DYNAMIC SYSTEM DESIGN OPTIMIZATION OF WAVE ENERGY CONVERTERS UTILIZING DIRECT TRANSCRIPTION

BY

DANIEL RONALD HERBER

THESIS

Submitted in partial fulfillment of the requirements
for the degree of Master of Science in Systems and Entrepreneurial Engineering
in the Graduate College of the
University of Illinois at Urbana-Champaign, 2014

Urbana, Illinois

Adviser:

Assistant Professor James T. Allison

Abstract

Dynamics are playing an increasingly important role in many engineering domains as these systems become more active and autonomous. Designing a dynamic engineering system can be challenging. In this thesis, both the problem formulation and solution methods will be discussed for designing a dynamic engineering system. A case is made for the inclusion of both the physical and control system design into a single design formulation. A particular class of numerical methods known as direct transcription is identified as promising solution method. These principles are then demonstrated on the design of a wave energy converter, a device that captures energy present in ocean waves. This system is of particular interest since a successful design hinges on exploiting the natural dynamics of the interaction between the ocean waves and the physical wave energy converter. A number of numerical studies are presented that identify both novel and previously observed strategies for the maximizing energy production of an ocean wave energy converter.

To Ashley and my parents,
for their love and support.

Acknowledgments

First and foremost, I would like to express my gratitude towards my adviser, Professor James T. Allison, for his invaluable guidance throughout my graduate studies and thesis work. What started off as a grading position quickly turned into a collaboration on wave energy research, stemming from his passion for research and teaching.

I would especially like to thank Ashley for her continuous support and love during my studies which includes, but is not limited to, listening to me talk about my research and always having time to review my writing. I want also to recognize my family who have always supported me. My mother and father have always encouraged me to pursue my academic and life interests, for which I am forever grateful.

There are many members of the Engineering System Design Lab who provided invaluable research and academic assistance throughout my graduate studies. This includes Jeff Arena, Anand Deshmukh, Chen Ge, Tinghao Guo, Allen Kaitharath, Ashish Khetan, Danny Lohan, Jason McDonald, Xin Niu, and Lakshmi Rao. Allen, Chen, and Xin also were invaluable collaborators on a number of wave energy related projects.

I would also like to thank the Department of Industrial & Enterprise Systems Engineering not only for their financial assistance through Teaching Assistantships, but their constant effort to create a challenging and engaging engineering curriculum throughout my graduate and undergraduate studies.

Finally, I would like to acknowledge the support of Deere & Company and in particular the John Deere Technology Innovation Center in Champaign. My work with them was an instrumental step from my undergraduate to graduate studies, and made for an enjoyable transformation from student to researcher. I would like to thank Hank Roark especially for his guidance and patience; in addition to Prof. Allison, he sparked my interest in many research fields.

Contents

List of Figures

List of Tables

List of Abbreviations

AAO	All-at-Once
ANN	artificial neural network
BS	Bretschneider spectrum
BVP	boundary value problem
DAE	differential algebraic equation
DT	direct transcription
$D \to O$	discretize-then-optimize
HC	heaving cylinder
LG	Legendre-Gauss
LGL	Legendre-Gauss-Lobatto
LGR	Legendre-Gauss-Radau
LTI	linear time-invariant
MDF	Multidisciplinary Feasible
MDO	multidisciplinary design optimization
NLP	nonlinear programming
OCSD	optimal control-system design
ODE	ordinary differential equation
ODSD	optimal dynamic system design
OPSD	optimal physical-system design
$O \to D$	optimize-then-discretize
PMP	Pontryagin's maximum principle
PTO	power take-off
QCQP	quadratically constrained quadratic program
QP	quadratic program
SWL	still water level
WEC	wave energy converter

List of Symbols

a	cylinder radius [m]
$\mathbf{a}_U$	acceleration vector for the translation modes [m/s^2]
$\mathbf{a}_\Omega$	acceleration vector for the rotation modes [rad/s^2]
A	wave amplitude [m]
$\mathbf{A}$	state matrix (also constant linear constraint matrix)
α	empirical coefficient in Bretschneider spectrum
b	cylinder draft [m]
$\mathbf{b}$	constant linear constraint vector
$\mathbf{B}$	input matrix
β	empirical coefficient in Bretschneider spectrum
c	wave celerity [m/s]
$\mathcal{C}$	control subspace
$\mathbf{C}$	path constraint function
$\mathbf{C}[t_k]$	discretized path constraint vector at time point t_k
C_D	drag coefficient [0.81 for HC]
$\mathbf{D}$	differentiation matrix
e	disturbance
E	energy [J]
ϵ	penalty method termination tolerance [$\epsilon > 1$]
η	wave elevation [m]
f	objective function
f_{Ratio}	ratio of successive objective functions in penalty method
$\mathbf{f_d}$	state derivative function
$\mathbf{f_d}[t_k]$	discretized state derivative function at time point t_k
F_b	buoyancy force [N]
F_e	excitation force [N]

F_{PTO}	power take-off force [N]
F_r	radiation force [N]
F_v	viscous force [N]
F_w	wave force [N]
$\mathbf{F}$	external force vector [N]
g	gravitational constant [9.81 m/s^2]
$\mathbf{g}$	inequality constraint function
$\mathbf{g_p}$	plant constraint function
$\mathbf{G}$	gradient
γ_s	Runge-Kutta constant for stage s
h	height above the ocean floor [m]
h_k	kth time step size [s]
$\mathbf{h}$	equality constraint function
H	wave height [m]
$H(\cdot)$	Hamiltonian
$\hat{H}$	augmented Hamiltonian
$H_{1/3}$	mean wave height of the highest third of the wave [m]
$\mathbf{H}$	Hessian
I_k	kth time segment
$\mathbf{I}_g$	moment of inertia tensor at the center of mass [kgm^2]
k	wave number [1/m]
k_b	buoyancy stiffness coefficient [Nm]
k_r	impulse-response of the radiation force [N/m]
$\mathbf{K}$	disturbance matrix
$\mathbf{K}_{\mathrm{feed}}$	full-state feedback gain matrix
κ	penalty value update parameter [$0 < \kappa < 1$]
L	Lagrange interpolating polynomial
$\mathcal{L}$	Lagrange or running cost term
$\hat{\mathcal{L}}$	modified Lagrange term
$\mathcal{L}[t_k]$	discretized Lagrange term at time point t_k
$\mathbf{L}$	linkage constraint function
m	mass [kg]
m_r	added mass [kg]
$\overline{m}_r$	weighted added mass [kg]

$\mathbf{M}$	external moment vector [Nm]
$\mathcal{M}$	Mayer or terminal cost term
$\boldsymbol{\mu}$	path constraint Lagrange multiplier vector
n_g	number of inequality constraints
n_h	number of equality constraints
n_r	number of regular wave components
n_t	number of time points
n_u	number of control variables
n_x	number of optimization variables
n_C	number of path constraints
n_ϕ	number of boundary constraints
n_ξ	number of state variables
$\mathbb{N}$	set of natural numbers starting from 1
$\mathbb{N}_0$	set of natural numbers starting from 0
$\nu_{s\ell}$	Runge-Kutta constant for inner stage ℓ and outer stage s
ω	wave angular frequency [rad/s]
ω_0	natural angular frequency of the HCWEC [rad/s]
$\Delta\omega_i$	frequency width for wave component i [rad/s]
$\boldsymbol{\Omega}$	angular velocity vector [rad/s]
$\mathbf{p}$	costate vector
P	power [W]
$P(\tau)$	Legendre polynomial
$\overline{P}$	average power [W]
$\mathbf{P}$	quadratic constraint constant matrix
$\mathcal{P}$	plant subspace
ψ	discretized Lagrange term
$\boldsymbol{\phi}$	boundary constraint function
Q	constant coefficients when calculating sparsity patterns
R_{pen}	regularization penalty constant
R_r	radiation resistance [Nm/s]
$\overline{R}_r$	weighted radiation resistance [Nm/s]
R_v	viscous resistance [Nm/s]
$\mathbb{R}^+$	set of positive real numbers
ρ	sea water density [1025 kg/m^3]

ρ_s	Runge-Kutta constant for stage s
S	Runge-Kutta scheme order
$S(\omega)$	wave spectrum [m^{2}rad/s]
S_w	water plane area of the body [m^2]
t	time [s]
t_0	initial time [s]
t_f	final time [s]
$\mathbf{t}$	discretized time vector [s]
T	wave period [s]
T_p	modal period [s]
τ	dummy time variable
θ	wave phase [rad]
$\mathbf{u}$	control vector
$\bar{\mathbf{u}}$	intermediate discretized control vector
$\mathbf{u}[t_k]$	discretized control vector at time point t_k
$\mathbf{U}$	discretized control matrix
w	Gaussian quadrature weights
$\mathbf{x}$	optimization variable vector
$\mathbf{x_c}$	control optimization variable vector
$\mathbf{x_p}$	plant optimization variable vector
X_r	radiation reactance [Nm/s]
$\boldsymbol{\xi}$	state vector
$\boldsymbol{\xi}[t_k]$	discretized state vector at time point t_k
$\bar{\boldsymbol{\xi}}$	intermediate discretized state vector
$\dot{\boldsymbol{\xi}}$	state derivative vector
$\hat{\dot{\boldsymbol{\xi}}}$	approximated state derivative vector
$\boldsymbol{\Xi}$	discretized state matrix
z	coordinate of vertical translation or heave direction [m]
$\dot{z}$	heave velocity [m/s]
$\ddot{z}$	heave acceleration [m/s^2]
Z	radiation impedance [Nm/s]
$\boldsymbol{\zeta}$	defect constraint matrix or vector
$\boldsymbol{\zeta}[t_k]$	defect constraint vector at time point t_k
$\mathbf{0}$	matrix or vector of zeros

Chapter 1

Introduction

Dynamics are playing an increasingly important role in many engineering domains as these systems become more active and autonomous. Designing a dynamic engineering system can be challenging. Legacy design formulations need to be reevaluated, and newer methods should be considered that favor more natural formulations which directly account for the dynamics. Special numerical methods can efficiently and reliability find solutions for these problems. The design of wave energy converters (WECs) is promising application area for dynamic system design optimization.

1.1 The Design of Ocean Wave Energy Converters

Energy is the largest commodity in the world and its influence on modern society is ever-increasing [1]. A subset of the world energy resources is renewable energy, which is defined as energy produced through sources that are near inexhaustible or can be replenished in a short amount of time. Examples include: solar, wind, geothermal, hydropower, biomass, and ocean energy. Significant concerns have been raised on both the national and global level regarding nonrenewable energy sources including the dependence on foreign supplies (e.g., fossil fuels) and their influence on global warming [2–4]. Although renewable resources have the potential to alleviate these concerns, most are unable to compete with the low energy prices of nonrenewables, primarily fossil fuels. Ocean energy is a promising class of renewable energy but it is still considered to be in the early stages of technology development [5, p. 3]. The five categories that capitalize on a distinct ocean-based physical phenomenon include wave energy, tidal energy, marine currents, temperature gradients, and salinity gradients [6]. Wave energy is generated from the wind passing over the surface of the sea. This work will focus on improving the

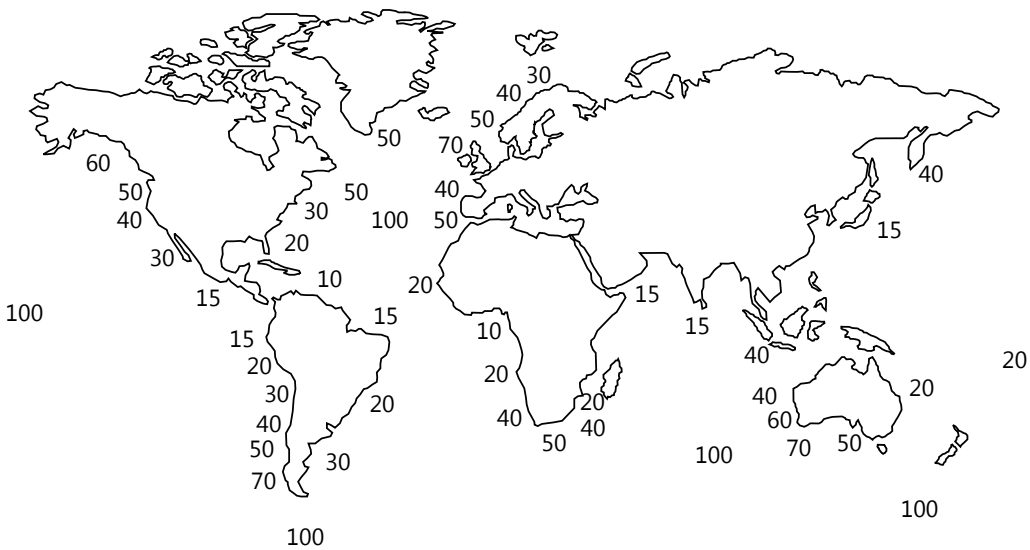

Figure 1.1 Approximate yearly average global distribution of wave power levels in kW per meter of wave front [7].

performance of WECs that capture wave energy and turn it into a usable energy resource.

The characteristics of wave energy provide strong evidence for the engineering investment required to capture usable energy. These positive characteristics include:

- Highest power density — When compared to other renewable sources [8].

- High availability — Wave energy is typically quantified by a high utility factor, which is the quotient between the rated power and the average energy production. Due to the storage and transport capacity of ocean waves, usable energy remains after the wind ceases [9]. This translates up to a 90% availability at a given site, while solar and wind power are typically available 20% to 30% of the time [10].

- Large resource — Estimates for the practical potential world-wide energy contribution of wave energy is estimated at 2,000 TWh/year [8] and the fraction available for United States (US) consumption is estimated at 117 TWh/year [11]. These large energy figures are due to the vast ocean regions where the power density is high. The average annual power density of the world's ocean waves can be seen in Fig. 1.1. The National

Renewable Energy Laboratory estimates harnessing 20% of the wave energy potential from coastal US with 50% efficiency would be equivalent to all of the hydrogeneration throughout the US in 2003, equating to nearly 24,000 MW [12].

- Low environmental impact — Wave energy has low negative interaction with the surroundings according to Electric Power Research Institute [13]. Offshore WECs have a relatively low visual profile. Visual disturbance and public acceptance have been major factors that have hindered the development of many energy projects.

There are a number of negatives associated with wave energy that need consideration during any development project, including:

- Large variations in power — WECs need to be designed to survive all possible conditions. The extreme circumstances of the "100-year" storm wave can be up to 100 times the average power. These large spikes in power can damage the WEC.

- Harsh operating environment — The ocean is an extremely corrosive environment and the device is constantly exposed to marine growth.

- Difficult access conditions — Access to offshore structures for deployment or maintenance can be difficult and costly.

The first wave power patent was granted in 1799 to Monsieur Girard of Paris [8]. A long period passed with little work on producing commercially viable WECs, but after the oil crisis in 1973, interest was elevated. Following a period of reduced funding and activity in the 1980's, funding for wave energy research increased again in the late 90's, mainly due to the Kyoto conference on the reduction of CO_2 emissions and the growing realization of shortness and insecurity of national energy supplies. An early book by McCormick provides a summary of some of the early proposals and patents [14]. In 2006, fifty-three different wave energy technologies were being developed [6].

All WECs transform wave power into electrical power through at least one mechanical intermediate system. One such system is a floating or submerged body that moves along with the waves and a power take-off (PTO) system

that converts this relative motion into electrical power [15, p. 1]. This implies that the most fundamental task of a WEC is to generate a wave that interferes destructively with the incident wave, thus imparting all of the wave's power into the mechanical component of the WEC, meaning WECs need to be exceptional wave generators [16, 17]. Radiation resistance, also known as the wave damping coefficient, is derived from the physical profile of the WEC and plays a key role in determining amount of power that can be absorbed and subsequently sold [18, p. 12].

There are reviews of available WEC technologies [19–21]. A few of the most prevalent classifications are summarized and some common WEC topologies (❶ to ❼) are shown in Fig. 1.2.

- Point absorber — This is typically a buoy-like device with horizontal dimensions that are small compared to the incident wavelengths and it oscillates according with one or more degrees of freedom. An example is Ocean Power Technology's Powerbuoy (❷) [22]. Some heaving multi-point absorber systems are the FO3 (collection of ❷) [23] and the Wave Star (similar to a collection of ❶) [24].

- Attenuator — These typically have a slender profile that is installed parallel to the wave propagation direction and "ride" the wave during its operation. An early design was Cockerell's Rafts (❹) [14, p. 101], and a current commercial design is the Pelamis (❹) [25].

- Terminator — Their installation direction is parallel to the wave front (perpendicular to the predominant wave direction) and physically intercept the incoming wave [19]. An example is Salter's duck (❺) [26].

There are others characterized by their modes of operation, including submerged pressure differential devices, oscillating wave surge converters, oscillating water columns, and overtopping devices (❼) [19].

To illustrate the basic principles behind wave energy conversion consider the simple point absorber WEC that is constrained to move in a heaving motion (❶) shown in Fig. 1.3. The mechanical component is connected to a PTO moored to the ocean floor. Various shapes have been proposed for the mechanical component including spheres and cylinders [27]. The vertical position of the device's mass center (z) is measured from the still water

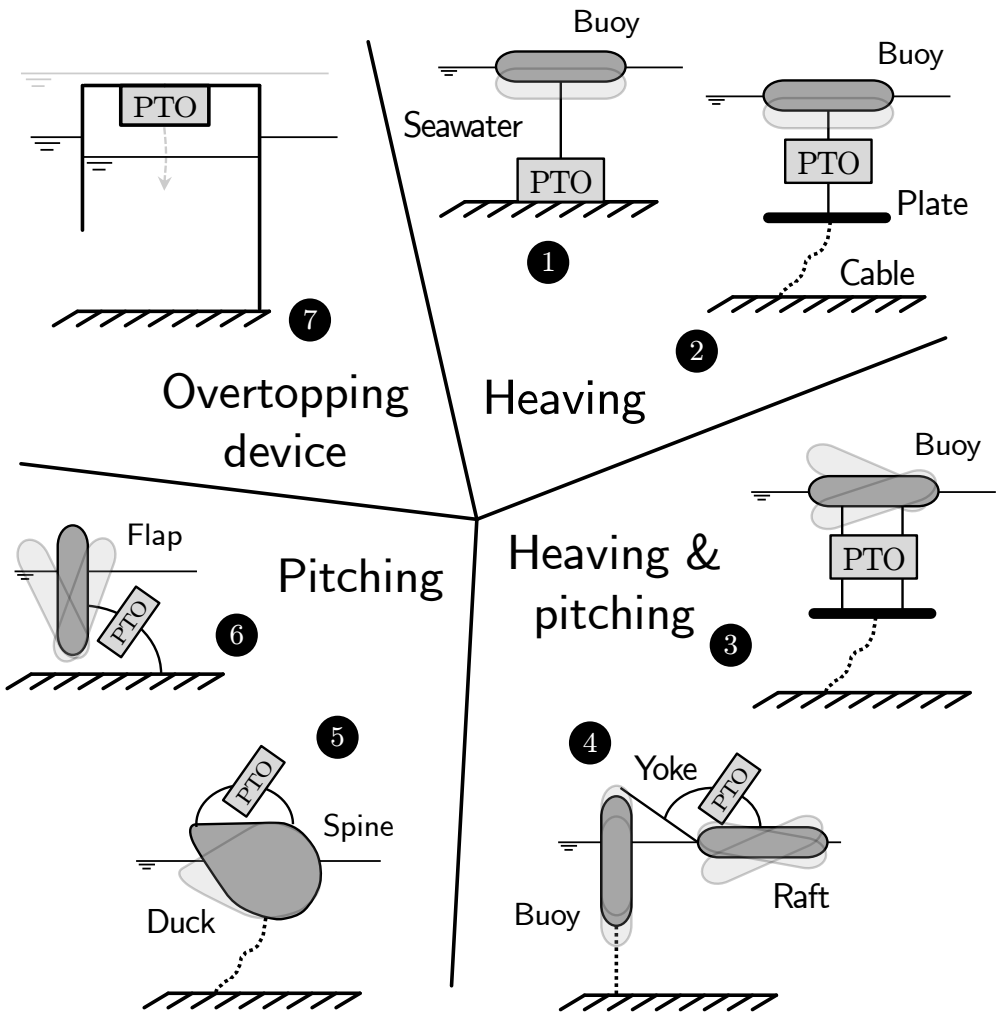

Figure 1.2 Illustrations of various common devices used to capture wave energy [20].

level (SWL), which is h meters above the ocean floor. The wave elevation is denoted $\eta(t)$. As buoyancy forces the heaving WEC upward, motion is resisted by the PTO. Work is done on the PTO at the rate:

$$P(t) = F_{\text{PTO}}(t)\dot{z}(t) \tag{1.1}$$

where $F_{\text{PTO}}(t)$ is the PTO force and $\dot{z}(t)$ is the vertical velocity of the device. The common goal when designing such a device is to maximize the energy

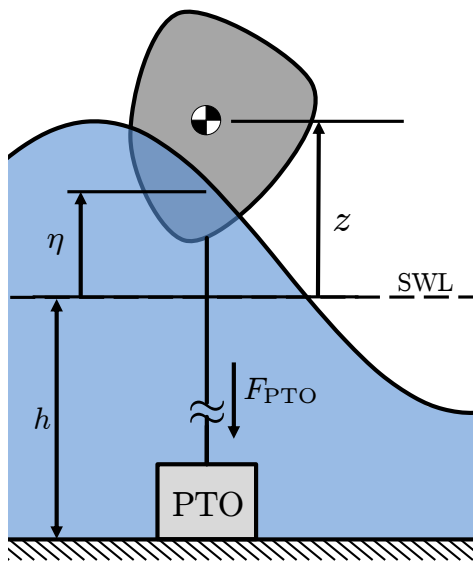

Figure 1.3 Simple heaving point absorber WEC.

absorbed over a desired time horizon, or mathematically:

$$\max \quad E(t) = \int_{t_0}^{t_f} P(t)dt \tag{1.2}$$

where the time horizon is defined between t_0 and t_f.

A number of different PTOs have been studied including simple mathematical models similar to Eqn. (1.1) [28, 29], hydraulic-electric apparatuses [19, 30], rotating electric machines [31], and linear electric machines [20, 32–34]. Most of these PTOs are actively controlled, i.e., the force produced by the PTO is determined by the operator. This control trajectory through time is frequently calculated through a feedback controller which utilizes the current state information from the system (such as the position and velocity of the device). Optimal control strategies for various design objectives have been developed for simple waves (e.g., reactive [27], latching [30], and declutching [28]). However, Tedeschi et al. demonstrated that these control strategies are inferior in more complex waves [31]. An alternative approach to feedback controllers (or any type of structured control) is open-loop control design. With these approaches, the control trajectory is directly designed, allowing for solutions that can produce the true system performance limits [28, 29, 35, 36]. This approach can also prove useful in the early stages of the design

process where the entire system has not been specified yet. For example, an engineer may not know which type of PTO is going to produce the optimal system-level performance, but directly designing $F_{\mathrm{PTO}}(t)$ could result in a optimal target trajectory for the future PTO design.

The key issue with the design of ocean WECs are the challenges associated with constructing a technology that is properly adapted to the constraints given by the natural resource [1, p. 16]. With some the previously discussed challenges, it is easy to see that the development of a WEC is a highly cross-disciplinary task [18, pp. 3-4]. The community has not converged to preferred WEC designs (see Fig. 1.2). The classifications provided have substantial diversity (e.g., the many ideas and concepts associated with point absorbers involving a variety of engineering disciplines [5, p. 5]). When an engineering optimization problem requires the analysis of multiple disciplines, it is classified as a multidisciplinary design optimization (MDO) problem [37]. Typical analysis domains include the wave-structure interaction and is coupled with the disciplines associated with the PTO (e.g., electrical, hydraulic, or both).

In addition to the complexity of the system-level analysis, the specific domains have their own associated complexity. Early work in WEC design was performed in the frequency domain [27]. This technique requires a number of assumptions, including linearity and regular incident waves. Regular waves are harmonic or sinusoidal waves (e.g., $\eta(t) = A \sin \omega t$), whereas irregular waves are a superposition of many regular wave components and better model real seas and their stochastic nature. Many authors have stated that there is a fundamental difference between designing WECs for irregular versus regular waves. Drew et al. asserted that designing for a single frequency of the incident sea wave will not predict the performance in real systems [19]. Tedeschi et al. emphasized the need to use time-dependent solutions since the instantaneous extracted power in irregular waves is required for realistic analysis [31].

Critical practical constraints also need to be accounted for when designing WECs. Initial research was based on unconstrained formulations. Only a small number of prototypes have been produced since practical constraints were ignored [5, p. 5]. Some practical constraints include:

- Stroke constraint — Intended to prevent the mechanical limitations on the stroke of the device, e.g., imposed by the limited height of a hydraulic

piston [5, 38].

- Control force restriction — Necessary to decrease the control forces to practical levels, particularly for the case where the tuning is to be delivered by the PTO system [5, 38]. This restriction is typically imposed by electromechanical and/or economic limitations.

- Slamming constraint — Intended to reduce the probability that the mechanical component rises out of the water, and therefore subjected to bottom slamming [5, 29]. This constraint is imposed by the hydrodynamic limitations, and special attention is typically required to model the complex water-entry phenomena associated with hydrodynamic pressures and loads.

- Other constraints include wave velocity, frequency, output voltage, output current, and physical constraints [39, p. 8]

Occasionally designs are based on engineering intuition. For example, Eriksson discusses the benefits of using a linear generator to reduce the complexity of the mechanical interface [20, p. 19]. While this is a valid strategy, engineering complexity should not be removed unless the final design is going to provide a satisfactory response. The designer cannot make this tradeoff without knowing the upper limits of both the wave-buoy system and wave-buoy-PTO system. These requirements motivate a method to compare fairly the various types of proposed designs. Such a method would result in the true system performance limits for each proposed design.

In summary, a proper WEC design formulation should directly address the multidisciplinary nature, the constraints, and the dynamics of the WEC system design problem.

1.2 The Design of Dynamic Engineering Systems

The framework established by multidisciplinary design optimization of dynamic engineering systems directly addresses the key points in WEC design [40]. Problems are posed as constrained mathematical optimization problems. Equation (1.2) is an example but may also be subject to constraints, such as the power in Eqn. (1.1), must always be positive (i.e., $P(t) \geq 0$).

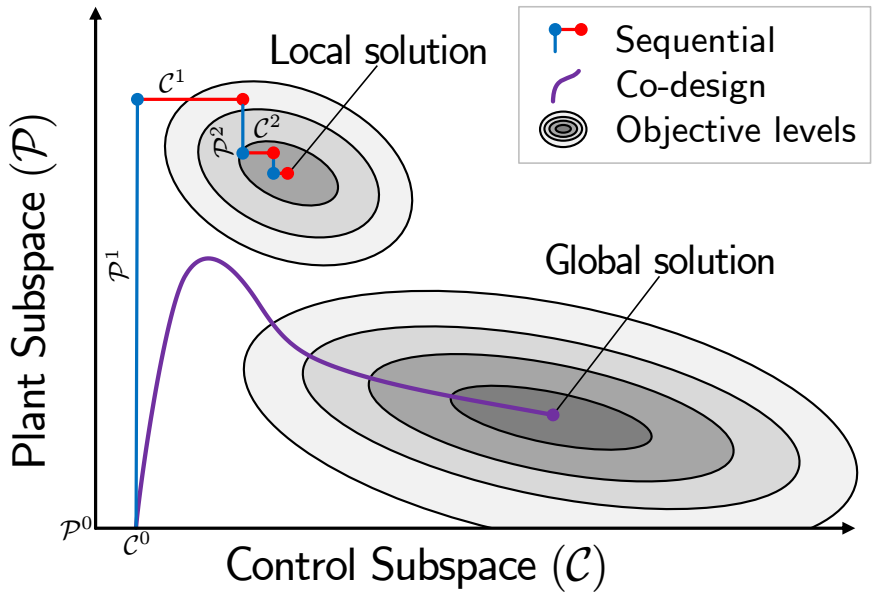

Figure 1.4 Illustration of the differences between sequential design and co-design.

A core principle in this framework is the integrated design of both the physical elements (or plant) of the system and the control in order to achieve the best possible system performance. The preferred approach simultaneously considers the plant and control design as a single system-level optimization problem. This approach is often referred to as co-design [41–45]. Using this approach, the designer can capitalize on the synergy between physical and control system design decisions to produce designs with superior performance [40, 46–48]. In comparison, a traditional sequential approach designs the physical system first, then is held fixed while the control is optimized. This procedure can be iterated [41, 42]. A graphic comparison of the sequential approach to co-design is shown in Fig. 1.4. The sequential approach can only make changes in either the plant subspace ($\mathcal{P}$) or control ($\mathcal{C}$) subspace and follows the sequence of design variable iterations as:

$$\left(\mathcal{C}^0, \mathcal{P}^0\right) \rightarrow \left(\mathcal{C}^0, \mathcal{P}^1\right) \rightarrow \left(\mathcal{C}^1, \mathcal{P}^1\right) \rightarrow \left(\mathcal{C}^1, \mathcal{P}^2\right) \rightarrow \left(\mathcal{C}^2, \mathcal{P}^2\right) \rightarrow \cdots$$

whereas the co-design sequence makes changes in both domains simultane-

ously:

$$\left(\mathcal{C}^0, \mathcal{P}^0\right) \to \left(\mathcal{C}^1, \mathcal{P}^1\right) \to \left(\mathcal{C}^2, \mathcal{P}^2\right) \to \left(\mathcal{C}^3, \mathcal{P}^3\right) \to \left(\mathcal{C}^4, \mathcal{P}^4\right) \to \cdots$$

These subspace iterations are likely not the same due to the differences in their update methods, i.e., $(\mathcal{C}^1, \mathcal{P}^1)_{\text{seq}} \neq (\mathcal{C}^1, \mathcal{P}^1)_{\text{co-design}}$. In addition, integrated approaches are sometimes necessary to find feasible solutions, especially in demanding dynamic systems [40]. Another advantage is the ability to exploit the passive dynamics (dynamic behavior without active control) of the system which has been shown to produce exceptional designs in robotic manipulators [48, 49]. A co-design approach is the natural way to handle the WEC design problem since a successful design hinges on exploiting the natural dynamics of the ocean wave-mechanical component interaction.

Often WEC studies consider both plant and control design at some point during the design process. For example, a set of optimization variables could include the mechanical component's shape and size (plant) and the PTO force (control). However, many studies fix the physical design before an optimal controller can be identified. Frequently the majority of the engineering costs are placed into a physical prototype which is difficult to change later in the design process. The control strategy, however, can be easily modified and tested with the physical prototype, producing a realized energy capture. A co-design approach aims to produce a better physical design before the prototype is created.

One final aspect of co-design is its ability to leverage other simultaneous design methods, i.e., methods which perform the system analysis and design in a simultaneously manner. The class of direct transcription (DT) methods are simultaneous approaches to solving an optimal control problem. These are direct methods where the problem is first discretized and then transcribed to a nonlinear programming (NLP) formulation. In other words, an infinite-dimensional optimal control problem is transcribed to a finite-dimensional NLP [50, 51]. DT can be used to solve the open-loop optimal control aspect on the WEC design problem [29]. Control and physical constraints are also easily incorporated in a DT setting (such as the practical WEC constraints) [29, 35, 36]. These methods have recently been extended to co-design problems with a high level of success [29, 47, 52].

1.3 Thesis Overview

Chapter 2 is split into two main sections. The first reviews dynamic system design optimization formulations and the second presents a qualitative discussion of various methods that can be used to solve dynamic system design problems. Chapter 3 outlines direct transcription with a focus on the additional defect constraints and favorable properties of the method. Chapter 4 focuses on the mathematical modeling of the wave energy converter design problem while reviewing previous work. Chapter 5 contains a number of numerical studies on the wave energy converter design problem employing a proper dynamic system design optimization formulation and direct transcription. Chapter 6 presents the conclusion. These chapters accomplish the following objectives:

(1) To present a unified framework for both control- and physical-system design of dynamic engineering systems

(2) To discuss the merits of current methods to solve dynamic system design optimization problems

(3) To demonstrate the usefulness of direct transcription when solving dynamic system design problems

(4) To better understand both the optimal control- and physical-system design of wave energy converters

Chapter 2

Dynamic System Design Optimization

Our first step in understanding how to design a dynamic engineering system is a discussion of how the solution to an NLP can produce useful engineering designs. The formulation of a general nonlinear program is:

$$\min_{\mathbf{x}} \quad f(\mathbf{x}) \tag{2.1a}$$

$$\text{subject to :}$$

$$\mathbf{h}(\mathbf{x}) = \mathbf{0} \tag{2.1b}$$

$$\mathbf{g}(\mathbf{x}) \leq \mathbf{0} \tag{2.1c}$$

where $\mathbf{x}$ are the optimization variables, the objective function, $f(\mathbf{x})$, is in Eqn. (2.1a), the equality constraints are Eqn. (2.1b), and the inequality constraints are Eqn. (2.1c) (see Refs. [53, 54] for NLP textbooks). The optimization variable vector is $\mathbf{x} = [x_1, \ldots, x_{n_x}]^T \in \mathbb{R}^{n_x}$. The constraint functions are vector-valued: $\mathbf{h}(\mathbf{x}) = [h_1, \ldots, h_{n_h}]^T$ and $\mathbf{g}(\mathbf{x}) = \left[g_1, \ldots, g_{n_g}\right]^T$.

This abstract problem can be related back to engineering design through an analytic representation of the design problem (see Ref. [55] for traditional physical-system design formulations and Refs. [51, 56] for control-system design formulations). Optimization variables are substituted for numeric design variables that are inputs to an analytic expression of the design objective. Transferring the design from a qualitative description to mathematical formulation can be decidedly challenging. For example, how does one quantify the aesthetics of an automobile? However, in the overall design of an automobile, average fuel economy might be more important during different stages of the design process and can be quantified naturally. Engineering intuition can often be used to quantify a dynamic system design problem in a format consistent with Prob. (2.1), but as we will explore soon, solving this type of problem can be exceedingly difficult.

2.1 Optimal Control-System Design

We will first discuss the optimal control-system design (OCSD) as it is an important part of the general dynamic system design formulation. The goal of an OCSD problem is to determine the state trajectories, $\boldsymbol{\xi}(t)$, and the control trajectories, $\mathbf{u}(t)$, that produce the best possible system performance. As the word trajectory implies, dynamics are fundamental to these systems. Constraints on trajectories must also be satisfied to produce feasible system performance. The OCSD problem is stated as:

$$\min_{\mathbf{u}(t),t_0,t_f} \quad \int_{t_0}^{t_f} \mathcal{L}\left(t, \boldsymbol{\xi}(t), \mathbf{u}(t)\right) dt + \mathcal{M}\left(t_0, \boldsymbol{\xi}(t_0), t_f, \boldsymbol{\xi}(t_f)\right) \tag{2.2a}$$

$$\text{subject to :}$$

$$\dot{\boldsymbol{\xi}} - \mathbf{f_d}\left(t, \boldsymbol{\xi}(t), \mathbf{u}(t)\right) = \mathbf{0} \tag{2.2b}$$

$$\mathbf{C}\left(t, \boldsymbol{\xi}(t), \mathbf{u}(t)\right) \leq \mathbf{0} \tag{2.2c}$$

$$\boldsymbol{\phi}\left(t_0, \boldsymbol{\xi}(t_0), t_f, \boldsymbol{\xi}(t_f)\right) \leq \mathbf{0} \tag{2.2d}$$

Problem (2.2) consists of a number of critical components reminiscent of Prob. (2.1): the cost functional or objective function in Eqn. (2.2a), the dynamic constraints in Eqn. (2.2b), the algebraic path constraints in Eqn. (2.2c), and the boundary constraints in Eqn. (2.2d).

Optimal control is a well-developed subject; many scholars date its origins in the storied Brachystochrone challenge set forth by Johann Bernoulli in 1697 [57]. However, the very nature of these formulations lead to extremely challenging solution efforts. An OCSD problem is infinite-dimensional since we are designing a trajectory that varies in time, whereas many traditional engineering design problems operate on a finite-dimensional optimization vector. Another way of viewing the minimization procedure in Prob. (2.2) is the selection of the best trajectory among all feasible trajectories for the system [58, p. 2]. Initial work with infinite-dimensional optimization started with calculus of variations, which seeks an optimal path without the framework of a actively controlled system [57, 58].

First, we should understand the how powerful a problem placed in this formulation can be, i.e., the ability to find novel optimal solutions both beyond the bounds of human creativity and encompassing an incredibly useful problem archetype. Even with these claims, one might point out the lack

of physical-system design in this formulation; this will be discussed in the following sections.

Objective function, Eqn. (2.2a) — The first term is an integral calculated over the time horizon t_0 to t_f. Inside this integral is the Lagrange term or running cost, $\mathcal{L}(\cdot)$, which could depend on time, state, and control. Some common engineering design problems have running costs of fuel consumption rate, extracted power, or limited motion. These sample running costs all share the property that they are trajectories that are integrated, which we might be interested in minimizing or maximizing to produce the desired system performance. The second term is known as the Mayer term or terminal cost, $\mathcal{M}(\cdot)$, and depends only on the initial and final behavior of the system where t_0 and t_f may be included as optimization variables. This term allows us to pose a diverse set of problems including minimum time to climb for an aircraft, or the maximum height of a fuel-limited rocket. If both these terms are present, the problem is often term a Bolza objective problem.

Simple transformations exist to convert a Bolza objective problem into a Lagrange only ($\mathcal{M} \equiv 0$) or Mayer only($\mathcal{L} \equiv 0$) problem if certain assumptions are met [58, p. 87]. Starting with a converting $\mathcal{M} \to \mathcal{L}$, we must assume the $\mathcal{M}$ only depends on the initial or final state values. The transformation then is:

$$\mathcal{M}\big|_{t_f} = \mathcal{M}\big|_{t_0} + \int_{t_0}^{t_f} \Big(\mathcal{M}_t(t, \boldsymbol{\xi}) + \mathcal{M}_x(t, \boldsymbol{\xi}) \cdot \mathbf{f_d}\left(t, \boldsymbol{\xi}, \mathbf{u}\right) \Big) dt \tag{2.3}$$

where $\mathcal{M}\big|_t \equiv \mathcal{M}(t, \boldsymbol{\xi})$. We now can see why $\mathcal{M}$ can only depend on the initial or final state; Eqn. (2.3) can either remove $\mathcal{M}\big|_{t_f}$ or $\mathcal{M}\big|_{t_0}$ depending on which term is not present. Thus, the equivalent Mayer cost now only contains an integral over the time horizon completing the conversion to Lagrange only form. Converting $\mathcal{L} \to \mathcal{M}$ can be done through an additional state variable ξ_0 with the assumption that $\mathcal{L}$ satisfies the same regularity conditions as $\mathbf{f_d}(\cdot)$ [58, p. 87]. The dynamics of ξ_0 will naturally be equivalent to $\mathcal{L}$ with an arbitrary initial value for the ordinary differential equation (ODE):

$$\int_{t_0}^{t_f} \mathcal{L}\left(t, \boldsymbol{\xi}, \mathbf{u}\right) dt = \xi_0(t_f) \tag{2.4a}$$

$$\dot{\xi}_0 = \mathcal{L}\left(t, \boldsymbol{\xi}, \mathbf{u}\right), \quad \xi_0(t_0) = 0 \tag{2.4b}$$

These transformations will provide important insights later when trying to solve Prob. (2.2) numerically.

Dynamic constraints, Eqn. (2.2b) — The distinction between the state derivatives and the functions that calculate the state derivatives is a subtle one: there are different methods of finding $\dot{\boldsymbol{\xi}}$. One way is to use the actual derivative function based on natural phenomenon while another is with derivative function approximation using only the states. But the set of dynamic constraints specifies that these two approaches must arrive at the same values. As stated before, this is an infinite-dimensional problem so these constraints can be viewed as pointwise over the entire time interval [56, p. 123]. These are first-order differential equations and in general are nonlinear [59, p. 11]. A linear time-invariant (LTI) system is:

$$\dot{\boldsymbol{\xi}}(t) = \mathbf{A}\boldsymbol{\xi}(t) + \mathbf{B}\mathbf{u}(t) \tag{2.5}$$

where $\mathbf{A}$ is the state matrix and $\mathbf{B}$ is the input matrix. Although LTI systems are typically taught in early university courses on control, they are the exception rather than the rule when it comes to the dynamic behavior of realistic physical systems [59, pp. 6-11]. Linear voltage versus current laws for resistors and linear force versus velocity laws for friction are really just approximations of more complex nonlinear behavior [59, p. 11]. Meaningful formulations of realistic engineering design problems will need to capture this behavior. For an LTI system, state trajectories can be computed with the following equation:

$$\boldsymbol{\xi}(t) = e^{\mathbf{A}(t-t_0)}\boldsymbol{\xi}_0 + \int_{t_0}^{t} e^{\mathbf{A}(t-\tau)}\mathbf{B}\mathbf{u}(\tau)d\tau \tag{2.6}$$

where $e^{\mathbf{A}t}$ is the state transition matrix and the integral term is a convolution integral [59, p. 43]. This equation will be revisited in the discussions of additional dynamic system design formulations.

Path constraints, Eqn. (2.2c) — Many traditional engineering constraints can be formulated naturally as path constraints. Two examples include preventing an aircraft from crashing into the ground or requiring an automobile to follow a desired drive cycle. Other important states or derived states (such as power) often need to be constrained. Temperature, position, force, pressure, current, stress, and power are all common examples. These constraints

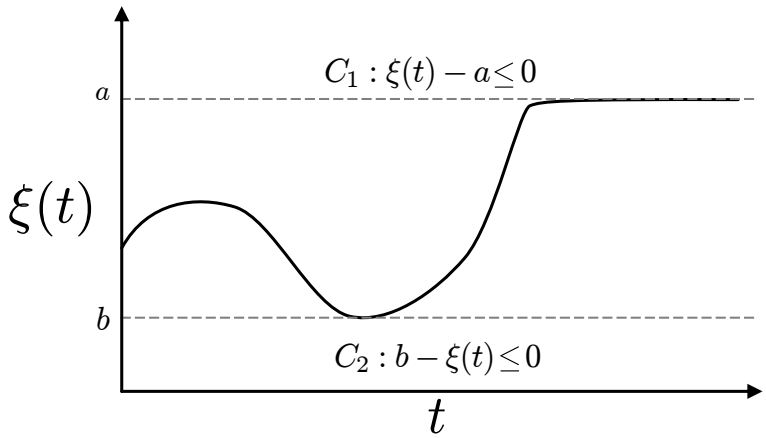

Figure 2.1 Visualization of two simple path constraints.

create a multipoint boundary value problem (BVP) where the locations in time when the path constraints become active are not known a priori since the constraints may enter or exit activity multiple times throughout the time horizon [56, p. 126]. They are also known as algebraic path constraints since the ODE system is transformed into a system of differential algebraic equations (DAEs) when inequality constraints become active. For every degree of freedom lost by imposing an algebraic relationship through an active path constraint, one state or control variable will now be determined via an algebraic constraint. In active systems, control inputs normally become the algebraic variable since they are independent, while state variables still must satisfy physics or other natural phenomena [60]. As additional inequality constraints become active, the DAE index may increase, increasing solution difficulty due to numerical errors [56, pp. 124-125]. Two simple path constraints are shown in Fig. 2.1. The lower path constraint becomes active at only a single point during the time horizon while C_1 remains active for an extended period of time. If active control is present when C_1 is active, the state value is already known and assuming this is the only state, the control can be calculated through an algebraic relationship.

Boundary constraints, Eqn. (2.2d) — These constraints have some similarities with path constraints but are viewed as discrete since they only are considered at the boundary time values [56, p. 123]. Unlike path constraints, we know when boundary constraints are active even if time boundaries vary

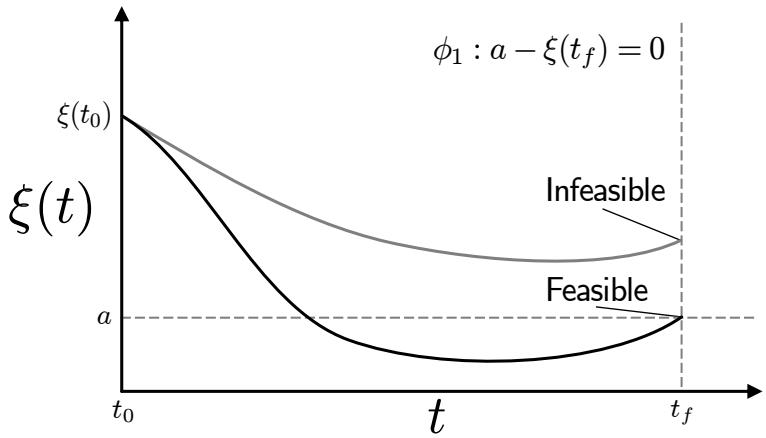

Figure 2.2 Visualization of a simple boundary constraint.

in the problem (i.e., we still know the values of t_0 and t_f when evaluating a boundary constraint). Final or initial states values might be set for a particular problem, i.e., the solution must guide the system to/from a specific target. A simple boundary constraint that requires the state to be equal to a at t_f is shown in Fig. 2.2. This requirement is only enforced at a single discrete point. The upper trajectory in this visualization is infeasible since the constraint is not satisfied but the general state trend is similar to the feasible path. Final time state boundary constraints can be challenging to satisfy since they are an accumulation of previous derivative values. Alternative paths may exist that satisfy the boundary condition.

Other common boundary constraints include kinematic relationships in robotics [61]. These constraints might require an algebraic variable that depends on the states (e.g., the end position of the robotic manipulator depends on the state joint angles). In Ref. [62], the state derivative at the boundary is constrained in the space station attitude control problem. One final example is a periodic constraint, i.e., the initial and final values need to be equivalent so the system can undergo an optimal repetitive cycle. This constraint type will prove to be especially useful in WEC design problems [29].

Time dependence — We can remove the time dependence in Prob. (2.2) by

making the following substitution:

$$\xi_{n+1} = t, \quad \dot{\xi}_{n+1} = 1, \quad \xi_{n+1}(t_0) = t_0 \tag{2.7}$$

where time is now another state variable.

Multiple phases — In many problems, it is necessary or convenient to view the dynamic trajectory as a collection of phases. A phase is defined as a portion of the overall trajectory where the set of DAEs remain unchanged. If the problem has different sets of DAEs, the sets must be in different phases [56, p. 108]. There are other numerical reasons to create a multiphase problem, even if the DAEs remain unchanged. These reasons will be explored in Section 2.4.2.

The addition of phases requires the addition of a new type of constraint to the formulation in Prob. (2.2) known as linkage constraints:

$$\mathbf{L}\left(t_f^{p_l}, \boldsymbol{\xi}^{p_l}(t_f), t_0^{p_r}, \boldsymbol{\xi}^{p_r}(t_0)\right) \leq \mathbf{0} \tag{2.8}$$

where p_l and p_r are the "left" and "right" phase numbers in the set of possible phase numbers [63] . In many cases, the states need to be continuous between the phases, which would be represented by a special case of Eqn. (2.8):

$$\boldsymbol{\xi}^{p_l}(t_f) - \boldsymbol{\xi}^{p_r}(t_0) = \mathbf{0} \tag{2.9}$$

In addition, Prob. (2.2) needs to be modified with some combination of phase objectives, and the boundary constraints need to include indicators for switching from one phase to another, known as events. Events are often based on specific time or state values. For example in a multistage rocket, one might have an event condition active when a specific stage is out of fuel. The linkage conditions would not be continuous since mass is lost instantaneously between the stages [64].

Closed-loop control — In most practical implementations, we need to design a feedback controller (and often we need to design an observer to estimate states that cannot be measured directly). A simple form of feedback control is a full-state feedback regulator, where the control input is defined as $\mathbf{u}(t) = -\mathbf{K}_{\text{feed}}\boldsymbol{\xi}(t)$. Assuming this control structure, the OCSD problem may be solved with respect to the gain matrix $\mathbf{K}_{\text{feed}}$ instead of the $\mathbf{u}(t)$. The set of

trajectories possible will feedback controllers are only a subset of all possible trajectories, which might limit the performance. Limiting the performance of the system should be a calculated decision, not a modeling convenience. The true system performance limits can only be identified while directly designing the control with open-loop control. Karbowski et al. makes the case that a "fair" comparison between hybrid vehicles designs can only be made if the open-loop optimal control is used [65]. General control laws may be identified from the open-loop solutions. In Prob. (2.2), $\mathbf{u}(t)$ should be replaced with the control design variables, $\mathbf{x_c}$, if we are using a parametrized version of the control.

2.2 Optimal Physical-System Design

Many dynamic engineering systems existed before control theory. The design of these systems was solely dependent on what could be changed within the physical-system. These systems relied much more heavily on passive dynamics without the possibility of active control. Due to a number of reasons, many optimal physical-system design (OPSD) efforts forgo more comprehensive treatment of the system dynamics for simplified versions (such as steady-state or pseudostatic models) or static analysis that neglects dynamic effects altogether [40]. Approximations of actual dynamic system performance metric are also commonly made (such as mass [66] or gravity balance [67]). While some problems can be adequately solved with these simplifications, the overall performance of the system could be improved with more complete dynamic models, and potentially support the solution of more demanding dynamic systems [40].

Even if comprehensive dynamic models are in use, they are normally developed for control design, and do not allow physical design changes. OPSD requires system models that incorporate realistic dynamics while providing flexibility in the physical design space. These models have the form:

$$\dot{\boldsymbol{\xi}}(t) = \mathbf{f_d}\left(t, \boldsymbol{\xi}(t), \mathbf{x_p}\right) \tag{2.10}$$

where $\mathbf{x_p}$ is a vector of plant design variables. If we consider once again an

LTI system, the state trajectories could be computed with the following:

$$\boldsymbol{\xi}(t) = e^{\mathbf{A}(\mathbf{x_p})t}\boldsymbol{\xi}_0 \tag{2.11}$$

where the system matrix $\mathbf{A}(\mathbf{x_p})$ depends on the plant design variables $\mathbf{x_p}$. With this system, it is obvious that the plant design affects the state trajectories, and OPSD on these systems will only be possible if models of the form shown in Eqn. (2.10) are available. Models of this form will require more development effort than models with the form given in Eqn. (2.2b) [40]. For example, dynamic models for linear electric generators are commonly parameterized by lumped, dependent parameters such as the inductance and capacitance [34]. We cannot directly change these quantities as a designer, but they have a substantial impact on the dynamic performance of the system. Independent quantities such as geometric variables should be used instead.

The goal of the OPSD problem is to identify the best possible system performance by modifying the plant variables, which will produce different state trajectories. The OPSD problem is stated as:

$$\min_{\mathbf{x_p},t_0,t_f} \quad \int_{t_0}^{t_f} \mathcal{L}\left(t, \boldsymbol{\xi}(t), \mathbf{x_p}\right) dt + \mathcal{M}\left(t_0, \boldsymbol{\xi}(t_0), t_f, \boldsymbol{\xi}(t_f), \mathbf{x_p}\right) \tag{2.12a}$$

$$\text{subject to :}$$

$$\dot{\boldsymbol{\xi}} - \mathbf{f_d}\left(t, \boldsymbol{\xi}(t), \mathbf{x_p}\right) = \mathbf{0} \tag{2.12b}$$

$$\mathbf{C}\left(t, \boldsymbol{\xi}(t), \mathbf{x_p}\right) \leq \mathbf{0} \tag{2.12c}$$

$$\boldsymbol{\phi}\left(t_0, \boldsymbol{\xi}(t_0), t_f, \boldsymbol{\xi}(t_f), \mathbf{x_p}\right) \leq \mathbf{0} \tag{2.12d}$$

which similar to Prob. (2.2) but lacking $\mathbf{u}(t)$. This problem contains similar constraints as before, but they may also depend on $\mathbf{x_p}$. In the physical-system design community, it is common to combine the path and boundary constraints into a single plant constraint that accounts for the influence of the dynamic response on the physical design requirements denoted:

$$\mathbf{g_p}\left(t, \boldsymbol{\xi}(t), \mathbf{x_p}\right) \leq \mathbf{0} \tag{2.13}$$

This single constraint does not provide the same insights found with path and boundary constraints in the optimal control-system formulation [29]. This distinction in Prob. (2.2) is made because the solution methods treat these

constraints differently. The OPSD solution approaches can also benefit from these classifications. As stated in the previous section, path constraints are continuous while boundary constraints are discrete. A common continuous plant constraint is bounding the stress or deflection of a member, while a boundary constraint might involve geometric requirements or mass calculation [47, 55].

A number of researchers have studied Prob. (2.12). Wang and Arora reviewed methods for solving the OPSD based on DT where the states were discretized [68]. Guo and Allison also used DT to solve the OPSD of genetic regulatory circuits [69]. Structural optimization problems have long been formulated as OPSD when considering the dynamics. Kang et al. provided a review of approaches for optimizing structures subject to transient loads [70], and Barthelemy and Haftka reviewed approximation methods relevant to this problem class [71]. Finally, OPSD has been used in designing more general mechanical systems [72, 73].

2.3 Optimal Dynamic System Design

In the previous two sections we separately discussed problem formulations for OCSD and OPSD. However, treating these as separate problems provides no guarantee that the result will be the optimal system-level design. Let us consider for a final time an LTI system with active control and dynamic models in the same form as Eqn. (2.10):

$$\boldsymbol{\xi}(t) = e^{\mathbf{A}(\mathbf{x_p})(t-t_0)}\boldsymbol{\xi}_0 + \int_{t_0}^{t} e^{\mathbf{A}(\mathbf{x_p})(t-\tau)}\mathbf{B}(\mathbf{x_p})\mathbf{u}(\tau)d\tau \tag{2.14}$$

Here the convolution integral, which directly impacts the states, depends on both plant and control variables! An integrated solution approach is required to capitalize on the synergistic relationship between physical- and control-system designs [40, 46–48]. Creating a single system-level optimization problem that combines OCSD and OPSD is known as co-design [41–45]. We will define the optimal dynamic system design (ODSD) problem by

combining Prob. (2.2) and Prob. (2.12):

$$\min_{\mathbf{x_p},\mathbf{u}(t),t_0,t_f} \quad \int_{t_0}^{t_f} \mathcal{L}\left(t,\boldsymbol{\xi}(t),\mathbf{u}(t),\mathbf{x_p}\right) dt + \mathcal{M}\left(t_0,\boldsymbol{\xi}(t_0),t_f,\boldsymbol{\xi}(t_f),\mathbf{x_p}\right) \tag{2.15a}$$

$$\text{subject to :}$$

$$\dot{\boldsymbol{\xi}} - \mathbf{f_d}\left(t,\boldsymbol{\xi}(t),\mathbf{u}(t),\mathbf{x_p}\right) = \mathbf{0} \tag{2.15b}$$

$$\mathbf{C}\left(t,\boldsymbol{\xi}(t),\mathbf{u}(t),\mathbf{x_p}\right) \leq \mathbf{0} \tag{2.15c}$$

$$\boldsymbol{\phi}\left(t_0,\boldsymbol{\xi}(t_0),t_f,\boldsymbol{\xi}(t_f),\mathbf{x_p}\right) \leq \mathbf{0} \tag{2.15d}$$

where all appropriate functions of the problem may depend on the plant and control variables, and plant and control constraints are categorized as either path and boundary constraints.

Differing from Prob. (2.15), a traditional approach is to use a sequential strategy, where the alternating physical- and control-system design problems are optimized (also see Fig. 1.4) [41, 42]. However, some formulations and/or models can only accommodate the effect of plant design on the control design problem. Therefore, iterating between the two problems is not possible [40]. If a dynamic system can be simulated in a passive mode, the dynamics can be directly considered during the plant design iterations. For example, with a passive-active automotive suspension, the passive suspension (i.e., mechanical links, spring, damper, etc.) can be optimized first for comfort and handling [44]. Then the optimal passive design could be used by the OCSD problem. But many systems require active control for simulations (e.g., robotic manipulators). In these cases the sequential approach cannot directly account for the dynamics in both domains. In some systems, methods have been developed to help guide the physical design towards improved active dynamic performance which require active control without directly including it in the design formulation [74].

Still considering the sequential approach, Allison and Herber discussed five different classes of plant design problems that include different levels of approximated system objectives, dynamics, and control [40]. They made the case against approximated system objectives in favor of the true system performance objective being used in the plant design problem. In addition when considering the effect of the active control in the plant design phase, the solution quality will be improved and iterated sequential co-design will

be possible.

A number of researchers have asserted that co-design problems are fundamentally multiobjective, i.e., there are at least two independent objectives [75–77]. While intrinsic tradeoffs in the system (e.g., cost vs. performance) may require a specific co-design problem to be multiobjective, a problem is not automatically multiobjective if it is a co-design problem. Legacy design practices can lead to OPSD problems that have different design objectives than the control problem [40]. When separate plant and control objectives are used, the plant objective is often an approximation of the real system objective (e.g., gravity balance approximating energy efficiency or reduced mass leading to more favorable dynamics).

Legacy design processes may also lead to separate plant objectives. When physical design is performed in isolation (e.g., the mechanical engineers and control engineers do not collaborate during the design process), using a plant objective that is not directly connected to dynamics or active control (such as mass or other static measures) is a logical choice. It might be challenging to adopt an integrated systems design approach, but abandoning familiar design objectives and adopting objectives that more accurately reflect overall system will design components that produce the best overall system behavior. Integrated system design requires consistent use of the same system objective (or objectives even if this is an inherently multiobjective problem) across all system elements.

We can now analysis a reduced but still equivalent statement of Prob. (2.15) using some of the items discussed in the previous section to get at the core of ODSD:

$$\min_{\mathbf{x_p},\mathbf{u}(t),t_0,t_f} \quad \mathcal{M}\left(\boldsymbol{\xi}(t_0),\boldsymbol{\xi}(t_f),\mathbf{x_p}\right) \tag{2.16a}$$

$$\text{subject to :}$$

$$\dot{\boldsymbol{\xi}} - \mathbf{f_d}\left(\boldsymbol{\xi}(t),\mathbf{u}(t),\mathbf{x_p}\right) = \mathbf{0} \tag{2.16b}$$

$$\mathbf{C}\left(\boldsymbol{\xi}(t),\mathbf{u}(t),\mathbf{x_p}\right) \leq \mathbf{0} \tag{2.16c}$$

$$\boldsymbol{\phi}\left(\boldsymbol{\xi}(t_0),\boldsymbol{\xi}(t_f),\mathbf{x_p}\right) \leq \mathbf{0} \tag{2.16d}$$

We now have a problem that only has a terminal cost (using the transformation in Eqn. (2.4)) and no time dependence (using the transformation in Eqn. (2.7)). This presentation of the ODSD problem might be more easily

compared to a traditional constrained engineering design problem. The key difference is the system of ODEs that need to be satisfied in Eqn. (2.16b), which will be at the core of the methods used to solve this problem.

2.4 Solving Optimal Dynamic System Design Problems

This section will focus on the methods developed to solve the various problems posed in the previous sections. First, indirect methods for OCSD will be discussed with direct methods following. We will go deeper into the many direct approaches in order to identify the best approaches for ODSD. Finally, we will discuss ways to combine the methods for OCSD and OPSD in order to solve the ODSD problem.

2.4.1 Indirect Methods for OCSD

The earliest methods for solving OCSD were indirect methods, which are based on the elegant mathematics of calculus of variations [78, p. 201]. The two common approaches are Pontryagin's maximum principle (PMP) and dynamic programming (which leads to the Hamilton-Jacobi-Bellman equation) [58, pp. 102,156]. These approaches can be compared: PMP satisfies only the necessary condition for optimality while the HJB satisfies the sufficient condition [58, pp. 168-170]. Therefore, we will proceed by describing an approach aligned with PMP. This method relies on a derived quantity known as the Hamiltonian:

$$H(\boldsymbol{\xi}, \mathbf{u}, \mathbf{p}, p_0) = p_0 \mathcal{L}\left(\boldsymbol{\xi}, \mathbf{u}\right) + \langle \mathbf{p}, \mathbf{f_d}\left(\boldsymbol{\xi}, \mathbf{u}\right)\rangle \tag{2.17}$$

where $\mathbf{p}$ is the adjoint vector or costate, p_0 is the nonpositive scalar abnormal multiplier, and $\langle \mathbf{p}, \mathbf{f_d}\rangle$ is the inner product $\sum_{i=1}^{n} \mathbf{p}_i \mathbf{f_d}_i$ [58, p. 103]. The abnormal multiplier is zero only in degenerate cases, so assuming this is not the case, we can normalize the problem to $p_0 = -1$. An augmented Hamiltonian can be constructed to include path constraints [56, p. 125]:

$$\hat{H}(\boldsymbol{\xi}, \mathbf{u}, \mathbf{p}, p_0, \boldsymbol{\mu}) = H(\boldsymbol{\xi}, \mathbf{u}, \mathbf{p}, p_0) + \langle \boldsymbol{\mu}, \mathbf{C}(\boldsymbol{\xi}, \mathbf{u})\rangle \tag{2.18}$$

Using the first-order necessary condition, it can be shown that the following conditions are required at an optimum solution to an OCSD problem [58, 79]:

$$\hat{H}(\boldsymbol{\xi}^*, \mathbf{u}^*, \mathbf{p}^*, p_0^*, \boldsymbol{\mu}^*) \leq \hat{H}(\boldsymbol{\xi}^*, \mathbf{u}, \mathbf{p}^*, p_0^*, \boldsymbol{\mu}^*) \ \forall t \tag{2.19a}$$

$$\dot{\boldsymbol{\xi}}^* = \frac{\partial \hat{H}(\boldsymbol{\xi}^*, \mathbf{u}^*, \mathbf{p}^*, p_0^*, \boldsymbol{\mu}^*)}{\partial \mathbf{p}} \tag{2.19b}$$

$$\dot{\mathbf{p}}^* = -\frac{\partial \hat{H}(\boldsymbol{\xi}^*, \mathbf{u}^*, \mathbf{p}^*, p_0^*, \boldsymbol{\mu}^*)}{\partial \boldsymbol{\xi}} \tag{2.19c}$$

$$\langle \mathbf{p}^*, \mathbf{f_d}\left(\boldsymbol{\xi}^*, \mathbf{u}^*\right)\rangle = \mathbf{0}, \ p_0^* \leq 0, \ [p_0^*, \mathbf{p}^*] \neq \mathbf{0} \ \forall t \tag{2.19d}$$

$$\langle \boldsymbol{\mu}^*, \mathbf{C}(\boldsymbol{\xi}^*, \mathbf{u}^*)\rangle = \mathbf{0}, \ \boldsymbol{\mu}^* \geq \mathbf{0} \tag{2.19e}$$

$$\text{Appropriate boundary or transversality conditions} \tag{2.19f}$$

where Eqn. (2.19a) is the augmented Hamiltonian minimization condition, Eqn. (2.19b) is the state equation, Eqn. (2.19c) is the Euler-Lagrange equation, and Eqns. (2.19d) and (2.19e) are analogous to the Karush-Kuhn-Tucker conditions in constrained finite-dimensional optimization [55, p. 195]. In addition, there are typically a number of boundary or transversality conditions based on the particular problem. Often the state variables have initial conditions specified and the adjoint variables have final conditions [51, pp. 243-246]. Additional conditions can typically be applied regarding $\hat{H}(\cdot)$ such as it is constant or zero depending on the problem [58, p. 103].

Indirect approaches can lead to important insights into the structure of the solution, such as with the linear quadratic regulator (LQR) [78, p. 201]. However, it can be quite challenging to solve these equations analytically. Hamiltonian derivatives are required and finding analytic expressions necessitate "an intelligent user with at least some knowledge of optimal control theory" [56, p. 129]. Many problems deal with complicated black box functions or use table interpolation which do not have analytic forms for their derivatives [78, p. 162]. Finally, this approach is not flexible since for every new problem, the relevant derivatives need to be recalculated [56, p. 129]. Therefore, numerical methods are often employed.

Numeric indirect methods are termed optimize-then-discretize ($O \rightarrow D$) methods since the relevant optimality conditions are explicitly derived using Eqns. (2.19) and then are discretized through the state and Euler-Lagrange

equations into a boundary value problem (BVP) [51, pp. 243-246]. With path constraints, multiple BVPs will need to be linked for each arc that a path constraint is active since a new set of DAEs will need to be solved. However, the number of constrained subarcs and the sequence of constrained/unconstrained arcs are unknown a priori, so it is quite difficult or even impossible to construct the correct BVP. Another issue with numeric indirect methods is standard solution procedures are not robust. An initial guess for the costates must be given, but these are not physical quantities, so we have no good way of providing a reasonable estimate [56, p. 129]. Furthermore, even with a reasonable guess, the numerical solution of the adjoint equations in Eqn. (2.19c) can be very ill-conditioned. Since Eqns. (2.19b) and (2.19c) are coupled together, the numerical integration procedure can produce "wild" trajectories even with a reasonable guess, and these trajectories are challenging to perform iterations on [79, pp. 214-215]. One method used to remedy this numerical issue is to perform the integration over short time intervals, known as indirect multiple shooting, and adding the necessary additional variables and boundary constraints.

2.4.2 Direct Methods for OCSD

Direct methods of optimal control are known as discretize-then-optimize ($D \rightarrow O$) methods [51, pp. 243-246]. These methods do not use calculus of variations or directly state the optimality conditions. Instead, the control and/or state are parametrized using function approximations and the cost is approximated using numerical quadrature [78, p. 141]. This creates a discrete, finite-dimensional problem that then is optimized using large-scale NLP solvers [51, pp. 243-246].

This formulation requires an accurate level of parameterization of the control (and possibly the state) profiles. The mathematics are not as elegant as indirect methods (e.g., finite-difference methods may need to be used) which produces a solution that is challenging to use to gain insight into the structure of the problem. Also, no costate is produced from NLP solution so it is difficult to know if we are at the true optimal solution [78, p. 201]. There are two main classes of direct methods: sequential and simultaneous. Sequential methods only parametrize the control while simultaneous methods

parametrize both the state and control. Sequential methods will be discussed first.

Single shooting — This is the most basic sequential method and is also known as direct shooting [78, p. 181]. Given initial conditions and a set of control parameters, the DAE model is solved in an inner loop through conventional DAE solvers (forward simulation) such as a Runge-Kutta based method. The OCSD problem using a shooting method is expressed as:

$$\min_{\mathbf{u}(t),t_0,t_f} \quad \int_{t_0}^{t_f} \mathcal{L}\left(t, \boldsymbol{\xi}(t), \mathbf{u}(t)\right) dt + \mathcal{M}\left(t_0, \boldsymbol{\xi}(t_0), t_f, \boldsymbol{\xi}(t_f)\right) \tag{2.20a}$$

$$\text{subject to :}$$

$$\mathbf{C}\left(t, \boldsymbol{\xi}(t), \mathbf{u}(t)\right) \leq \mathbf{0} \tag{2.20b}$$

$$\boldsymbol{\phi}\left(t_0, \boldsymbol{\xi}(t_0), t_f, \boldsymbol{\xi}(t_f)\right) \leq \mathbf{0} \tag{2.20c}$$

$$\text{where :}$$

$$\dot{\boldsymbol{\xi}} - \mathbf{f_d}\left(t, \boldsymbol{\xi}(t), \mathbf{u}(t)\right) = \mathbf{0} \tag{2.20d}$$

where the use of a DAE solver is expressed with "where:" since it is no longer a constraint. This is a Multidisciplinary Feasible (MDF) formulation[1] since all the analysis tasks are nested inside a single optimization algorithm loop [37].

The parameters representing the control variables are then updated by the NLP solver in the outer loop. For example, if the control variables are represented as polynomials, the optimization is performed with respect to the polynomial coefficients. Due to the use of conventional DAE solvers, this approach has the advantage of easily finding feasible solutions to the state equations, but needs to a perform full simulation for each perturbation in the optimization algorithm. Repeated numerical integration of the DAE model, however, does not guarantee convergence with open-loop unstable systems [51, pp. 243-246] and the resulting solution can be very sensitive to the choice of control [78, p. 181]. This strategy is the easiest to construct out of all the direct methods, since reliable and efficient codes for DAE and NLP solvers are naturally linked [51, pp. 243-246].

Multiple shooting — A more robust version of the single shooting, multiple shooting better handles unstable DAEs (similar motivation for using indirect

[1] One of the basic forms of MDO in Ref. [37]

multiple shooting to mitigate unstable costate dynamics). This approach partitions the time horizon into smaller time segments and separate DAE models are constructed on each element [51, pp. 243-246]. This can now be viewed as a multiphase problem that requires continuity constraints, i.e., continuous states at each time segment (see Eqn. (2.9)). This introduces additional variables at the beginning and end of each time segment.

A number of of the numerical issues with shooting methods were discussed with a numeric case study [80]. Sequential approaches typically produce low-accuracy solutions and are computationally inefficient, i.e., compared to the soon to be discussed local and global collocation methods. Even with a large number of control variables, the solution may not converge to the optimal solution with shooting but may with the same number of control variables using local or global collocation. Many of these issues are due to the inability to efficiently handle path and boundary constraints. Since the states are calculated through a forward simulation, we have to numerically approximate how local control perturbations will affect the global state trajectory (see Figs. 2.1 and 2.2). This leads to simultaneous approaches that forgo the nested analysis of sequential methods for a large set of constraints.

Simultaneous approaches, also as known as direct transcription, parametrize both the state and control trajectories. These approaches no longer require any nested calculations with DAE solvers but instead add a large number of equality constraints that ensure feasible dynamics. These constraints will be analogous to the dynamic constraints in Eqn. (2.2b). These additional constraints are termed defect constraints and take the general form:

$$\boldsymbol{\zeta}\left(\mathbf{t}, \boldsymbol{\Xi}, \mathbf{U}\right) = \mathbf{0} \tag{2.21}$$

where $\mathbf{t}$, $\boldsymbol{\Xi}$, and $\mathbf{U}$ are the discretized time, state, and control. However, we can only guarantee a feasible solution if the optimization algorithm terminates properly. There are a number of ways to form these constraints, which will be explored in Chapter 3.

DT is a special case of the All-at-Once (AAO) MDO formulation[2] due to ability to perform simultaneous analysis and design [37, 81]. Path constraints

[2]One of the basic forms of MDO in Ref. [37]

are now no more complicated than dynamic constraints, mitigating the computational issues that can be experienced with shooting methods [50, 78, p. 200]. This new large NLP formulation has a specific structure and sparsity pattern that can be exploited in NLP solvers to reduce total computational effort [51, pp. 243-246]. Simultaneous approaches have been shown to have good convergence properties and handle unstable DAEs [50, 82–84]. Finally, these approaches have specific advantages for singular control problems and high-index path constraints [50]. This collection of desirable properties make DT a strong candidate for use in solving the OPSD problem. There are two basic classifications of DT: local and global.

Local collocation — In a local method, low degree polynomial approximations are used and the problem is divided into a large number of finite elements (located at the values of the discretized time vector, $\mathbf{t}$). Typically, polynomials with degrees less than four are used in local collocation without varying the degree from element to element, hence another common term being time-marching methods. This is typically accomplished with Runge-Kutta methods such as Euler's, trapezoidal, and Hermite-Simpson [82]. The details of local collocation will be discussed in Section 3.2.1.

Global collocation — Also known as pseudospectral methods, the state is approximated using an appropriate set of global trial (basis) functions (e.g., Lagrange or Chebyshev polynomials) and the dynamics are orthogonally collocated (i.e., the collocation points are the roots of an orthogonal polynomial) [82]. These are higher order methods that can have higher accuracy with a smaller degree of discretization [78, p. 222]. The details of global collocation will be discussed in Section 3.2.2.

In Fig. 2.3, the multitude of methods available to solve an OCSD are categorized. Figure 2.4 illustrates the location of potential defect constraints for each of the direct methods, highlighting the main features of each approach (although the illustrations may vary slightly for the exact method used). In the single shooting case, the dynamics are always feasible. There is no need for any defect constraints since the state value used in the optimization algorithm is always the same as the predicted value. In multiple shooting, a defect constraint will be required between phases since the initial value used in the simulation from t_4 to t_8 needs to be equal to the final value of the simulation

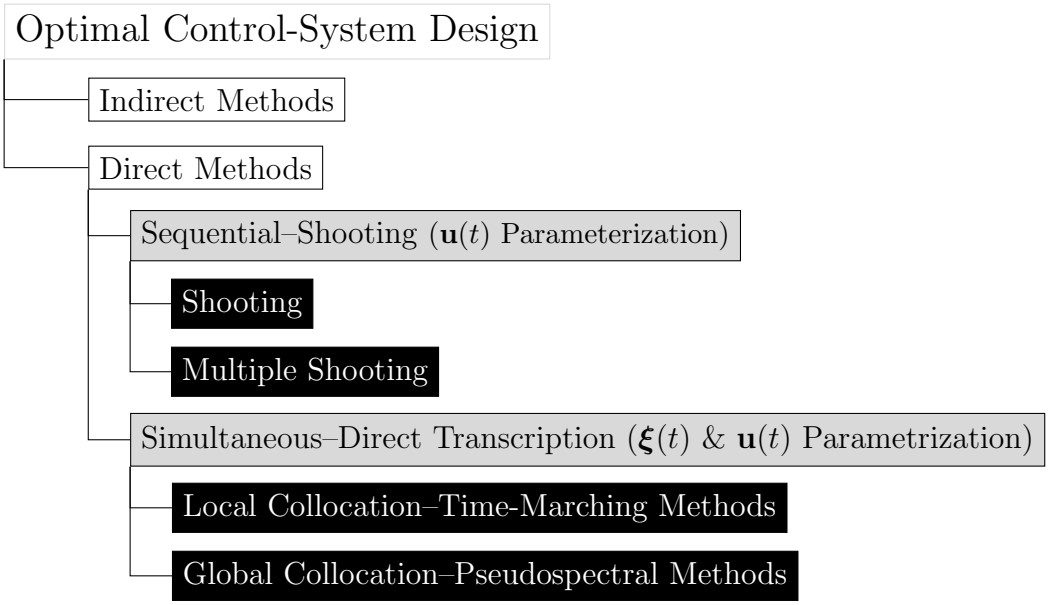

Figure 2.3 Methods of solving an optimal control-system design problem.

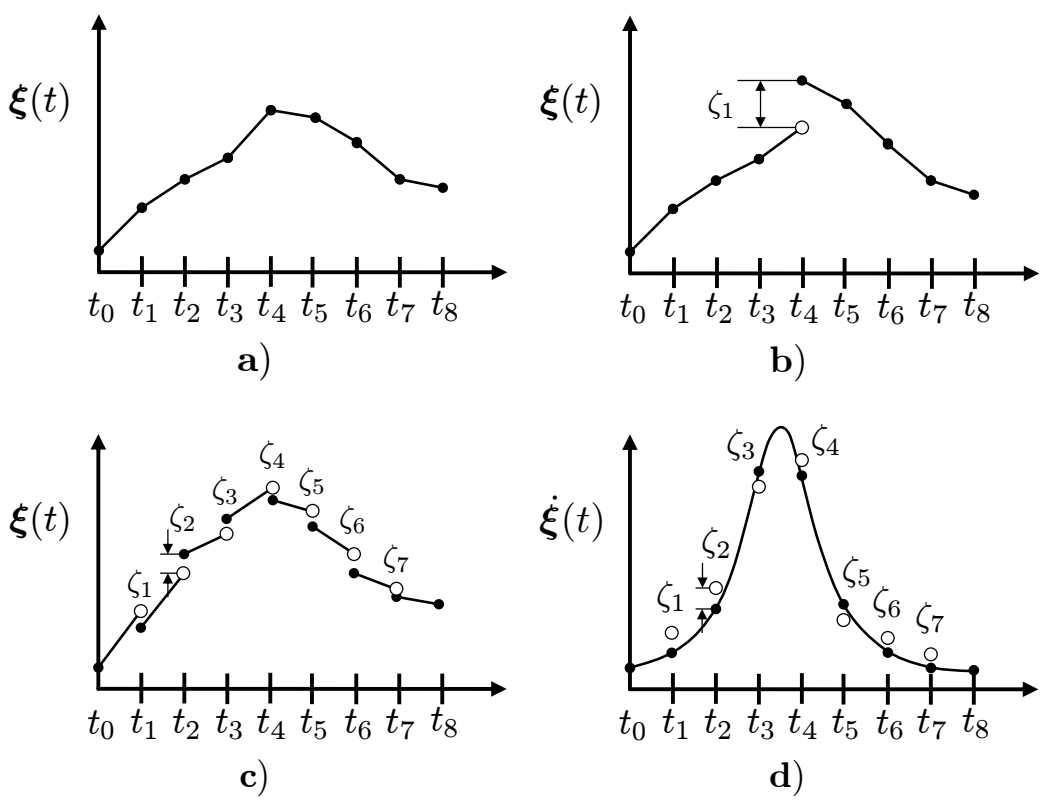

Figure 2.4 Illustration of time discretization and potential defect constraints where • is the current state value used in the optimization algorithm and ∘ is the predicted state value for: **a**) single shooting, **b**) multiple shooting, **c**) DT local collocation, **d**) DT global collocation.

from t_1 to t_4. Multiple shooting will require a smaller number of defect constraints and have a higher level of feasibility during the optimization routine when compared to DT. On the other hand, DT will require a larger number of defect constraints, namely at every interior value of $\mathbf{t}$ (and possibly the endpoints). Local collocation will use the current state and control values to predict the next state value. Global collocation will have defect constraints at the same locations as local collocation and will have defect constraints on the states if they are written in integral form [78, p. 234]. In all cases, the current state value used in the optimization algorithm ($\bullet$) and the predicted value ($\circ$) should coincide. This implies the discretized state trajectory is feasible.

2.4.3 Combining Methods for OCSD and OPSD

Key to the solving the ODSD problem is an integrated approach that solves the OCSD and OPSD together. This can be accomplished with co-design. There are two main co-design approaches: nested and simultaneous. Another co-design approach uses the Augmented Lagrangian Coordination to decompose the ODSD problem and utilizes coupling variables to link the OCSD and OPSD problems [46]. These approaches have been shown to produce better results than sequential system design [48]. We will now review the two main approaches and discussed their applicability to challenging ODSD problems.

Sequential system design — This is the conventional approach to solve an ODSD problem [41, 85–89]. Here, there are at least two separate optimization problems: one to solve the OPSD problem and one for the OCSD problem (illustrated in Fig. 2.5a). Changes to the plant variables can only be made during the optimization of the OPSD problem then must be held fixed when trying to solve the OCSD problem (see Fig. 1.4). As stated previously, iterative sequential design can be performed if dynamics can be directly accounted for in both domains (dashed line in Fig. 2.5a). This approach does not account for the coupling between the domains but does often produce feasible system designs. A taxonomy of sequential design formulations was presented in Ref. [40]. The OCSD problem can be solved with the previously discussed methods while the OPSD problem may utilize simplified dynamics or direct

Table 2.1 Proposed effectiveness of problem formulations for ODSD.

		ODSD		
		Sequential	Nested	Simultaneous
OCSD	Indirect	✗	✗	✗
	Shooting	✗	—	—
	DT	✗	✓	✓✓

methods to properly account for the dynamics (i.e., shooting approaches using forward simulation [40] or direct transcription for simultaneous dynamics and plant design [68, 69]).

Nested co-design — Also known as bi-level co-design, this approach requires two optimization routines: an outer-loop that solves the OPSD problem and an inner-loop that finds the optimal control for each candidate plant design considered by the outer-loop (illustrated in Fig. 2.5b) [90]. Nested co-design is a special case of the MDF formulation [42, 91] but the classification of the OCSD subproblem depends on the specific method used (e.g., nested co-design with DT contains both MDF and AAO formulations). The main advantage of nested co-design is the ability to leverage existing OCSD methods to solve the inner-loop problem efficiently without the complication of managing plant-design variables [40]. A number of studies have utilized nested co-design with many resulting in the optimal system-level design [29, 44, 47, 52].

Simultaneous co-design — Both plant and control design decisions are made concurrently in simultaneous co-design. Therefore, this formulation will account for all dynamic system interactions and plant-control design coupling to lead to the system-level optimal value [90]. The key to using this approach is having dynamic models available that can directly handle changes in the plant design, and then be used with a sequential or simultaneous method for handling the dynamics. Simultaneous co-design has been shown to produce excellent results in demanding dynamic systems [47–49, 52, 67].

Table 2.1 lists all of the OCSD and ODSD methods, and a proposed effectiveness is presented for each possible combination (✓: desirable and ✗: undesirable). Indirect methods for OCSD are denoted "undesirable" since their

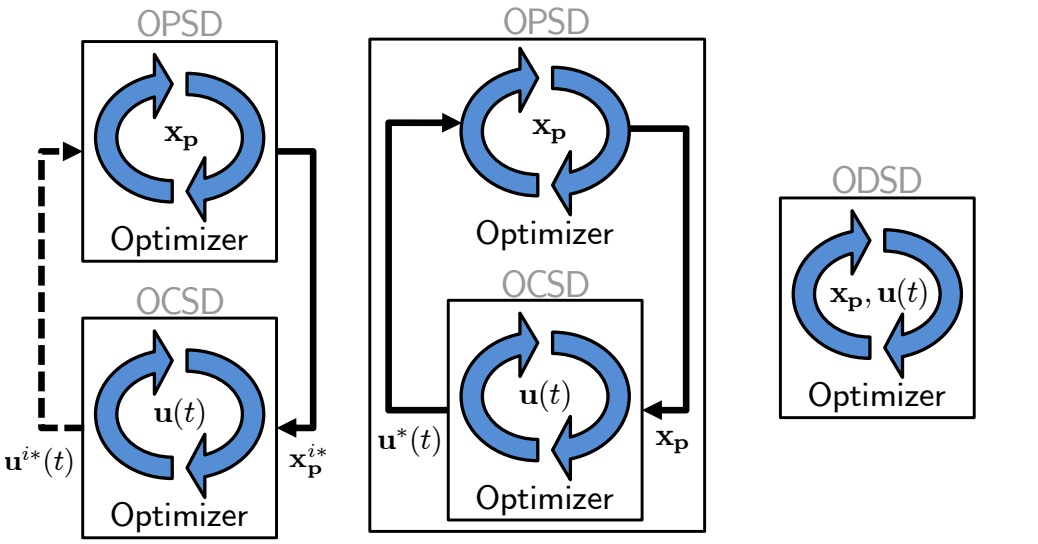

a) Sequential design **b**) Nested co-design **c**) Simultaneous co-design

Figure 2.5 Methods for solving a optimal dynamic system design problem.

formulations contain multiple BVPs and numerically sensitive costate calculations. Sequential system design is also always undesirable since it does not account for the coupling between the plant and control designs. Shooting methods are potentially tractable if the problem is well-behaved and contains a limited number of path and boundary constraints. However, the models need to be in the same form as Eqn. (2.10). Co-design methods utilizing DT are the most promising methods. The ability to naturally include path and boundary constraints is essential in an ODSD problem [47]. A simultaneous co-design formulation combined with DT performs the analysis and design of both the control and plant concurrently.

Now that a general discussion of both the problem formulation and solution approaches for ODSD has been presented, we can focus on the details of a promising ingredient for solving ODSD: direct transcription.

Chapter 3

Direct Transcription

This chapter will discuss the class of DT methods introduced in Section 2.4.2. DT has become quite popular and has been used to solve many challenging engineering problems. The value of these methods to solve complex, real-world, industrial-strength problems was demonstrated in 2007 when DT was used to calculate a 180-degree maneuver of the International Space Station without using any propellant, saving NASA millions [92]. A number of commercial [63, 93–98] and open-source [99, 100] DT software implementations are available. First, some preliminaries will be given. Then two different approaches for approximating the ordinary differential equations will be presented, followed by a discussion on the problem structure and some additional comments.

3.1 Direct Transcription Preliminaries

We need to convert the continuous ODSD problem in Prob. (2.15) into a discrete problem with a finite number of optimization variables. This is known as transcription [56, p. 132]. We start by dividing the entire time horizon into multiple segments such that:

$$t_0 < t_1 < \cdots < t_{n_t-1} < t_{n_t} \tag{3.1}$$

where $n_t + 1$ is the number of discrete time values, $t_{n_t} = t_f$, $h_k = t_k - t_{k-1}$ is the kth time step, and I_k is the segment $[t_{k-1}, t_k]$. The discretized time vector will be:

$$\mathbf{t} = \begin{bmatrix} t_0 & t_1 & \cdots & t_{n_t} \end{bmatrix}^T_{(n_t+1)\times 1} \tag{3.2}$$

where the components of $\mathbf{t}$ are also called node, grid, or mesh points. The

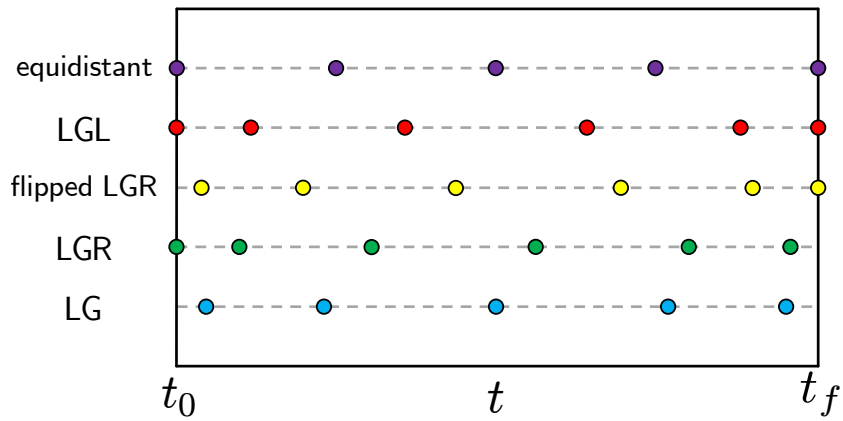

Figure 3.1 Illustration of the location of equidistant and Legendre grid points.

simplest choice for $\mathbf{t}$ is a uniform grid, i.e., each grid point is equidistant from one another:

$$t_k = t_0 + k\frac{t_f - t_0}{n_t} \qquad \{k \mid k \in \mathbb{N}_0, k \leq n_t\} \tag{3.3}$$

Other discretization schemes are based on orthogonal polynomials and their roots [101, pp. 229-230]. Legendre-Gauss-Lobatto (LGL) points, Legendre-Gauss (LG) points, and Legendre-Gauss-Radau (LGR) points are all common sets used in DT [83, p. 41]. Locations of these points are obtained from the roots of a Legendre polynomial, $P_{n_t+1}(\tau)$, or a linear combination of a $P_{n_t+1}(\tau)$ and its derivatives. These schemes may contain neither, one, or both endpoints and tend to be distributed more densely towards the edges of the interval. This is to avoid Runge's phenomenon (divergent interpolation) which can occur while using equidistant mesh points with a polynomial approximation [83, p. 45]. An illustration of these discretization schemes over the time horizon can be seen in Fig. 3.1. Additional points can be added for an arbitrary value of $n_t + 1$. Please refer to Ref. [83, pp. 39-45] for a more detailed discussion of the family of Legendre-Gauss points.

Concurrently with increasing the number of collocation points in the discretization scheme, the time horizon can be broken up into small segments to better approximate the continuous problem. Additional linkage constraints need to be applied to make the segments continuous (see Eqns. (2.8) and (2.9)). Each segment will have its own collocation points designed to best approximate the local behavior of the dynamics. This approach is especially useful

for nonsmooth problems [102].

In addition to discretizing the time horizon, the states and controls need to be moved from the continuous function to a discrete approximation. Most of these will be included as optimization variables. When the ODSD problem has been solved, the discrete states and controls will be defined at all time points:

$$\boldsymbol{\Xi} = \begin{bmatrix} \boldsymbol{\xi}[t_0] \\ \boldsymbol{\xi}[t_1] \\ \vdots \\ \boldsymbol{\xi}[t_{n_t}] \end{bmatrix} = \begin{bmatrix} \xi_1[t_0] & \xi_2[t_0] & \cdots & \xi_{n_\xi}[t_0] \\ \xi_1[t_1] & \xi_2[t_1] & \cdots & \xi_{n_\xi}[t_1] \\ \vdots & \vdots & \ddots & \vdots \\ \xi_1[t_{n_t}] & \xi_2[t_{n_t}] & \cdots & \xi_{n_\xi}[t_{n_t}] \end{bmatrix}_{(n_t+1)\times n_\xi} \tag{3.4a}$$

$$\mathbf{U} = \begin{bmatrix} \mathbf{u}[t_0] \\ \mathbf{u}[t_1] \\ \vdots \\ \mathbf{u}[t_{n_t}] \end{bmatrix} = \begin{bmatrix} u_1[t_0] & u_2[t_0] & \cdots & u_{n_u}[t_0] \\ u_1[t_1] & u_2[t_1] & \cdots & u_{n_u}[t_1] \\ \vdots & \vdots & \ddots & \vdots \\ u_1[t_{n_t}] & u_2[t_{n_t}] & \cdots & u_{n_u}[t_{n_t}] \end{bmatrix}_{(n_t+1)\times n_u} \tag{3.4b}$$

where n_ξ is the number of state variables, n_u is the number of control variables, and the notation $[\cdot]$ indicates this is using the discretized version of the preceding variable. It is important to note that not all the discretization schemes in Fig. 3.1 include both endpoints. Therefore, the numerical method used to obtain the values in Eqn. (3.4) may not be directly including these points as optimization variables. The defect constraints will use $\boldsymbol{\Xi}$ and $\mathbf{U}$ and are organized as:

$$\boldsymbol{\zeta} = \begin{bmatrix} \boldsymbol{\zeta}[t_1] \\ \vdots \\ \boldsymbol{\zeta}[t_{n_t}] \end{bmatrix} = \begin{bmatrix} \zeta_1[t_1] & \zeta_2[t_1] & \cdots & \zeta_{n_\xi}[t_1] \\ \vdots & \vdots & \ddots & \vdots \\ \zeta_1[t_{n_t}] & \zeta_2[t_{n_t}] & \cdots & \zeta_{n_\xi}[t_{n_t}] \end{bmatrix}_{n_t\times n_\xi} \tag{3.5}$$

We also need to discretize the Lagrange term:

$$\int_{t_0}^{t_f} \mathcal{L}\left(t, \boldsymbol{\xi}(t), \mathbf{u}(t), \mathbf{x_p}\right) dt \approx \psi\left(\mathbf{t}, \boldsymbol{\Xi}, \mathbf{U}, \mathbf{x_p}\right) \tag{3.6}$$

Path and boundary constraints are algebraic expressions that need to be

evaluated as well:

$$\mathbf{C} = \begin{bmatrix} \mathbf{C}[t_0] \\ \mathbf{C}[t_1] \\ \vdots \\ \mathbf{C}[t_{n_t}] \end{bmatrix} = \begin{bmatrix} C_1[t_0] & C_2[t_0] & \cdots & C_{n_C}[t_0] \\ C_1[t_1] & C_2[t_1] & \cdots & C_{n_C}[t_1] \\ \vdots & \vdots & \ddots & \vdots \\ C_1[t_{n_t}] & C_2[t_{n_t}] & \cdots & C_{n_C}[t_{n_t}] \end{bmatrix}_{(n_t+1)\times n_C} \tag{3.7a}$$

$$\boldsymbol{\phi} = \begin{bmatrix} \phi_1 & \phi_2 & \cdots & \phi_{n_\phi} \end{bmatrix}_{1\times n_\phi} \tag{3.7b}$$

where n_C is the number of path constraints and n_ϕ is the number of boundary constraints. We note that path constraints are evaluated at each point in $\mathbf{t}$, while boundary constraints are evaluated only once. The discretized version of Prob. (2.15) utilizing DT is:

$$\min_{\mathbf{x_p},\boldsymbol{\Xi},\mathbf{U},t_0,t_f} \quad \psi\left(\mathbf{t},\boldsymbol{\Xi},\mathbf{U},\mathbf{x_p}\right) + \mathcal{M}(\boldsymbol{\xi}[t_0],t_0,\boldsymbol{\xi}[t_f],t_f,\mathbf{x_p}) \tag{3.8a}$$

subject to:

$$\boldsymbol{\zeta}\left(\mathbf{t},\boldsymbol{\Xi},\mathbf{U},\mathbf{x_p}\right) = \mathbf{0} \tag{3.8b}$$

$$\mathbf{C}\left(\mathbf{t},\boldsymbol{\Xi},\mathbf{U},\mathbf{x_p}\right) \leq \mathbf{0} \tag{3.8c}$$

$$\boldsymbol{\phi}(\boldsymbol{\xi}[t_0],t_0,\boldsymbol{\xi}[t_f],t_f,\mathbf{x_p}) \leq \mathbf{0} \tag{3.8d}$$

where the discretized states are included as optimization variables and defect constraints replace the dynamic constraints.

For clarity, the discretized derivative function and Lagrange term may be denoted as:

$$\mathbf{f_d}[t] \equiv \mathbf{f_d}(t,\boldsymbol{\xi}[t],\mathbf{u}[t],\mathbf{x_p}) \tag{3.9a}$$

$$\mathcal{L}[t] \equiv \mathcal{L}(t,\boldsymbol{\xi}[t],\mathbf{u}[t],\mathbf{x_p}) \tag{3.9b}$$

3.2 Numerical Approximation of Differential Equations

Consider the time interval I_k over which the solution of $\dot{\boldsymbol{\xi}} = \mathbf{f_d}(\cdot)$ is desired. Integrating this differential equation over I_k results in the following solution:

$$\boldsymbol{\xi}[t_k] = \boldsymbol{\xi}[t_{k-1}] + \int_{t_{k-1}}^{t_k} \mathbf{f_d}\left(\tau, \boldsymbol{\xi}(\tau), \mathbf{u}(\tau), \mathbf{x_p}\right) d\tau \tag{3.10}$$

In single shooting, we use a DAE solver to sequentially solve Eqn. (3.10) (i.e., given $\boldsymbol{\xi}[t_{k-1}]$ solve for $\boldsymbol{\xi}[t_k]$). Thus the final result is a feasible solution to the system of differential equations. The calculation of defect constraints can use the same underlying methods but instead of a solving the states in a sequential manner through the time horizon, the entire collection of mesh points will be solved in an iterative manner, searching for both a feasible and optimal collection of states. The underlying methods used here are termed collocation methods which provide a numerical solution of ordinary differential equations. We need to select a finite-dimensional space of candidate solutions (typically polynomials up to a certain degree). Then we will need to find values for the optimization variables that satisfy the given equations at the collocation points (namely the time points in Eqn. (3.2)). The next two sections will look at local or global collocation implementations of DT.

3.2.1 Local Collocation: Runge-Kutta Methods

In a local method, low degree polynomial approximations are used and the problem is divided into a large number of finite elements (located at the values of the discretized time vector, $\mathbf{t}$). Consider the integration over I_k in Eqn. (3.10). We can divide this integration step into S subintervals:

$$\tau_s = t_{k-1} + h_k \rho_s \qquad \text{with: } 0 \leq \rho_1 \leq \cdots \leq \rho_S \leq 1 \tag{3.11}$$

We now apply a numerical integration formula (or quadrature) within an-

other quadrature formula to arrive at a S-stage Runge-Kutta scheme:

$$\boldsymbol{\xi}[t_k] \approx \boldsymbol{\xi}[t_{k-1}] + h_k \sum_{s=1}^{S} \gamma_s \mathbf{f}_{\mathbf{d}ks} \tag{3.12a}$$

$$\mathbf{f}_{\mathbf{d}ks} \equiv \mathbf{f}_{\mathbf{d}ks}\left(\tau_s, \bar{\boldsymbol{\xi}}_{ks}, \bar{\mathbf{u}}_{ks}, \mathbf{x}_{\mathbf{p}}\right) \tag{3.12b}$$

$$\bar{\boldsymbol{\xi}}_{ks} = \boldsymbol{\xi}[t_{k-1}] + h_k \sum_{\ell=1}^{S} \nu_{s\ell} \mathbf{f}_{\mathbf{d}k\ell} \tag{3.12c}$$

where the parameters $\{\rho_s, \gamma_s, \nu_{s\ell}\}$ are known constants and can be represented in the Butcher array [56, p. 98] and $\bar{\mathbf{u}}_{ks}$ is the estimated control value at stage s. We will assume that $\bar{\mathbf{u}}_{ks}$ is estimated as a piecewise linear function:

$$\bar{\mathbf{u}}_{ks} = u[t_{k-1}] + \frac{u[t_k] - u[t_{k-1}]}{h_k} h_k \rho_s \tag{3.13}$$

Since Runge-Kutta methods are single step (i.e., they have no "memory" and only use the local time points), adjustment of the time step h_k is easy to implement and independent of previous profile information. Directly controlling the time step allows accurate location of nonsmooth events in the state profiles. In addition, accurate solutions require that the state profile be smooth only within a step and continuous across steps [51, p. 256]. There are both explicit and implicit Runge-Kutta methods (implicit methods have $\boldsymbol{\xi}[t_k]$ show up on the right side of Eqn. (3.12a)). Explicit Runge-Kutta methods are generally unsuitable for stiff equations since their region of absolute stability is small. We will now discuss four common Runge-Kutta schemes and how they are included in the discrete ODSD problem formulation.

Euler forward — An explicit first-order scheme is the Euler forward method:

$$\boldsymbol{\xi}[t_k] \approx \boldsymbol{\xi}[t_{k-1}] + h_k \mathbf{f}_{\mathbf{d}}[t_{k-1}] \tag{3.14}$$

This equation needs to hold true for all mesh points for feasible dynamics. Rearranging this constraint into negative null form gives the defect constraints

for the Euler forward method:

$$\boldsymbol{\zeta}[t_k] = \mathbf{0} \qquad \forall k \in \{k \mid k \in \mathbb{N}, k \leq n_t\} \tag{3.15a}$$

where:

$$\boldsymbol{\zeta}[t_k] = \boldsymbol{\xi}[t_k] - \boldsymbol{\xi}[t_{k-1}] - h_k \mathbf{f_d}[t_{k-1}] \tag{3.15b}$$

Trapezoidal — The trapezoidal rule is an implicit second-order method:

$$\boldsymbol{\zeta}[t_k] = \boldsymbol{\xi}[t_k] - \boldsymbol{\xi}[t_{k-1}] - \frac{h_k}{2}\left(\mathbf{f_d}[t_k] + \mathbf{f_d}[t_{k-1}]\right) \tag{3.16}$$

which needs to satisfy the same condition as Eqn. (3.15a).

Hermite-Simpson — The Hermite-Simpson is an implicit third-order method:

$$\boldsymbol{\zeta}[t_k] = \boldsymbol{\xi}[t_k] - \boldsymbol{\xi}[t_{k-1}] - \frac{h_k}{6}\left(\mathbf{k_1} + 4\mathbf{k}_2 + \mathbf{k}_3\right) \tag{3.17a}$$

$$\mathbf{k}_1 = \mathbf{f_d}[t_{k-1}] \tag{3.17b}$$

$$\mathbf{k}_2 = \mathbf{f_d}\left(\frac{t_{k-1} + t_k}{2}, \bar{\boldsymbol{\xi}}_k, \bar{\mathbf{u}}_k, \mathbf{x_p}\right) \tag{3.17c}$$

$$\mathbf{k}_3 = \mathbf{f_d}[t_k] \tag{3.17d}$$

$$\bar{\boldsymbol{\xi}}_k = \frac{1}{2}\left(\boldsymbol{\xi}[t_{k-1}] + \boldsymbol{\xi}[t_k]\right) + \frac{h_k}{8}\left(\mathbf{f_d}[t_{k-1}] - \mathbf{f_d}[t_k]\right) \tag{3.17e}$$

$$\bar{\mathbf{u}}_k = \frac{1}{2}\left(\mathbf{u}[t_{k-1}] + \mathbf{u}[t_k]\right) \tag{3.17f}$$

which once again needs to satisfy the same condition as Eqn. (3.15a).

Classical fourth-order Runge-Kutta — This is another popular explicit scheme given by:

$$\boldsymbol{\zeta}[t_k] = \boldsymbol{\xi}[t_k] - \boldsymbol{\xi}[t_{k-1}] - \frac{h_k}{6}\left(\mathbf{k}_1 + 2\mathbf{k}_2 + 2\mathbf{k}_3 + \mathbf{k}_4\right) \tag{3.18a}$$

$$\mathbf{k}_1 = \mathbf{f_d}[t_{k-1}] \tag{3.18b}$$

$$\mathbf{k}_2 = \mathbf{f_d}\left(\frac{t_{k-1} + t_k}{2}, \boldsymbol{\xi}[t_{k-1}] + \frac{h_k \mathbf{k}_1}{2}, \bar{\mathbf{u}}_k, \mathbf{x_p}\right) \tag{3.18c}$$

$$\mathbf{k}_3 = \mathbf{f_d}\left(\frac{t_{k-1} + t_k}{2}, \boldsymbol{\xi}[t_{k-1}] + \frac{h_k \mathbf{k}_2}{2}, \bar{\mathbf{u}}_k, \mathbf{x_p}\right) \tag{3.18d}$$

$$\mathbf{k}_4 = \mathbf{f_d}\left(t_k, \boldsymbol{\xi}[t_{k-1}] + h_k \mathbf{k}_3, \mathbf{u}[t_k], \mathbf{x_p}\right) \tag{3.18e}$$

$$\bar{\mathbf{u}}_k = \frac{1}{2}\left(\mathbf{u}[t_{k-1}] + \mathbf{u}[t_k]\right) \tag{3.18f}$$

which once again needs to satisfy the same condition as Eqn. (3.15a).

Recall the conversion from $\mathcal{L} \to \mathcal{M}$ in Eqn. (2.4) where we appended an additional state, ξ_0. If we calculate the final value of ξ_0, we will have the running cost for the problem. Any of the Runge-Kutta schemes can be used to find this final value. Since the Euler forward and trapezoidal rules only depend on the collocated points (i.e., all values of ρ_s are integers), compact expressions can be shown for the approximation of $\mathcal{L}$.

Quadrature using Euler forward — The simplest calculation requires only $\mathcal{L}$ at the initial time:

$$\int_{t_0}^{t_f} \mathcal{L}\left(t, \boldsymbol{\xi}(t), \mathbf{u}(t), \mathbf{x_p}\right) dt \approx \left(t_f - t_0\right) \mathcal{L}\left[t_0\right] \tag{3.19}$$

A composite method uses a set of points to better approximate the definite integral [101, p. 255]. Composite Euler forward on a non-uniform grid is:

$$\int_{t_0}^{t_f} \mathcal{L}\left(t, \boldsymbol{\xi}(t), \mathbf{u}(t), \mathbf{x_p}\right) dt \approx \sum_{k=0}^{n_t-1} h_k \mathcal{L}\left[t_k\right] \tag{3.20}$$

where composite Euler forward on a uniform grid is given by:

$$\int_{t_0}^{t_f} \mathcal{L}\left(t, \boldsymbol{\xi}(t), \mathbf{u}(t), \mathbf{x_p}\right) dt \approx \frac{t_f - t_0}{n_t} \sum_{k=0}^{n_t-1} \mathcal{L}\left[t_k\right] \tag{3.21}$$

Quadrature using trapezoidal rule — The simplest calculation using trapezoidal rule requires the values of $\mathcal{L}$ at both endpoints [101, p. 247]:

$$\int_{t_0}^{t_f} \mathcal{L}\left(t, \boldsymbol{\xi}(t), \mathbf{u}(t), \mathbf{x_p}\right) dt \approx \frac{t_f - t_0}{2} \left(\mathcal{L}\left[t_0\right] + \mathcal{L}\left[t_f\right]\right) \tag{3.22}$$

The composite trapezoidal rule on a non-uniform grid is [101, p. 255]:

$$\int_{t_0}^{t_f} \mathcal{L}\left(t, \boldsymbol{\xi}(t), \mathbf{u}(t), \mathbf{x_p}\right) dt \approx \frac{1}{2} \sum_{k=1}^{n_t} h_k \left(\mathcal{L}\left[t_k\right] + \mathcal{L}\left[t_{k-1}\right]\right) \tag{3.23}$$

Finally, the composite trapezoidal rule on a uniform grid is given by:

$$\int_{t_0}^{t_f} \mathcal{L}\left(t, \boldsymbol{\xi}(t), \mathbf{u}(t), \mathbf{x_p}\right) dt \approx \frac{t_f - t_0}{n_t} \left(\frac{\mathcal{L}\left[t_0\right]}{2} + \sum_{k=1}^{n_t-1} \mathcal{L}\left[t_k\right] + \frac{\mathcal{L}\left[t_f\right]}{2} \right) \tag{3.24}$$

Note the similarities between the composite Euler forward and the trapezoidal rule. For large values of n_t, these approximations will contain almost the same terms, whereas the trapezoidal rule will only include the additional value $\mathcal{L}[t_f]$. These simple expressions can directly be used in the objective of Prob. (3.8) rather than appending an additional state.

3.2.2 Global Collocation: Pseudospectral Methods

In pseudospectral methods, the state is approximated using an appropriate set of global trial (basis) functions and the dynamics are orthogonally collocated (i.e., the collocation points are the roots of an orthogonal polynomial) [82]. These are higher-order methods that can have higher accuracy with a smaller degree of discretization [78, p. 222]. Instead of integrating $\mathbf{f_d}(\cdot)$ over a small interval I_k, we can use a Lagrange interpolating polynomial to approximate $\boldsymbol{\xi}$ over the entire time horizon. We will proceed assuming flipped LGR points although modifications can readily be made to use other discretization schemes. Given a set of $n_t + 1$ support points of the continuous function $\boldsymbol{\xi}(t)$, there exists a unique polynomial representation of degree n_t such that:

$$\hat{\boldsymbol{\xi}}(t_k) = \boldsymbol{\xi}(t_k) \qquad \forall k \in \{k \mid k \in \mathbb{N}_0, k \leq n_t\} \tag{3.25}$$

The unique polynomial approximation of the continuous function is given by the Lagrange polynomial approximation formula:

$$\boldsymbol{\xi}(t) \approx \hat{\boldsymbol{\xi}}(t) = \sum_{p=0}^{n_t} \boldsymbol{\xi}[t_p] L_p(t) \tag{3.26}$$

where the Lagrange polynomials defined as [101, p. 224]:

$$L_p(t) = \prod_{\substack{m=0 \\ m \neq p}}^{n_t} \frac{t - t_m}{t_p - t_m} \tag{3.27}$$

These polynomials satisfy the so-called isolation property:

$$L_p(t_m) = \begin{cases} 1 & \text{if } p = m \\ 0 & \text{if } p \neq m \end{cases} \tag{3.28}$$

This is an advantageous property since the interpolated value that the support points are equivalent to the actual function value. Since it is not a linear combination of all the support points, the NLP formulation can utilize sparse matrices, particularly for the Jacobian matrix of the constraints [83, p. 38].

The derivative of the Lagrange interpolating polynomial in Eqn. (3.26) is given by:

$$\dot{\boldsymbol{\xi}}(t) \approx \hat{\dot{\boldsymbol{\xi}}}(t) = \sum_{p=1}^{n_t} \boldsymbol{\xi}[t_p] \dot{L}_p(t) \tag{3.29}$$

and we recall that:

$$\dot{\boldsymbol{\xi}}(t) = \mathbf{f_d}(t, \boldsymbol{\xi}, \mathbf{u}, \mathbf{x_p}) \approx \hat{\dot{\boldsymbol{\xi}}}(t) \tag{3.30}$$

Therefore at the support points:

$$\mathbf{f_d}[t_k] = \sum_{p=1}^{n_t} \boldsymbol{\xi}[t_p] \dot{L}_p[t_k] = \sum_{p=1}^{n_t} D_{kp} \boldsymbol{\xi}[t_p] \tag{3.31}$$

where $D_{kp} = \dot{L}_p[t_k]$ is termed the differentiation matrix. We now have arrived at the following set of defect constraints:

$$\boldsymbol{\zeta}[t_k] = \mathbf{0} \qquad \forall k \in \{k \mid k \in \mathbb{N}, k \leq n_t\} \tag{3.32a}$$

where:

$$\boldsymbol{\zeta}[t_k] = \mathbf{f_d}[t_k] - \sum_{p=1}^{n_t} D_{kp} \boldsymbol{\xi}[t_p] \tag{3.32b}$$

The flipped LGR collocation scheme does not include the initial time point but it is either a free optimization variable or known and an appropriate constraint is introduced [78, p. 231].

The Lagrange term is approximated with Gaussian quadrature:

$$\int_{t_0}^{t_f} \mathcal{L}\left(t, \boldsymbol{\xi}(t), \mathbf{u}(t), \mathbf{x_p}\right) dt \approx \sum_{k=0}^{n_t} w_k \mathcal{L}[t_k] \tag{3.33}$$

where w_k are the quadrature weights that are dependent on the discretization scheme [101, pp. 251-253].

Flipped LGR is currently the favored discretization scheme due to a number of properties: 1) the state, control, and costate converge exponentially, 2) utilizes implicit Gaussian quadrature schemes, 3) no redundancy in control at mesh points, 4) is most natural to implement [78].

3.3 Additional Comments

3.3.1 Mesh Refinement

After Prob. (3.8) is solved, we typically need to assess the accuracy of the finite-dimensional approximation. The first step is to construct a continuous solution using only the results of Prob. (3.8). Pseudospectral methods already have a continuous approximation in Eqn. (3.26). Time-marching methods can use Lagrange interpolating polynomials or any other interpolation method [101, p. 219]. This continuous approximation will be used instead of the exact solution because it is not generally available.

The solution error for a particular set of time points is evaluated by examining how closely the differential-algebraic constraint equations are satisfied between collocation points [84, p. 100]. If the accuracy on this interval does not satisfy the allowable tolerance, either the number of collocation points can be increased or the interval can be subdivided into more approximating subintervals. The mesh refinement algorithm iterates until all mesh tolerances are met. Betts discusses mesh refinement algorithms suitable for time-marching methods in Ref. [56, pp. 152-162]. Darby presents a few *hp*-mesh refinement algorithms for LGR-based pseudospectral methods, which determines the segment widths (denoted h) and the polynomial degree (denoted p) in each segment simultaneously [84].

3.3.2 Problem Structure and Sparsity

Many modern NLP algorithms can use a sparsity pattern to more efficiently and reliably solve the problem. A matrix is said to be "sparse" when many of the elements are zero. The problem structure that arises from DT has a number of sparse matrices. Consider the following matrices that are used in common NLP algorithms such as sequential quadratic programming and interior-point methods [56, pp. 60-90]. The gradient of the objective is defined as:

$$\nabla_{\mathbf{x}} \begin{bmatrix} \psi \\ \mathcal{M} \end{bmatrix} = \begin{bmatrix} \frac{\partial \psi}{\partial \boldsymbol{\xi}} & \frac{\partial \psi}{\partial \mathbf{u}} & \frac{\partial \psi}{\partial \mathbf{x_p}} & \frac{\partial \psi}{\partial t_0} & \frac{\partial \psi}{\partial t_f} \\ \frac{\partial \mathcal{M}}{\partial \boldsymbol{\xi}} & \frac{\partial \mathcal{M}}{\partial \mathbf{u}} & \frac{\partial \mathcal{M}}{\partial \mathbf{x_p}} & \frac{\partial \mathcal{M}}{\partial t_0} & \frac{\partial \mathcal{M}}{\partial t_f} \end{bmatrix} \tag{3.34}$$

The subsequent derivative produces the Hessian:

$$\nabla_{\mathbf{xx}} \begin{bmatrix} \psi \\ \mathcal{M} \end{bmatrix} = \begin{bmatrix} \frac{\partial^2 \psi}{\partial \boldsymbol{\xi}^2} & \frac{\partial^2 \psi}{\partial \boldsymbol{\xi} \partial \mathbf{u}} & \frac{\partial^2 \psi}{\partial \boldsymbol{\xi} \partial \mathbf{x_p}} & \frac{\partial^2 \psi}{\partial \boldsymbol{\xi} \partial t_0} & \frac{\partial^2 \psi}{\partial \boldsymbol{\xi} \partial t_f} \\ \frac{\partial^2 \psi}{\partial \boldsymbol{\xi} \partial \mathbf{u}} & \frac{\partial^2 \psi}{\partial \mathbf{u}^2} & \frac{\partial^2 \psi}{\partial \mathbf{u} \partial \mathbf{x_p}} & \frac{\partial^2 \psi}{\partial \mathbf{u} \partial t_0} & \frac{\partial^2 \psi}{\partial \mathbf{u} \partial t_f} \\ \frac{\partial^2 \psi}{\partial \boldsymbol{\xi} \partial \mathbf{x_p}} & \frac{\partial^2 \psi}{\partial \mathbf{u} \partial \mathbf{x_p}} & \frac{\partial^2 \psi}{\partial \mathbf{x_p}^2} & \frac{\partial^2 \psi}{\partial \mathbf{x_p} \partial t_0} & \frac{\partial^2 \psi}{\partial \mathbf{x_p} \partial t_f} \\ \frac{\partial^2 \psi}{\partial \boldsymbol{\xi} \partial t_0} & \frac{\partial^2 \psi}{\partial \mathbf{u} \partial t_0} & \frac{\partial^2 \psi}{\partial \mathbf{x_p} \partial t_0} & \frac{\partial^2 \psi}{\partial t_0^2} & \frac{\partial^2 \psi}{\partial t_0 \partial t_f} \\ \frac{\partial^2 \psi}{\partial \boldsymbol{\xi} \partial t_f} & \frac{\partial^2 \psi}{\partial \mathbf{u} \partial t_f} & \frac{\partial^2 \psi}{\partial \mathbf{x_p} \partial t_f} & \frac{\partial^2 \psi}{\partial t_0 \partial t_f} & \frac{\partial^2 \psi}{\partial t_f^2} \\ \frac{\partial^2 \mathcal{M}}{\partial \boldsymbol{\xi}^2} & \frac{\partial^2 \mathcal{M}}{\partial \boldsymbol{\xi} \partial \mathbf{u}} & \frac{\partial^2 \mathcal{M}}{\partial \boldsymbol{\xi} \partial \mathbf{x_p}} & \frac{\partial^2 \mathcal{M}}{\partial \boldsymbol{\xi} \partial t_0} & \frac{\partial^2 \mathcal{M}}{\partial \boldsymbol{\xi} \partial t_f} \\ \frac{\partial^2 \mathcal{M}}{\partial \boldsymbol{\xi} \partial \mathbf{u}} & \frac{\partial^2 \mathcal{M}}{\partial \mathbf{u}^2} & \frac{\partial^2 \mathcal{M}}{\partial \mathbf{u} \partial \mathbf{x_p}} & \frac{\partial^2 \mathcal{M}}{\partial \mathbf{u} \partial t_0} & \frac{\partial^2 \mathcal{M}}{\partial \mathbf{u} \partial t_f} \\ \frac{\partial^2 \mathcal{M}}{\partial \boldsymbol{\xi} \partial \mathbf{x_p}} & \frac{\partial^2 \mathcal{M}}{\partial \mathbf{u} \partial \mathbf{x_p}} & \frac{\partial^2 \mathcal{M}}{\partial \mathbf{x_p}^2} & \frac{\partial^2 \mathcal{M}}{\partial \mathbf{x_p} \partial t_0} & \frac{\partial^2 \mathcal{M}}{\partial \mathbf{x_p} \partial t_f} \\ \frac{\partial^2 \mathcal{M}}{\partial \boldsymbol{\xi} \partial t_0} & \frac{\partial^2 \mathcal{M}}{\partial \mathbf{u} \partial t_0} & \frac{\partial^2 \mathcal{M}}{\partial \mathbf{x_p} \partial t_0} & \frac{\partial^2 \mathcal{M}}{\partial t_0^2} & \frac{\partial^2 \mathcal{M}}{\partial t_0 \partial t_f} \\ \frac{\partial^2 \mathcal{M}}{\partial \boldsymbol{\xi} \partial t_f} & \frac{\partial^2 \mathcal{M}}{\partial \mathbf{u} \partial t_f} & \frac{\partial^2 \mathcal{M}}{\partial \mathbf{x_p} \partial t_f} & \frac{\partial^2 \mathcal{M}}{\partial t_0 \partial t_f} & \frac{\partial^2 \mathcal{M}}{\partial t_f^2} \end{bmatrix} \tag{3.35}$$

Finally, the constraint Jacobian is given by:

$$\nabla_{\mathbf{x}} \begin{bmatrix} \boldsymbol{\zeta} \\ \mathbf{C} \\ \boldsymbol{\phi} \end{bmatrix} = \begin{bmatrix} \frac{\partial \boldsymbol{\zeta}}{\partial \boldsymbol{\xi}} & \frac{\partial \boldsymbol{\zeta}}{\partial \mathbf{u}} & \frac{\partial \boldsymbol{\zeta}}{\partial \mathbf{x_p}} & \frac{\partial \boldsymbol{\zeta}}{\partial t_0} & \frac{\partial \boldsymbol{\zeta}}{\partial t_f} \\ \frac{\partial \mathbf{C}}{\partial \boldsymbol{\xi}} & \frac{\partial \mathbf{C}}{\partial \mathbf{u}} & \frac{\partial \mathbf{C}}{\partial \mathbf{x_p}} & \frac{\partial \mathbf{C}}{\partial t_0} & \frac{\partial \mathbf{C}}{\partial t_f} \\ \frac{\partial \boldsymbol{\phi}}{\partial \boldsymbol{\xi}} & \frac{\partial \boldsymbol{\phi}}{\partial \mathbf{u}} & \frac{\partial \boldsymbol{\phi}}{\partial \mathbf{x_p}} & \frac{\partial \boldsymbol{\phi}}{\partial t_0} & \frac{\partial \boldsymbol{\phi}}{\partial t_f} \end{bmatrix} \tag{3.36}$$

For many problems (which do not consider plant design), the number of nonzero elements in the Hessian matrix and Jacobian matrix is less than 1% [56, p. 51]. This is primarily due to the special mathematical form for the defect and path constraint equations. Recalling the trapezoidal rule in Eqn. (3.16), each defect constraint depends on two sets of state and control

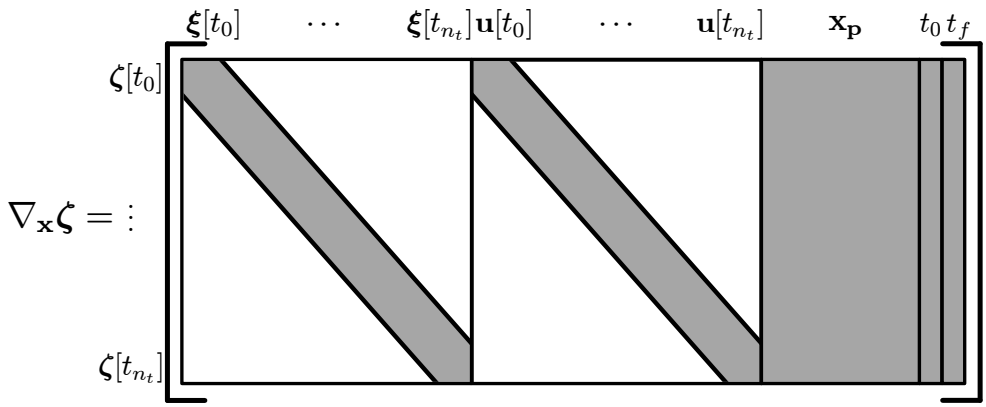

Figure 3.2 Illustration of the sparsity pattern of defect constraint Jacobian (shaded region indicates possible nonzero elements).

variables defined at t_{k-1} and t_k. As we increment through the possible values of k, the previously used state and control values in $\boldsymbol{\zeta}[t_{k-1}]$ are also used in $\boldsymbol{\zeta}[t_k]$ and nowhere else in the defect constraint equations. As illustrated in Fig. 3.2, this creates a zigzag diagonal pattern and a large number of zero elements. If these matrices are not given analytically, sparse finite differencing can be used to numerically approximate them [56, pp. 52-54].

These patterns have been studied for both local and global collocation methods. Betts demonstrates the sparsity pattern for most of the time-marching methods [56, pp. 134-152]. In addition, he defines a reduced optimization vector for certain forms of the defect constraint (namely the Hermite-Simpson method). Patterson and Rao discuss computationally efficient methods for computing the sparse matrices that arise from the pseudospectral discretization [103]. Recently, Allison et al. have discussed the sparsity pattern in co-design formulations [47]. The problem structure and sparsity pattern of the trapezoidal rule on the WEC design problem is discussed in Appendix A.

3.3.3 Singular Arcs

A singular arc is characterized by having both $\frac{\partial H(\cdot)}{\partial \mathbf{u}} = \mathbf{0}$ and $\det\left(\frac{\partial^2 H(\cdot)}{\partial \mathbf{u}^2}\right) = 0$. This is likely to occur if the Hamiltonian is a linear function of $\mathbf{u}$ [56, p. 125]. Singular problems are notoriously hard to solve numerically. The Goddard rocket problem is a common example where there are three distinct phases of the optimal solution trajectory [56, p. 213]. The second phase is a singular

arc and the control is highly oscillatory. This is because the control is not uniquely determined on a singular arc unless the higher-order conditions are imposed, such as:

$$\frac{d^2}{dt^2}\left(\frac{\partial H}{\partial \mathbf{u}}\right) = \mathbf{0}$$

Adding this condition is a hybrid technique between direct and indirect methods because the analytic necessary conditions must be derived and the arc sequence must be guessed. If mesh refinement is being used, it typically attempts to correct the perceived inaccuracy on the singular arc by adding grid points to this region; potentially not converging.

Betts discusses another approach to solve a different singular problem of minimizing task time for an industrial robot [56, pp. 304-310]. Regularization is performed by using a modified Lagrange term:

$$\hat{\mathcal{L}} = \mathcal{L} + R_{\text{pen}} \langle \mathbf{u}, \mathbf{u} \rangle \tag{3.37}$$

where $R_{\text{pen}} \in \mathbb{R}^+$ is a small penalty parameter and $\langle \cdot \rangle$ is the inner product. The control is now uniquely defined with this quadratic regularization and if R_{pen} is small enough, the optimal solution will be close to the original problem (i.e., $|\mathcal{L}^*| \gg |R_{\text{pen}} \langle \mathbf{u}^*, \mathbf{u}^* \rangle|$) [56, p. 307]. This term is analogous to the energy required to make control decisions. This term has been used in Refs. [29, 36, 104]. Methods for selecting the penalty parameter will be discussed in Section 5.1.

3.3.4 Open-Loop Control in Early Stage Design

In addition to the computational efficiency and numerical stability properties of DT, another quality motivates a more fundamental level the investigation of DT formulations for ODSD. Since DT is open-loop, no assumptions on the control structure are imposed. This may prove especially helpful during early-stage design when the control architecture is undefined. Open-loop control solutions can provide insights into upper system performance limits without the restrictions imposed by specific physical- and/or control-system design [40, 105].

Consider the following design problems that could benefit from an open-

loop control formulation: a novel hybrid powertrain for an automobile and the PTO for a WEC converter. In the first problem, a hybrid powertrain must determine actively the ratio of energy supplied by the hybrid power sources (e.g., an internal combustion engine and electric machine) to the various components of the automobile. For novel designs, control strategies may not exist in the current state of the art. If we let this ratio be an open-loop control decision, we can solve the ODSD problem to find the upper system performance limits before a realistic controller is even designed. The open-loop solutions can also provide insights into complex system dynamics, and serve as a basis for developing implementable feedback control systems [106–109].

The second problem is more pertinent to this work. Many different PTOs have been proposed for WECs (see Sec. 4.4). However without knowing the true upper performance limit of the wave-mechanical system, we will not know how close we are to a truly optimal system design. The open-loop solutions can provide possible directions for physical-system design, such as which PTO architecture will closely match the optimal open-loop trajectories [29, 36, 105].

With the general ODSD problem defined and the main numerical solution approach described, we can formulate the design of WECs as an ODSD problem.

Chapter 4

Wave Energy Converter Design

A general overview of the design of ocean WECs was discussed in the Introduction. This included an examination of the positive and negative characteristics of this resource. The basic principles behind wave energy conversion were shown including the some of the challenges associated with WEC design. This chapter will expand on this description by first discussing the mathematical models for ocean waves and then the equations of motion that describe the dynamics of a specific WEC architecture (namely ❶). Previous work on maximizing energy extraction through both plant and control design modifications will be reviewed along with various PTO mechanisms. Finally, the ODSD formulation in Prob. (2.15) will be determined for WECs by stating the relevant objectives and constraints.

4.1 Modeling Ocean Waves

To successfully extract energy from ocean waves, we need to understand their general behavior. At a quick glance, ocean waves might seem random and unpredictable. A wide array of phenomena contribute to wave generation including the wind, astronomical forces, earthquakes, submarine landslides, and other objects oscillating in the ocean. No single mathematical solution exists for all types of ocean waves so approximations need to be utilized. There are two primary categories of wind generated waves: sea and swell. The latter have rounded crests and are traveling waves that have left their region of primary wind energy transfer. This category is a candidate for the simplest wave model: regular or harmonic waves. Seas, on the other hand, are a train of waves driven by the prevailing local wind field. They are more stochastic in nature than swells, i.e., the apparent wave length and period vary continuously. Therefore, seas are more appropriately modeled as irreg-

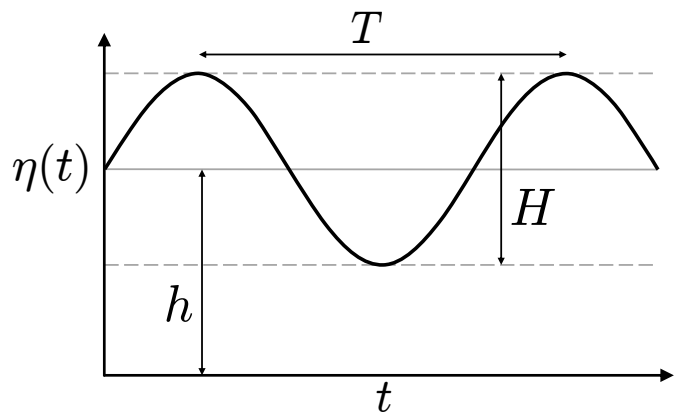

Figure 4.1 Regular wave definitions.

ular waves or a superposition of regular waves at many different frequencies [110, pp. 5-2]. The irregular wave models can represent the natural wave behavior in real locations.

4.1.1 Regular Waves

Assuming the wave moves in the positive x-direction, the wave profile, or the shape of the water's surface, can now be expressed as a function of both x and t as follows:

$$\eta(t) = \frac{H}{2}\cos(kx - \omega t) \tag{4.1}$$

where H is the wave height, k is the wave number, and ω is the wave angular velocity. The wave period, T, for a regular wave along with H and h are shown in Fig. 4.1. We now can apply potential theory if we make a number of assumptions: the wave amplitude is small enough for linear theory and the fluid is homogeneous, incompressible, and irrotational. Glossing over these details (please refer to Refs. [27, 110]), a relationship between ω and k can be found:

$$\omega^2 = kg\tanh(kh) \tag{4.2}$$

where $g = 9.81$ m/s^2 is the gravitational constant. This is known as the dispersion relation for any arbitrary water depth h. In deep water, $\tanh(kh) =$

1, reducing Eqn. (4.2) to:

$$\omega^2 = kg \tag{4.3}$$

With the dispersion relation in Eqn. (4.2), the wave celerity ($c = \lambda/T = \omega/k$) becomes:

$$c = \sqrt{\frac{g}{k}\tanh(kh)} \tag{4.4}$$

Applying the deep water conditions, the phase velocity is found to be:

$$c = \sqrt{\frac{g}{k}} = \frac{g}{\omega} \tag{4.5}$$

The total wave energy comes from summing the kinetic and potential energies inside in the wave:

$$E = \frac{1}{8}\rho g H^2 \tag{4.6}$$

where $\rho = 1025$ kg/m^3 is the sea water density and the calculated energy is per unit horizontal sea surface area. Continuing, the average work done or power becomes:

$$\overline{P} = \frac{1}{8}\rho g H^2 \frac{c}{2}\left(1 + \frac{2kh}{\sinh(2kh)}\right) \tag{4.7}$$

Once again applying the deep water conditions:

$$\overline{P} = \frac{1}{16}\rho g H^2 c = \frac{1}{16}\frac{\rho g^2 H^2}{\omega} \tag{4.8}$$

4.1.2 Irregular Waves

Irregular waves can be approximated as a superposition of a series of sinusoidal waves:

$$\eta(t) = \sum_{i=1}^{n_r} \eta_i(t) = \sum_{i=1}^{n_r} \frac{H_i}{2}\cos(k_i x - \omega_i t + \theta_i) \tag{4.9}$$

where n_r is the number of regular wave components used to represent the

irregular wave field, and $\{H_i, \omega_i, \theta_i\}$ are the wave height, angular frequency, and phase for component i, respectively. The wave phase components, θ_i, are random phase shifts. Increasing n_r will improve the fidelity of the wave field approximation. McTaggart noted that a minimum of 20 wave components are needed to ensure accurate modeling of an irregular seaway [111].

Many of the equations in Section 4.1.1 can be directly applied using the superposition principle. First, Eqn. (4.6) can quantify the total energy in the irregular wave per unit horizontal sea surface area as:

$$E = \sum_{i=1}^{n_r} \frac{1}{8} \rho g H_i^2 \tag{4.10}$$

Next, modifying Eqns. (4.7) and (4.8) will show the average power to be:

$$\text{(finite-depth)} \qquad \overline{P} = \sum_{i=1}^{n_r} \frac{1}{8} \rho g H_i^2 \frac{c_i}{2} \left(1 + \frac{2k_i h}{\sinh(2k_i h)}\right) \tag{4.11a}$$

$$\text{(deep-water)} \qquad \overline{P} = \sum_{i=1}^{n_r} \frac{1}{16} \frac{\rho g^2 H_i^2}{\omega_i} \tag{4.11b}$$

4.1.3 Wave Energy Spectra

For a particular location, Fourier series analysis can be performed over a large time horizon to extract the frequency characteristics of the irregular wave field. An implicit assumption made during this analysis is the time horizon will repeat itself after some lengthy period. This is from the fact that an irregular wave is composed of regular components; therefore the irregular wave itself will have a period. The goal of the Fourier series analysis is to find the statistical properties of the location in terms of frequency and amplitude.

The statistical properties can be conveniently denoted by a wave spectrum, $S(\omega)$. The amplitude of the ith component in Eqn. (4.9) is:

$$A_i = \frac{H_i}{2} = \sqrt{2S(\omega_i)\Delta\omega_i} \tag{4.12}$$

where $\Delta\omega_i$ is the wave frequency interval for component i. Another method for finding the wave spectrum other than data collection is through standardized empirical expressions, which are accurate under certain assumptions.

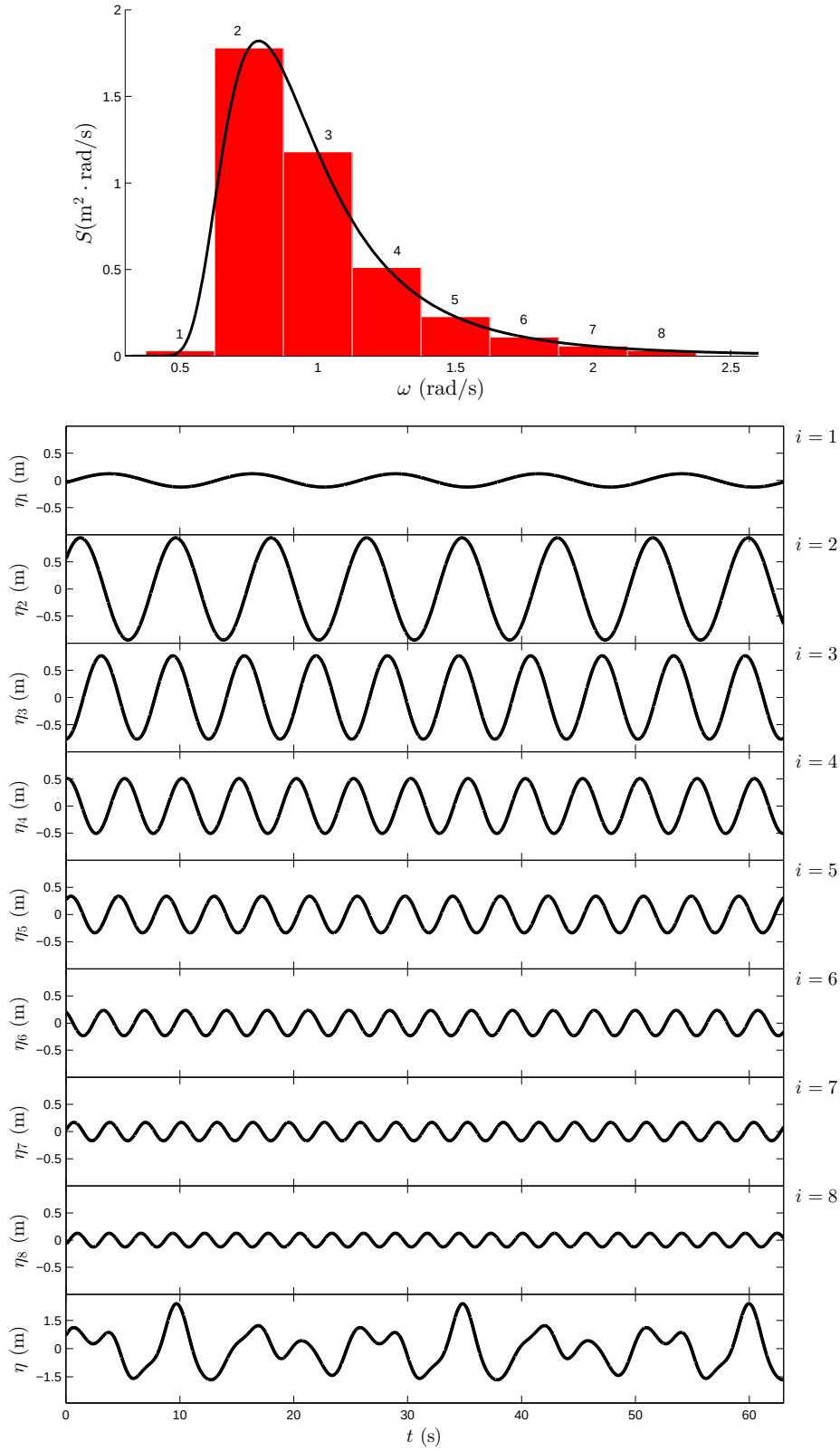

Figure 4.2 Superposition of 8 regular wave components to create an irregular wave using the Bretschneider spectrum with $S(\omega)$ on the top and $\eta(t)$ on the bottom.

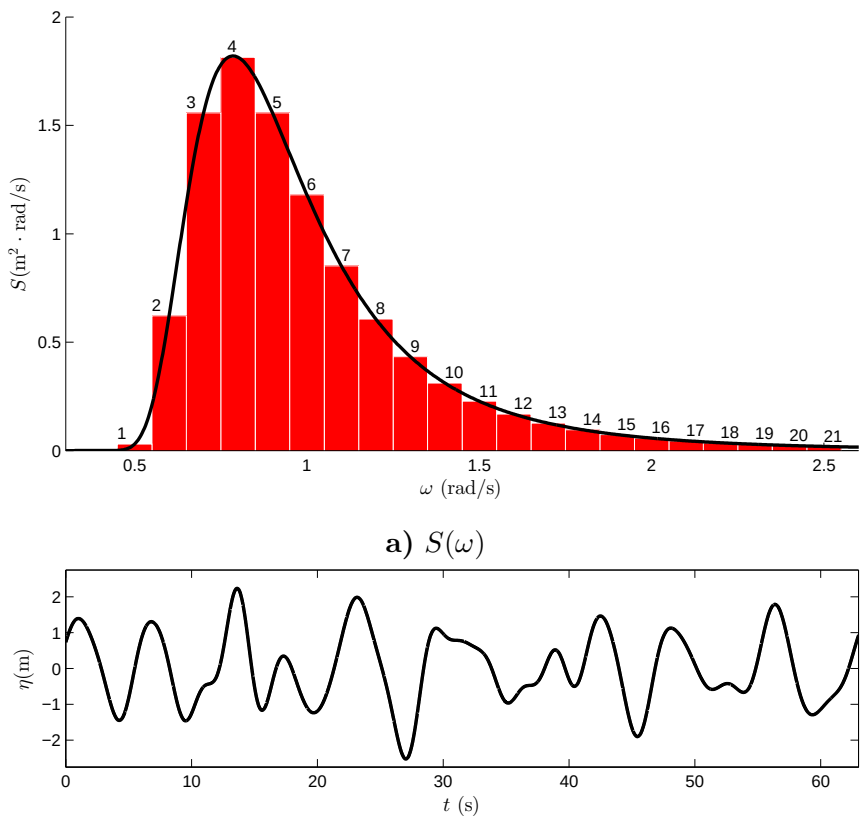

Figure 4.3 Bretschneider spectrum with $H_{1/3} = 4$ m and $T_p = 8$ s.

One common standardized spectrum is the Bretschneider (BS) spectrum that describes a developing sea, also known as the two-parameter ITTC spectrum [112]. The spectrum has the general form:

$$S(\omega) = \frac{\alpha}{\omega^5} e^{-\beta/\omega^4} \tag{4.13}$$

where α and β are the empirical coefficients given by:

$$\alpha = 487 \left(\frac{H_{1/3}}{T_p^2} \right)^2 \qquad \beta = \frac{1948.2}{T_p^4} \tag{4.14}$$

where $H_{1/3}$ is the mean wave height of the highest third of the wave and T_p is the modal period or the period associated with peak energy density.

A representative BS spectrum can be seen at the top of Fig. 4.2 with 8 discrete components. The bottom of this figure includes all 8 regular wave components with varying frequency, amplitude, and phase shift along with

their superposition to create an irregular wave. However, this is not an accurate enough approximation of $S(\omega)$ so n_r was increased to 21 in Fig. 4.3 to create a higher fidelity irregular wave.

Other common wave spectra include the one and two parameter Pierson-Moskowitz, ISSC, Liu, JONSWAP, Scott, Ochi-Hubble bi-modal, TMA, and Mitsuyasu [112]. Potential locations for WEC deployment are not described by a single value for the wave spectrum parameters, but rather a set of them. These sets usually are monthly approximations of the parameters [113, 114] or frequency distributions of sea states [114].

4.2 Equations of Motion

Early work in HCWEC analysis was performed in the frequency domain [17, 27]. This technique requires a number of assumptions including regular incident waves. Many authors have stated that there is a fundamental difference between designing WECs for irregular versus regular waves. Drew et al. asserted that a single frequency of the incident sea wave will not predict the performance in real systems [19]. Additionally, Tedeschi et al. emphasized the need to use time-dependent solutions since the instantaneous extracted power in irregular waves is required for realistic analysis [31]. Time-domain formulations allow the inclusion of unavoidable losses while frequency domain solutions do not [27, p. 182]. While irregular waves may appear to be a hinderance to WEC design, WECs in irregular waves have the potential to produce better results than WECs in regular waves under similar energy assumptions [38]. Real world WEC engineering systems also require constraints (such as an inequality path constraint on the PTO power) [29]. Nonlinear path constraints are impossible to account for in the frequency domain. Therefore, the analysis of the WEC dynamics will need to be performed in the time domain to account of irregular waves and realistic design constraints.

There are six modes of WEC body motion possible: surge (U_x), sway (U_y), heave (U_z), roll (Ω_x), pitch (Ω_y), and yaw (Ω_z) (see Ref. [27, p. 119] for the notation convention). These modes are due to the interaction between ocean waves and oscillating bodies. The dynamics of a WEC can be expressed

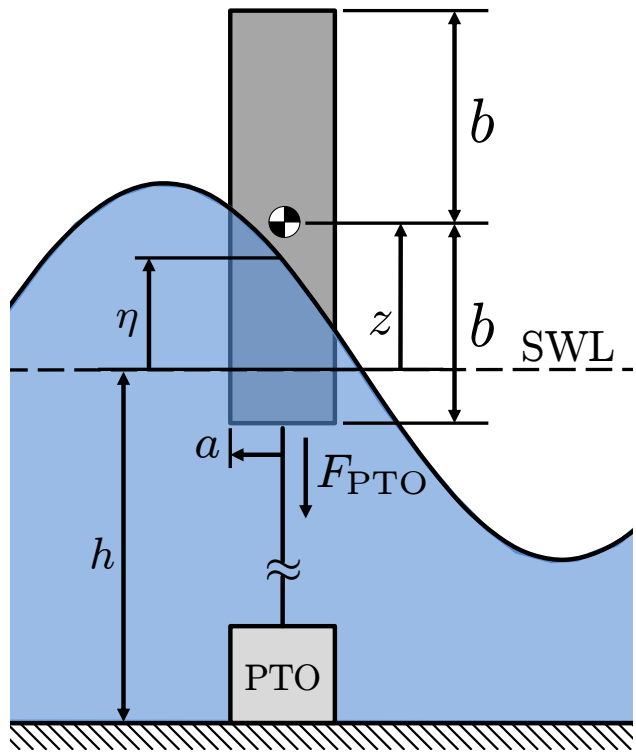

Figure 4.4 Heaving cylinder wave energy converter.

using Newton's law for rigid body dynamics in 3-dimensions:

$$m\mathbf{a}_U = \mathbf{F}_w + \mathbf{F}_v + \mathbf{F}_b + \mathbf{F}_{\mathrm{PTO}} \tag{4.15a}$$

$$\mathbf{I}_g\mathbf{a}_\Omega + \mathbf{\Omega} \times \mathbf{I}_g\mathbf{\Omega} = \mathbf{M}_w + \mathbf{M}_v + \mathbf{M}_b + \mathbf{M}_{\mathrm{PTO}} \tag{4.15b}$$

where m is the mass of the body, $\mathbf{a}_U$ is the acceleration vector for the translation modes (U_x, U_y, U_z), $\mathbf{\Omega}$ is the angular velocity vector, $\mathbf{a}_\Omega$ is the acceleration vector for the rotation modes $(\Omega_x, \Omega_y, \Omega_z)$, $\mathbf{I}_g$ is the moment of inertia tensor at the center of gravity, and $\mathbf{F}$ and $\mathbf{M}$ are the resulting forces and moments acting on the WEC [115]. The subscripts denote forces and moments from a specific effect: $_w$ indicates effects directly from the wave, $_v$ indicates effects from viscous losses, $_b$ indicates effects due to buoyancy, and $_{\mathrm{PTO}}$ indicates effects from the PTO. The wave force is typically broken up into two different components: the radiation force and the excitation force (i.e., $\mathbf{F}_w = \mathbf{F}_r + \mathbf{F}_e$).

We will consider one of the more simple WECs, a heaving cylinder WEC (HCWEC) connected to a PTO moored to the ocean floor (see Fig. 4.4)

similar to the systems described in Refs. [32, 116]. This system is similar to a point absorber, i.e., a heaving body WEC whose size is much smaller than ocean wavelength and has only one mode of oscillation in the vertical direction ($U_z \equiv z$) [17, 27]. The cylinder radius is a, while the draft of the cylinder, b, is the submerged length in still water. In order to simplify the plant design, the buoy is assumed to be of constant density and of length $2b$. Therefore, the vertical position of the buoy mass center is measured from the SWL. Using Eqn. (4.15) for only the heave mode, no moments will be present and a single equation of motion is required:

$$m\ddot{z} = -F_r + F_e - F_v - F_b - F_{\mathrm{PTO}} \tag{4.16}$$

Each of these forces will now be described.

Radiation force — In the absence of an incident wave, an oscillating WEC will generate a water wave. This wave will act on the WEC through a radiation force. This concept is similar to the membrane of a loudspeaker where an acoustic wave will be generated as a result of the oscillation of the system [27, p. 49]. Considering a single mode of oscillation, this force can be written as:

$$F_r = Z\dot{z} \tag{4.17}$$

where Z is the radiation impedance and $\dot{z}$ is the heave velocity [27, pp. 126-127]. It is convenient to split Z (since it is a complex function of ω) into real and imaginary parts:

$$Z(\omega, \mathbf{x_p}) = R_r(\omega, \mathbf{x_p}) + iX_r(\omega, \mathbf{x_p}) \tag{4.18}$$

where $R_r(\omega, \mathbf{x_p})$ is the radiation resistance or added damping and $X_r(\omega, \mathbf{x_p})$ is the radiation reactance. This both are functions of the plant design (typically just the geometry in many studies but may also be a function of the WEC architecture such as the differences between a cylinder and sphere). The first term in Eqn. (4.18) represents the energy lost due to this motion, namely the radiated power. In addition, some energy is stored in the water surrounding the WEC. The velocity of the water adds some kinetic energy while gravity acting on the deformed water surface adds some potential energy. This stored

energy can be added to the energy stored in the mechanical system [27, p. 50]. The radiation reactance is typically written as:

$$X_r(\omega, \mathbf{x_p}) = \omega m_r(\omega, \mathbf{x_p}) \tag{4.19}$$

where $m_r(\omega, \mathbf{x_p})$ is the added mass, which is usually positive [27, p. 50]. However, in certain cases the added potential energy is larger than the added kinetic energy; therefore, the added mass becomes negative [117].

We can relate R_r and m_r through Kramers-Kronig relations [27, p. 140]. The typical approach considers $\lim_{\omega\to\infty} m_r(\omega)$ since this quantity is nonzero. Then the total radiation force can be written as:

$$F_r = m_r(\infty, \mathbf{x_p})\ddot{z} + \int_{-\infty}^{t} k_r(t-\tau, \mathbf{x_p})\dot{z}(\tau)d\tau \tag{4.20}$$

where $m_r(\infty)$ is the infinite-frequency added mass and $k_r(\cdot)$ is the kernel of a convolution term known as the impulse-response of the radiation force or fluid memory term. This equation is also referred to as the Cummins equation [118]. The fluid memory function is then:

$$k_r(t, \mathbf{x_p}) = \frac{2}{\pi}\int_0^{\infty} \frac{R_r(\omega, \mathbf{x_p})}{\omega}\sin(\omega t)d\omega \tag{4.21}$$

Models that incorporate the convolution integral in Eqn. (4.20) are challenging to use with existing optimization algorithms as this integral results in integro-differential equations that are computationally expensive to simulate. Another approach uses an approximate state-space model to more efficiently calculate the radiation force [119]. However, this will add a large number of additional states to the system. If we assume only linear and monochromatic waves with only linear system elements, Eqn. (4.20) simply becomes:

$$F_r = m_r(\omega, \mathbf{x_p})\ddot{z} + R_r(\omega, \mathbf{x_p})\dot{z} \tag{4.22}$$

This leads to the most efficient (but also least accurate) approximation of the radiation force in irregular waves:

$$F_r = \overline{m}_r(\mathbf{x_p})\ddot{z} + \overline{R}_r(\mathbf{x_p})\dot{z} \tag{4.23}$$

where $\overline{m}_r(\mathbf{x_p})$ and $\overline{R}_r(\mathbf{x_p})$ are constants according to a weighted value within the range of relevant frequencies [18, p. 24]. One weight scheme uses weights based on $S(\omega)$:

$$\overline{m}_r = \frac{1}{\sum_{i=1}^{n_r} S(\omega_i)\Delta\omega_i} \sum_{i=1}^{n_r} m_r(\omega_i) S(\omega_i) \Delta\omega_i \tag{4.24a}$$

$$\overline{R}_r = \frac{1}{\sum_{i=1}^{n_r} S(\omega_i)\Delta\omega_i} \sum_{i=1}^{n_r} R_r(\omega_i) S(\omega_i) \Delta\omega_i \tag{4.24b}$$

Any WEC study needs to be able to efficiently calculate these radiation parameter functions such as m_r, R_r, and k_r. For simple geometries, such as the HCWEC considered here, analytic solutions for these parameters have been found [120, 121]. These solutions are exceedingly complex and would take a large percentage of total computation time of any optimization algorithm they were placed in (i.e., for every plant design change, these functions would need to be recomputed).

An alternative approach is to directly compute Eqn. (4.20) in the time domain by using seakeeping dedicated boundary element method codes such as SeaFEM, ACHIL3D [122], and TīMIT [123]. Other software codes exist to directly compute the parameters such as WAMIT [124], DIODORE, and AquaDyn [125]. These tools can also be applied to other shapes while the analytic solutions are only valid for a specific, simple topology. These software packages still have moderate computational demands that can slow down a design optimization study.

If execution efficiency is paramount, a surrogate model can be constructed that mimics the results of the more computationally expensive code as closely as possible, while being computationally cheaper to evaluate [126]. The strategy chosen for modeling the impedance coefficients involved data from Ref. [114], which calculated m_r and R_r from the analytic solution. The surrogate model was created using an artificial neural network (ANN) with 10 hidden layers. The objective used when fitting the ANN was to preserve the shape of the curves with the modeled points. Since a finite number of data points were used (14 curves for each coefficient), input constraints are needed

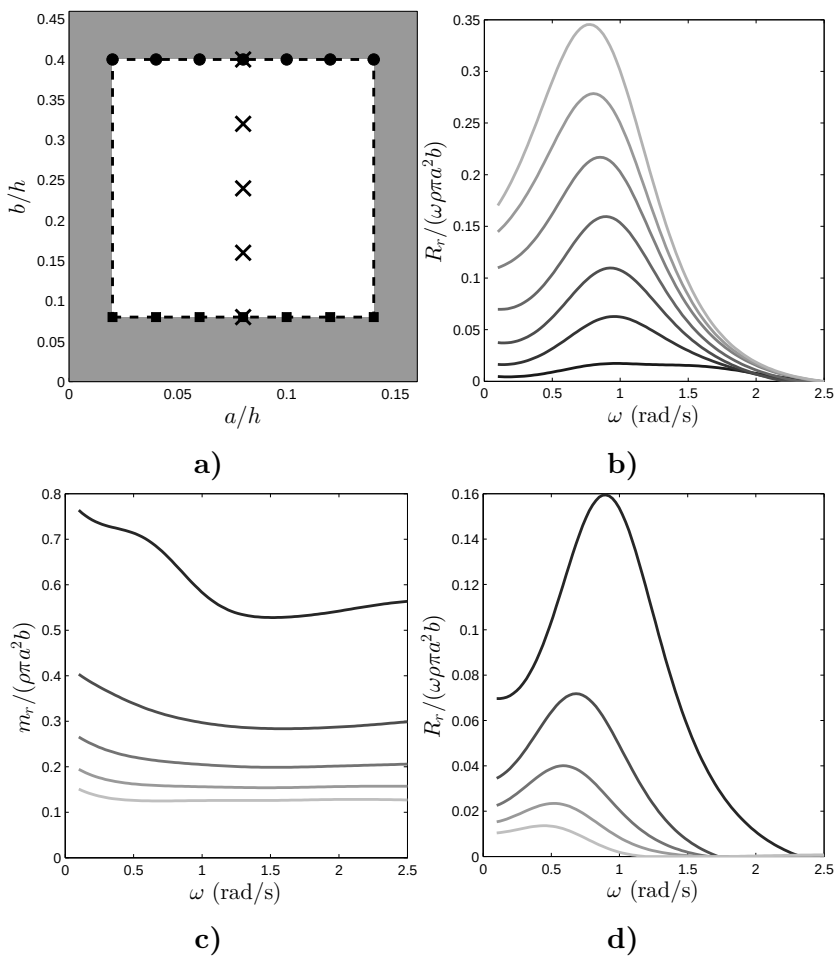

Figure 4.5 a) Design space of a/h and b/h with data points ■, ● from [114], white feasible region, all curves drawn using neural network, darker lines indicate smaller geometric ratio **b)** $R_r(\omega, \mathbf{x_p})$ using ■ points **c)** $m_r(\omega, \mathbf{x_p})$ using ✕ points **d)** $R_r(\omega, \mathbf{x_p})$ using ✕ points.

to preserve model accuracy:

$$0.02 \leq a/h \leq 0.14 \tag{4.25a}$$

$$0.08 \leq b/h \leq 0.40 \tag{4.25b}$$

The derivation is based on the data point locations shown in Fig. 4.5a. Figure 4.5b demonstrates the effect of a on $R_r(\omega)$. Figure 4.5c and Fig. 4.5d show the effect of b on both $m_r(\omega)$ and $R_r(\omega)$. Note that the 3 inner curves are at completely different locations than the collected data points. With more data for different values of b/h, the surrogate model accuracy could be improved.

Excitation force — The HCWEC will experience a dynamic pressure trajectory from the water when the wave passes [127, p. 22]. This force acts on the immersed body even if no motion is present and is modeled so the relative motion of the HCWEC does not effect its value [27, p. 51]. This force includes potentials from both the undisturbed incident wave and the diffracted wave. When considering bodies with a vertical axis of symmetry oscillating in heave in regular waves and deep water, the excitation force is given by:

$$F_e = \sqrt{\frac{2\rho g^3 R_r(\omega, \mathbf{x_p})}{\omega^3}}\eta(t) \tag{4.26}$$

which is a relationship between the radiation resistance and the excitation force [27, 30, 128]. In addition, since we are considering a point absorber in the heave mode, the excitation force will be in phase with the incident wave elevation although this is not the general case [27, p. 125]. For low frequencies, the heave excitation force has a magnitude that is predicted by Archimedes' law, which neglects effects of wave interference and of wave diffraction. For high frequencies, the force tends to zero, which was to be expected because of the mentioned effects, but also because of the decrease of hydrodynamic pressure with increasing submergence below the free water surface [27, p. 134].

In irregular waves, the excitation force will be a linear combination of n_r regular waves if linear theory is assumed. Then the total excitation force is:

$$F_e = \sum_{i=1}^{n_r} \sqrt{\frac{2\rho g^3 R_r(\omega_i, \mathbf{x_p})}{\omega_i^3}}\eta_i(t) \tag{4.27}$$

Buoyancy force — Using linear theory the hydrostatic buoyancy force F_b is proportional to the excursion z of the body from its equilibrium position:

$$F_b = \rho g S_w z \tag{4.28}$$

where S_w is the water plane area of the body. Due to the constant cross-sectional area of a HCWEC (i.e., the water plane area is independent of the heave position), the buoyancy force is given by the following formula [27,

p. 183]:

$$F_b = g\rho\pi a^2 z = k_b z \tag{4.29}$$

where k_b is the buoyancy stiffness coefficient.

Viscous force — The viscous drag force can be expressed as:

$$F_v = \frac{1}{2}\rho C_D S_w \dot{z}|\dot{z}| \tag{4.30}$$

where C_D is the drag coefficient (0.81 for a HC [129]). If the WEC moves at relatively slow speeds, a linearized version specific for a HCWEC is:

$$F_v = \frac{1}{2}C_D \rho\pi a^2 \dot{z}_{\max}\dot{z} = R_v \dot{z} \tag{4.31}$$

where R_v is the viscous resistance coefficient. This linearized version is not the same as the friction due to the mechanism or other means for transmission.

PTO force — The PTO force will be modeled here as an open-loop control force. Frequently, the PTO modeling is motivated by reactive control, i.e., modeled as a linear spring-damper system:

$$F_{\text{PTO}} = k_{\text{PTO}} z + R_{\text{PTO}} \dot{z} \tag{4.32}$$

where the PTO stiffness k_{PTO} corresponds to the capacitive term and the PTO damping R_{PTO} corresponds to the dissipative term. Assuming a regular wave input and that these coefficients can be tuned, a PTO design of this form can be found that maximizes energy extraction [28]. The PTO force in Eqn. (4.32), however, is fundamentally limited in the trajectories that it can produce. Many have used this PTO form to provide analytic solutions to a variety of WEC problems [28, 33, 35, 38], but their results are only optimal with respect to the specific simplified PTO architecture. In addition, this form of the PTO does not predict the behavior in real PTO systems. There is no reason to believe that this form for the PTO architecture will produce the true system performance limits or provide insights into the optimal system dynamics.

With all the forces defined, the general state space model can be written

as:

$$\dot{\boldsymbol{\xi}} = \mathbf{A}\boldsymbol{\xi} + \mathbf{B}u + \mathbf{K}e \tag{4.33}$$

where:

$$\mathbf{A} = \begin{bmatrix} 0 & a_{12} \\ a_{21} & a_{22} \end{bmatrix} \quad \mathbf{B} = \begin{bmatrix} 0 \\ b_{21} \end{bmatrix} \quad \mathbf{K} = \begin{bmatrix} 0 \\ k_{21} \end{bmatrix}$$

$$\boldsymbol{\xi} = \begin{bmatrix} z(t) \\ \dot{z}(t) \end{bmatrix} \quad u = F_{\mathrm{PTO}}(t) \quad e = F_e(t)$$

$$a_{21} = \frac{-k_b}{m + \overline{m}_r} \quad a_{22} = \frac{-\left(\overline{R}_r + R_v\right)}{m + \overline{m}_r} \quad a_{12} = 1$$

$$b_{21} = \frac{-1}{m + \overline{m}_r} \quad k_{21} = \frac{1}{m + \overline{m}_r}$$

4.3 WEC Design for Maximum Energy Extraction

Since the start of rigorous engineering research of the design of WECs in the 1970's, many researchers have identified both plant and control design principles to help maximize energy production.

While passive WECs (i.e., no active control of F_{PTO}) can produce energy, incorporating active control increases significantly energy production capability [28, 31, 130], increasing economic competitiveness. Reactive control was one of the earliest control strategies developed [27, p. 206]. Under the assumptions of linearity and regular waves, it can be shown that the HCWEC's dynamic behavior can be described by a second-order transfer function without zeros that will maximize energy production when the optimal velocity is given by:

$$\hat{\dot{z}}^* = \frac{\hat{F}_e}{2R_r} \tag{4.34}$$

where $\hat{\dot{z}}^*$ is the complex amplitude of the velocity trajectory and $\hat{F}_e$ is the complex amplitude of the excitation force. Maximum energy production is then produced when velocity is in phase with excitation force, but only when the particularly narrow assumptions described above are valid, including regularity of incident waves. Another important implication of Eqn. (4.34) is that a reactive control system—i.e., a PTO is required that can inject energy into the wave-mechanical system, not just extract it—is required for optimal

energy production. Bidirectional power flow helps exploit natural WEC dynamics [48, 49, 131] to maximize power production. Unfortunately, PTOs capable of bidirectional power flow are difficult to implement in practice. In addition, Tedeschi et al. demonstrated that reactive control in irregular waves is an inferior control strategy [31]. Another caveat of reactive control is large amplitudes for the heave position and velocity [132].

Wave energy extraction can be increased beyond what is possible through optimal control strategies alone.

Many WEC studies do consider both the physical system design (e.g., a and b for the design of a HCWEC) and the control system design (e.g., open-loop optimal control or a feedback controller). This is one form of co-design and is essential for the success of the WEC system since a successful design hinges on exploiting the natural dynamics of the ocean wave-buoy interaction [48, 49]. If the physical system is designed such that it resonates with incoming waves, similar to the behavior of electromagnetic antennae or acoustic microphones, energy extraction can be improved [27, p. 51]. Therefore, the natural dynamics can be partially expressed with the natural frequency of a heaving point oscillator in a regular wave is given by:

$$\omega_0 = \sqrt{\frac{k_b}{m + m_r(\omega)}} \tag{4.35}$$

Since real ocean waves are not regular, WECs cannot simply be designed according to the resonance conditions for a particular frequency. This can be addressed by employing a WEC control system that boosts power production in off-resonance conditions. One intuitive approach proposed by Budal and Falnes involves 'latching' the system in place (i.e., $\dot{z} = 0$ for a short period of time) [21]. The objective of latching control, sometimes referred to as phase control [27, 30, 132], is to keep $\dot{z}$ and F_e in phase (or at least to align the extrema of these trajectories with respect to time). This strategy is motivated by the phase requirement for reactive control presented in Eqn. (4.34).

Clement and Babarit has discussed another intuitive control strategy that involves decoupling the WEC from the PTO known as declutching (i.e., setting $F_{\text{PTO}} = 0$ for a short period of time). They showed that a hybrid latching and declutching (freewheeling) control strategy amplified power production substantially, increasing it beyond the sum of the two strategies individually

[28].

Optimal control formulations in the time domain have also been studied. These studies often treat buoy velocity as the control input [27, 38, 132]. While PTO force trajectory can be calculated using the results of a velocity-based solution, velocity (or any other system state) cannot be an independent control input. Treating velocity as the control input simplifies solution (e.g., it sidesteps singular optimal control formulations), but the PTO force is a more realistic independent control variable. Clement and Babarit used the simplified PTO model described in Eqn. (4.32) in formulating an optimal control problem based on PMP; the resulting controller exhibited latching behavior [28]. Lattanzio and Scruggs formulated a linear-quadratic-Gaussian optimal control problem, finding the optimal casual control for a particular generator arrangement [116].

DT has also been used to solve WEC problems. Abraham and Kerrigan used a PTO model composed of a linear damper and an active element, resulting in bang-bang control of both control inputs [35]. Allison et al. made no assumptions on PTO architecture to explore the upper limits of HCWEC performance and gain insight into principles of ideal WEC operation in regular and irregular ocean waves [29, 36]. Reactive, latching, and declutching behavior all emerged as valid optimal control strategies depending on particular combinations of design and operating constraints.

A variety of suboptimal but more implementable control strategies have been investigated. Valerio et al. have demonstrated a system than switches controllers depending on season [133]. This seems to be a very natural proposition since the sea states vary widely by season. Other methods such as model predictive control [38], internal model control [133], and feedback linearization [133] have been designed for realistic WEC control with varying levels of success. Realistic controller implementations are necessary, but the likelihood of success will depend on the initial controller architecture. A more comprehensive review of many WEC control strategies can be found in [134].

4.4 Power-Take Off Design

Realistic PTO systems have been develop that use hydraulics and electric machines. Hydraulic PTOs have been proposed by some due to their ability to absorb energy from the large, slow speeds of ocean waves and can utilize accumulators to provide bidirectional power flow [19, 30, 135]. Although they are able to drive generators at near constant speeds, they typically suffer from low transmission efficiency. Some have proposed designs based on linear electric machines [20, 32, 33]. This type of PTO has promise since it can provide bidirectional power flow, but in many cases cannot provide compressive (upward) force as it is typically connected via cables to the buoy. Tedeschi et al. have proposed a PTO where the WEC is attached to a rotational electric machine with power electronics via a gear box [31]. This PTO architecture has many advantages, including the ability to provide bidirectional power flow and PTO force, rendering it an especially promising PTO design strategy.

Using an open-loop trajectory to represent the PTO force, we only need to make very limited assumptions on the PTO architecture; thus, the linear PTO restriction has been removed, similar to the work performed in Ref. [29, 36]. Future studies could investigate the previously listed PTOs' ability to match the optimal open-loop trajectories or develop novel PTO architectures that will create the identified optimal system dynamics for maximum energy production.

4.5 Design Objectives and Constraints

We seek a formulation consistent with the ODSD problem in Prob. (2.15). The objective and constraints will depend on the plant variables where appropriate. The dynamic constraints (modeled with a state-space model that depends on plant variables) were already presented in Eqn. (4.33).

4.5.1 Objective Function

Reconsidering the Eqn. (1.1) and Prob. (1.2), the maximization of energy production over a finite time interval $0 \rightarrow t_f$ can be written as a uncon-

strained minimization problem:

$$\min_{\boldsymbol{\xi},u,a,b} \quad -\int_0^{t_f} \dot{z}(t)F_{\mathrm{PTO}}(t)dt \tag{4.36}$$

The states are included as optimization variables since DT methods will be utilized when solving this problem. An additional quadratic penalty term will be added since the control input appears linearly in the Hamiltonian (see Section 3.3.3):

$$H(\boldsymbol{\xi}, u, \mathbf{x_p}, \mathbf{p}) = \xi_2 u + \langle \mathbf{p}, \mathbf{A}\boldsymbol{\xi} + \mathbf{B}u + \mathbf{K}e \rangle \tag{4.37}$$

Consequently, maximizing energy production with respect to $F_{\mathrm{PTO}}(t)$ is a singular optimal control problem (which is difficult, but possible to solve) [56]. Kasturi and Dupont added a quadratic penalty term to an analogous mass-spring-damper system to enable efficient solution [104]. Clement and Babarit also noted that their WEC system design problem was a singular optimal control problem [28]. The unconstrained optimization formulation with the penalty term is:

$$\min_{\boldsymbol{\xi},u,a,b} \quad \int_0^{t_f} \left(-\dot{z}(t)F_{\mathrm{PTO}}(t) + R_{\mathrm{pen}}[F_{\mathrm{PTO}}(t)]^2\right) dt \tag{4.38}$$

where $R_{\mathrm{pen}} \in \mathbb{R}^+$ is the penalty weight. The addition of the penalty term perturbs the underlining problem, so using the smallest possible value of R_{pen} that still facilitates solution is desirable. It is analogous to the energy required for the PTO to make control decisions. This will be discussed more in Section 5.1.

4.5.2 Inequality Path Constraints

Position Constraint — If the buoy completely leaves the water it will impact the water on its way back down. This slamming of the HCWEC should be avoided. The following constraint prevents this event:

$$z(t) - (\eta(t) + b) \leq 0 \tag{4.39}$$

Power Constraint — Practical PTOs (at least so far) cannot provide bidirec-

Table 4.1 Four design cases of the power and control force constraint.

Case	$C_{\min}$	$u_{\min}$	
1	$-\infty$	$-\infty$	Unconstrained
2	$-\infty$	0	No compressive PTO force
3	0	$-\infty$	No reactive power
4	0	0	Both constraints

tional power flow [27] or would be cost prohibitive. Therefore, we would like to study the effects on applying a power inequality path constraint on the PTO force trajectory:

$$C_{\min} \leq \dot{z}(t) F_{\mathrm{PTO}}(t) \tag{4.40}$$

where $C_{\min}$ can be either $-\infty$ or 0. The former will be treated as an unconstrained power trajectory while the latter will ensure only positive power.

Control Force Constraint — Asymmetric control input bounds should be considered. Explicit bounds on the control would be of the form:

$$u_{\min} \leq u \leq u_{\max} \tag{4.41}$$

In most previous studies no explicit control input bounds are employed, although Hals and Falnes imposed symmetric PTO force constraints [38]. Asymmetric constraints (e.g., $0 \leq F_{\mathrm{PTO}} \leq F_{\max}$) are useful for modeling WECs where an upward force cannot be exerted on the buoy because of a cable connection between the buoy and the PTO. Asymmetric constraints are difficult to implement using conventional optimal control methods, highlighting the value of the DT.

Considering the variations of Eqns. (4.40) and (4.41), four different combinations of the power and control input constraints can be considered (see Table 4.1).

4.5.3 Boundary Constraints

Periodic Constraints — Irregular waves are periodic since they are a sum of periodic components. Typically, a few frequencies in wave spectrum are

dominant as evident in $S(\omega)$. Using these dominant frequencies, an approximation for the period of the irregular wave can be found. For the solution to be periodic as well, the states must be the same at the initial and final time:

$$\boldsymbol{\xi}\left(t_f\right) - \boldsymbol{\xi}\left(0\right) = \mathbf{0} \tag{4.42}$$

Adding this constraint results in a periodic optimal control problem, which arises in various applications including vibrating systems [104] and aircraft cruise control [136]. Using a periodic optimal control approach for the design of WEC control systems in irregular waves greatly reduces the computational expense when compared to the conventional strategy of using a large time horizon to achieve steady state behavior.

Time-Independent Plant Constraint — The mass of the HCWEC is equivalent to the submerged mass:

$$m = \rho \pi a^2 b \tag{4.43}$$

This is relating a dependent variable to independent geometric design variables. In addition, the bounds on a, b from Eqn. (4.25) need to be included.

4.5.4 Complete WEC Design Problem Formulation

The complete WEC design problem formulation considered here is as follows:

$$\min_{\boldsymbol{\xi},u,a,b} \quad \int_0^{t_f} \left(-\dot{z}(t)F_{\mathrm{PTO}}(t) + R_{\mathrm{pen}}[F_{\mathrm{PTO}}(t)]^2\right) dt \tag{4.38}$$

subject to:

$$\dot{\boldsymbol{\xi}} - (\mathbf{A}\boldsymbol{\xi} + \mathbf{B}u + \mathbf{K}e) = \mathbf{0} \tag{4.33}$$

$$z(t) - (\eta(t) + b) \leq 0 \tag{4.39}$$

$$C_{\min} - \dot{z}(t)F_{\mathrm{PTO}}(t) \leq 0 \tag{4.40}$$

$$u_{\min} - u \leq 0 \tag{4.41}$$

$$\boldsymbol{\xi}\left(t_f\right) - \boldsymbol{\xi}\left(0\right) = \mathbf{0} \tag{4.42}$$

$$m - \rho \pi a^2 b = 0 \tag{4.43}$$

With the complete WEC design problem defined, the next chapter will be devoted to numerical studies of a HCWEC in both regular and irregular waves. The studies will be designed to generate the optimal system dynamics under a variety of practical design constraints.

Chapter 5

Numerical Studies on WEC Design

This chapter will be devoted to a number of numerical studies on the WEC design problem in both regular and irregular waves. Direct transcription will be utilized in all of the examples.

5.1 Regularization Penalty Parameter

The first step is to investigate the appropriate values for the regularization penalty parameter added in Eqn. (4.38). As mentioned in Section 3.3.3, R_{pen} is a positive scalar, but we desire a small value in order to have minimal effect on the original problem. The effect of R_{pen} will be presented without analyzing the specifics of the solutions in order to first determine the appropriate value of R_{pen} to perform this analysis.

5.1.1 Regular Waves with a Local Collocation Method

In order to determine the effect of R_{pen} on the WEC design problem in a regular wave, a parameter sweep from 10^{-3} to 10^{-10} was performed with all other aspects of the problem fixed using a local collocation method. In Fig. 5.1a, we see the optimal total energy extracted with the additional penalty term removed post optimization versus various values of R_{pen}. For all four cases in Table 4.1, the energy consumption was monotonically decreasing with R_{pen}. However, we see that for small values of R_{pen}, the energy extraction is nearly the same, similar to the comment made by Betts with regard to this regularization procedure [56, p. 307]. Figure 5.1b demonstrates the relationship between R_{pen} and the relative effect of the penalty term, which is calculated

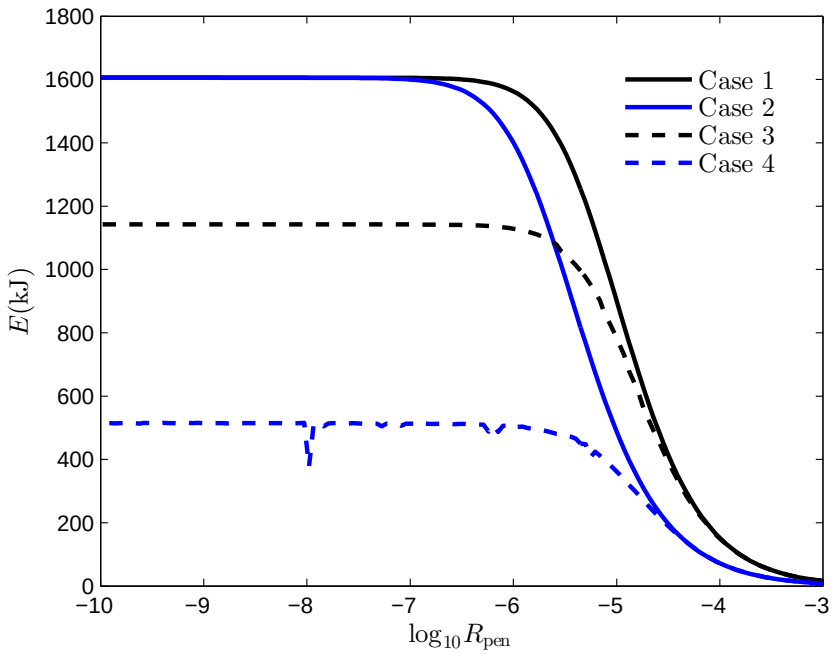

a)

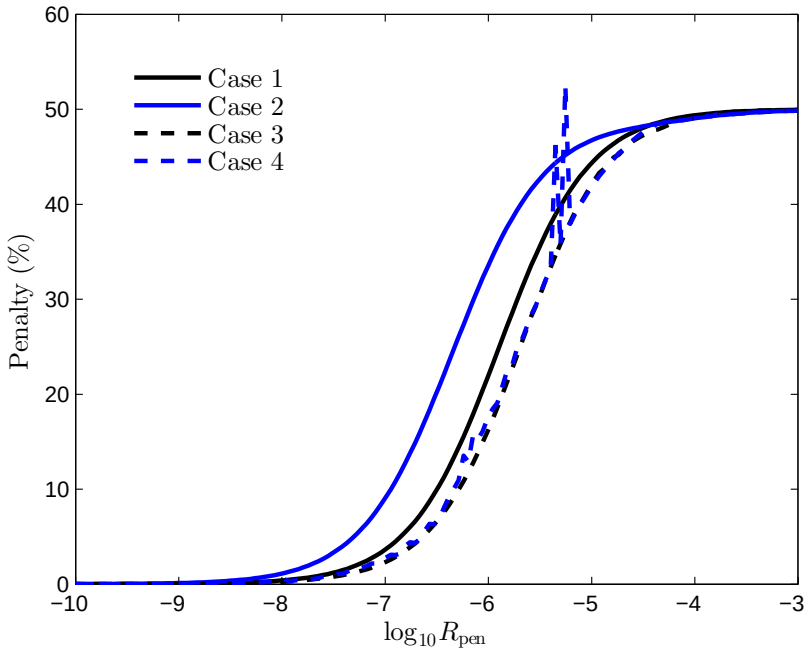

b)

Figure 5.1 Sensitivity studies to determine the appropriate value for R_{pen} in regular waves (all four cases considered).

by:

$$\text{Penalty} = \frac{R_{\text{pen}} \int \langle \mathbf{u}, \mathbf{u} \rangle \, dt}{\left| \int L dt \right| + \int R_{\text{pen}} \langle \mathbf{u}, \mathbf{u} \rangle \, dt} \tag{5.1}$$

The opposite trend is determined from this plot, which is expected. As we decrease the penalty parameter, the effect of the penalty term decreases until it is almost nonexistent around 10^{-8} for all four cases. However, there is a discrepancy between Fig. 5.1a and Fig. 5.1b because the location of R_{pen} for a nonchanging energy production is different than for a nearly zero penalty term effect. Since the original objective was to maximize energy production, it would be appropriate to stop when there is nonchanging energy production even if a moderate percentage of the modified objective is due to the penalty term (potentially near 20% for Cases 3 and 4). Also note the nonsmoothness at a few values of R_{pen}, which was caused by numerical difficulties at these points.

We still need to address the fact that we are now working with a modified objective function. The question is if this modification fundamentally changes the result and potentially produces unusable solutions. The phase space of the objective function (i.e., F_{PTO} vs. $\dot{z}$) was observed for different values of R_{pen}. The results for a widerange of R_{pen} values is shown in Fig. 5.2 for Case 1. Note that as R_{pen} decreases, the phase plots tend to converge to a specific ellipse (in both size and angle). As it will be discussed in the next section, for the smaller values, the optimal results are the same as for reactive control; therefore, for small enough values of R_{pen}, the problem is equivalent to the original objective. For Case 3 in Fig. 5.3, we once again see a general convergence in the phase plot. However, if R_{pen} is too small, we start to see singular control artifacts, such as instabilities in the phase plots. This is more prominent in the Case 3 plots. The same plots for Cases 2 and 4 are in Figs. B.1 and B.2 with similar conclusions drawn. Therefore, it seems reasonable to assume that results with a sufficiently small value for R_{pen} will produce optimal solutions aligned with the original objective.

From these studies, a simple algorithm was developed to determined the best value for R_{pen} outlined in Algorithm 1. The general idea is based on Fig. 5.1a: decrease R_{pen} until the objective function is no longer changing relative to the previous value. We first must select a large initial value for

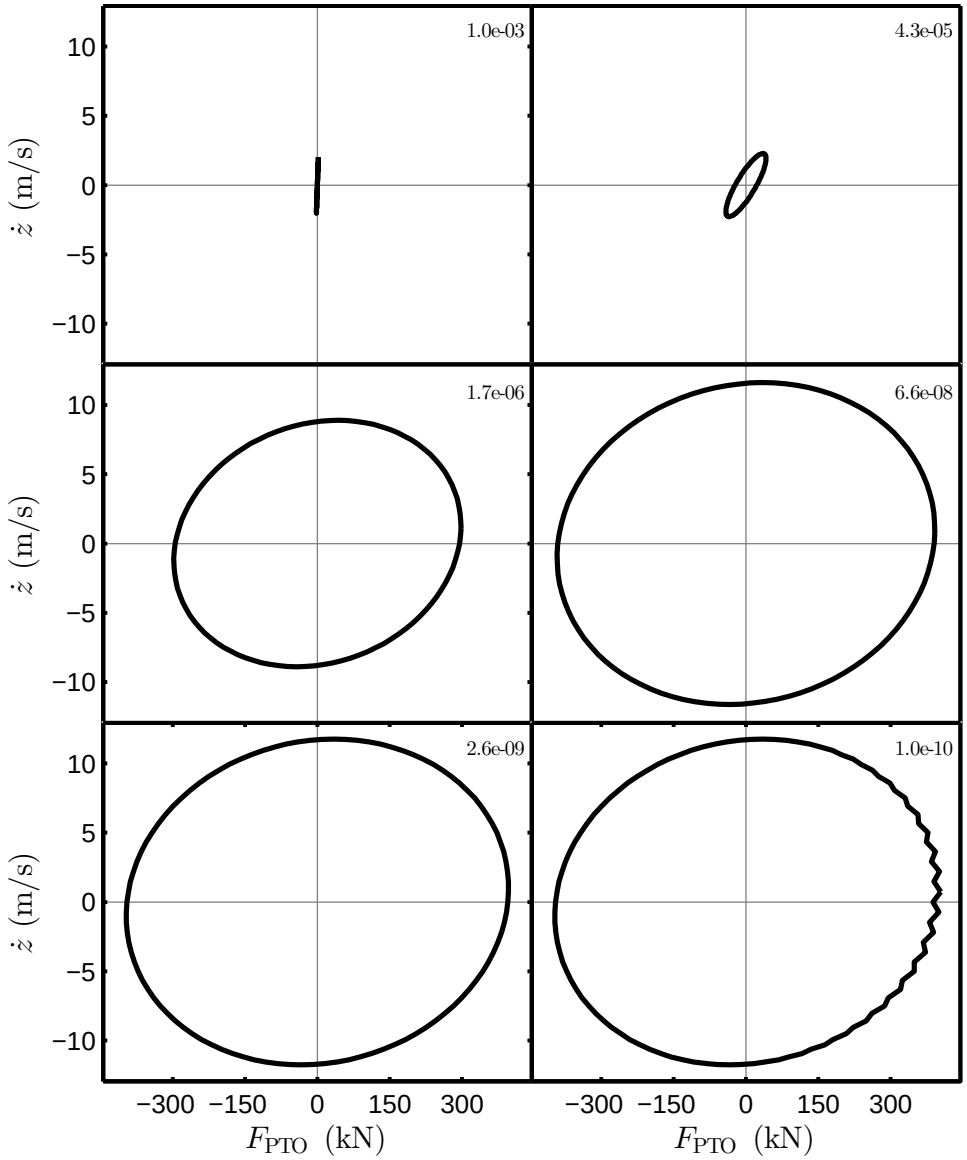

Figure 5.2 The effect of R_{pen} on the phase space of the objective function for Case 1 (note that the R_{pen} values are in the northeast corners).

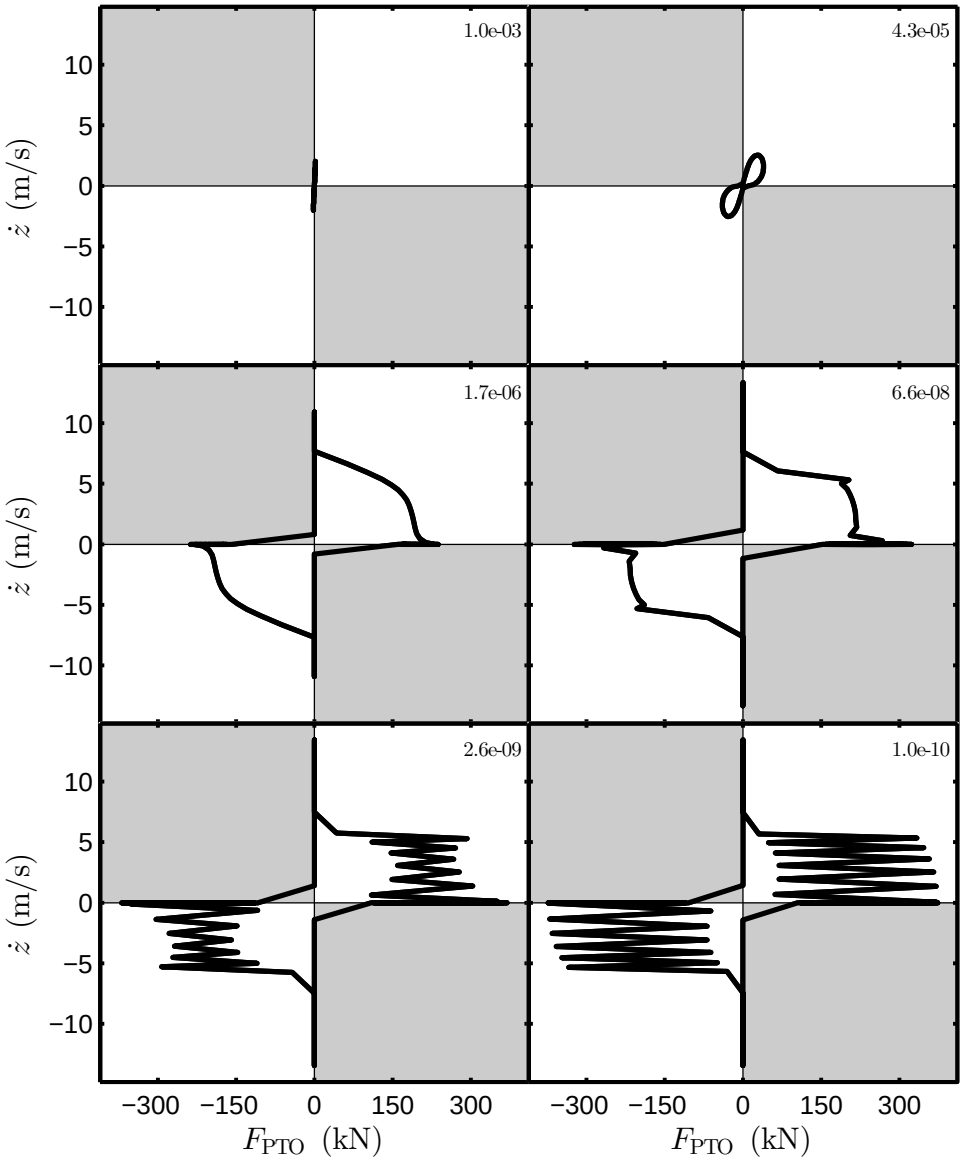

Figure 5.3 The effect of R_{pen} on the phase space of the objective function for Case 3 (note that the R_{pen} values are in the northeast corners, grey shading indicates infeasible regions).

Algorithm 1: Finding the appropriate regularization parameter.

Data: large R_{pen}, $0 < \kappa < 1$, $\epsilon > 1$
Result: f_i^*, R_{pen}

```
f_0 ← 0
f_Ratio ← ∞
while f_Ratio > ε do
    i ← i + 1
    f_i^* ← Solve minimization problem with R_pen
    f_Ratio ← f_i^* / f_{i-1}^*
    R_pen ← κ R_pen
end
```

R_{pen} such that the modified problem is sufficiently different than the original ($R_{\text{pen}} = 10^{-3}$ for regular wave cases). Next, a stopping tolerance ϵ should be set to a value greater than 1 since we are assuming that the modified objective is monotonically decreasing with respect to R_{pen} ($\epsilon = 1.01$ in this study). Finally, we need to set the update coefficient for R_{pen}, κ, which should be between 0 and 1 to ensure a decreasing value at each iteration ($\kappa = \frac{1}{2}$ in this study).

5.1.2 Irregular Waves with a Global Collocation Method

A similar sensitivity study was performed to determine R_{pen} in an irregular wave using a global collocation method. In Fig. 5.4, we see the optimal total energy extracted with the additional penalty term removed post optimization versus various values of R_{pen} for Case 1. From 10^{-6} to approximately 10^{-2}, the energy production is monotonically decreasing with R_{pen}; similar to what was observed in Fig. 5.1a. However below this value of R_{pen}, the energy production became negative (i.e., the final solution was no longer extracting energy)! In Fig. 5.5, we see the final solution at 10^{-6}. There are a number of segments where the velocity and PTO force are rapidly switching. It is important to note that this solution is feasible and the mesh tolerances are met according to the optimization algorithm. This is an artifact of the singular nature of the WEC design formulation. Unlike the local collocation R_{pen} sensitivity study, we cannot say that small enough values of R_{pen} will produce the similar energy results; these solutions are also completely

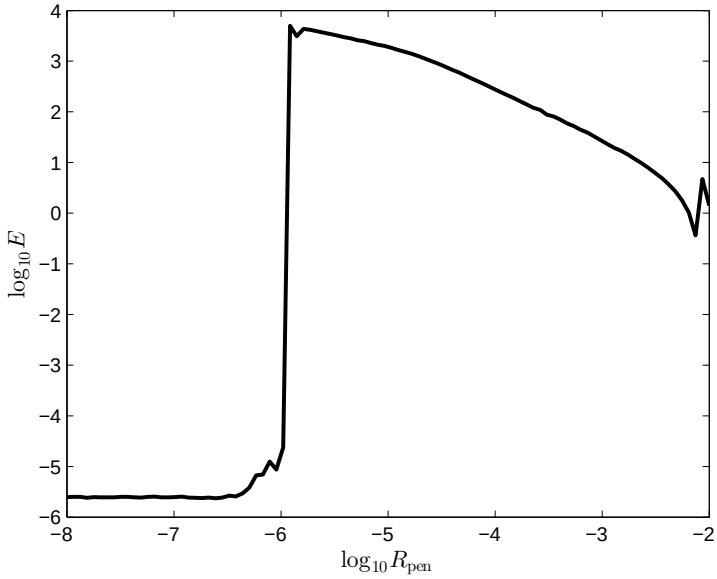

Figure 5.4 Sensitivity studies to determine the appropriate value for R_{pen} in irregular waves (only Case 1 considered).

impractical. Therefore, Algorithm 1 needs to be modified to stop near the point where the energy production switches signs.

We no longer can say that these are truly optimal results since we cannot arbitrarily decrease R_{pen} to converge to a final energy production value. In addition, we cannot make the same claim that the regularization procedure is not fundamentally perturbing the underlining problem. So why should we consider these results? Even with these shortcomings, using a global collocation method to optimize energy production in irregular waves will still provide design insights because these solutions strategies were seeking the optimal energy extraction. It is important to remember that no design guidelines were provided, only an objective and constraints. One example is the latching control strategy, where the velocity is held until it is approximately in phase with the excitation force. However, this is a suboptimal strategy [28]. Therefore, all phenomena that arise are due to the desired natural dynamics of the system.

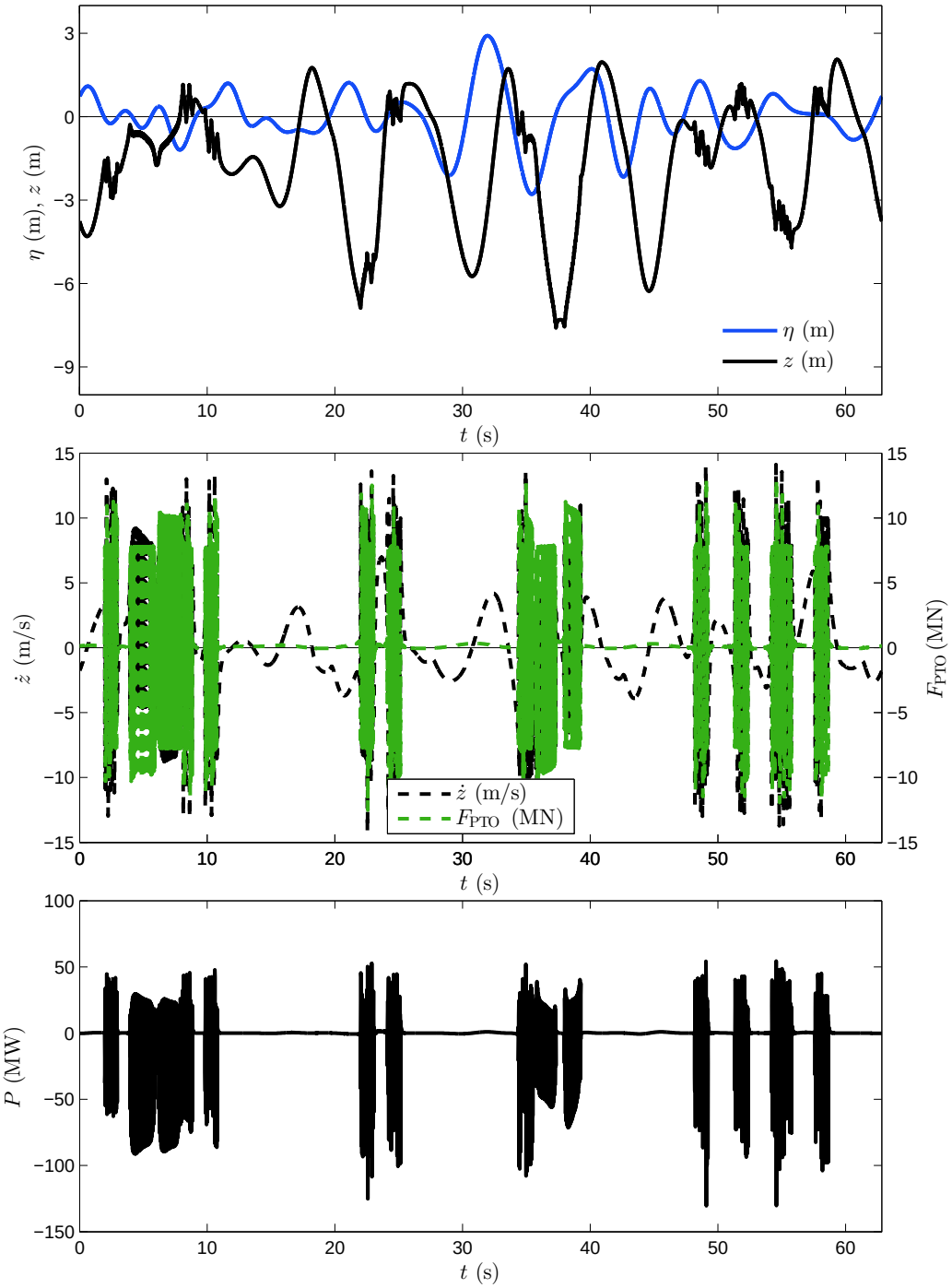

Figure 5.5 Poor solution with $R_{\text{pen}} = 10^{-6}$ in an irregular wave using a global collocation method (note that the solution is feasible and mesh tolerances are met according to the optimization algorithm).

Table 5.1 Parameters for regular wave studies.

Parameter	Value	Parameter	Value
H	4 m	n_t	100
T	8 s	R_{pen}	10^{-5}
h	10 m	ϵ	1.01
$F_{\text{PTO,max}}$	10^{10} N	κ	$\frac{1}{2}$
$\dot{z}_{\text{max}}$	10^3 m/s		

5.2 Regular Waves

Regular waves are studied first because the optimal results can be compared directly to the previously developed optimal control strategies such as reactive, latching, and declutching. The trapezoidal rule was used for both the defect constraints and numerical quadrature. The complete WEC design problem was considered except for the position path constraint defined in Eqn. (4.39) in order to investigate the more common unconstrained heave amplitude problem. Nested co-design was used in order to keep the defect constraints linear and therefore efficient to solve (see Appendix A). In addition, because there are only two plant design variables (a,b), enumerating many feasible combinations is possible. The NLP was solved using TOMLAB®[1] with SNOPT®[2]. Some parameters used are listed in Table 5.1. Many of the default values for SNOPT® were used except for the major optimality and minor optimality tolerances. They needed to be decreased to 10^{-11} to produce stable results.

5.2.1 Unrestricted Heaving Amplitude

First, no limits will be placed on the heaving amplitude. The parametric sweeps of (a, b) were performed for all four cases shown in Fig. 5.6. Adding more constraints (Case 4 has the most constraints) increased numerical difficulties, as evidenced by the numerical noise in Cases 3 and 4. The location of maximum energy extraction for each case is denoted by a white dot. Table 5.2 characterizes each of these solutions. The wave, states, and control

[1] `http://tomopt.com/tomlab/`
[2] `http://www.sbsi-sol-optimize.com/asp/sol_product_snopt.htm`

along with instantaneous power and phase space are plotted for each of the four cases in Figs. 5.7 and 5.8.

Observing Fig. 5.6, we can see that the energy results for Cases 1 and 2 are the same (i.e., $E_1 = E_2$). This implies that the addition of the force constraint does not degrade energy production. The power constraint, on the other hand, did degrade the performance of the WEC. The overall pattern in the results from Case 3 is similar to Cases 1 and 2, but has a lower in energy value. All cases favored the largest possible a value. A larger a value implies that there is more energy available to the WEC because the incident wave striking it is wider. Also recalling Fig. 4.5, a large radius increases the added resistance, which in turn increases the excitation force. Smaller b values were also preferred. When combined with the larger radius, disk-like cylinders were the desired design for all four cases. Case 4 had an optimal b value that was not as small as possible, which might be due to the numerical noise in this high energy region. This will be discussed more in Section 5.2.5.

We will now turn our attention to the optimal designs. For Case 1 in Fig. 5.7a, all optimal trajectories were harmonic. The phase space plot of the objective is an ellipse, which indicates that the instantaneous power was harmonic. Since larger portions of the ellipse are in quadrants 2 and 4, reactive power ($P < 0$) is used. The reactive control condition states that the excitation force and velocity should be in phase. This condition was met in Case 1 without any requirements that it should be met. Adding the force constraint in Case 2 simply shifted the harmonic solution in Case 1. Observe that the phase space is nearly the same except the ellipse is only in quadrants 1 and 4 as required by the constraint. The implies that the optimal velocity trajectories are identical. This solution requires large amounts of reactive power and extremely high control forces; thus, may prove to be an impractical design (not forgetting the maximum amplitudes of both Cases 1 and 2 would make a real HCWEC hit the sea floor or fly out of the water).

The addition of the power constraint in Case 3 restricts the phase space from entering quadrants 2 and 4 (see Fig. 5.8a). In this case we see both latching and declutching. Note when the phase trajectory stays in contact with the velocity axis, the system is latched; and when it comes into contact with the control axis, it is declutched. This behavior aligns the extremums of the velocity and excitation force, the same condition as reactive control, but

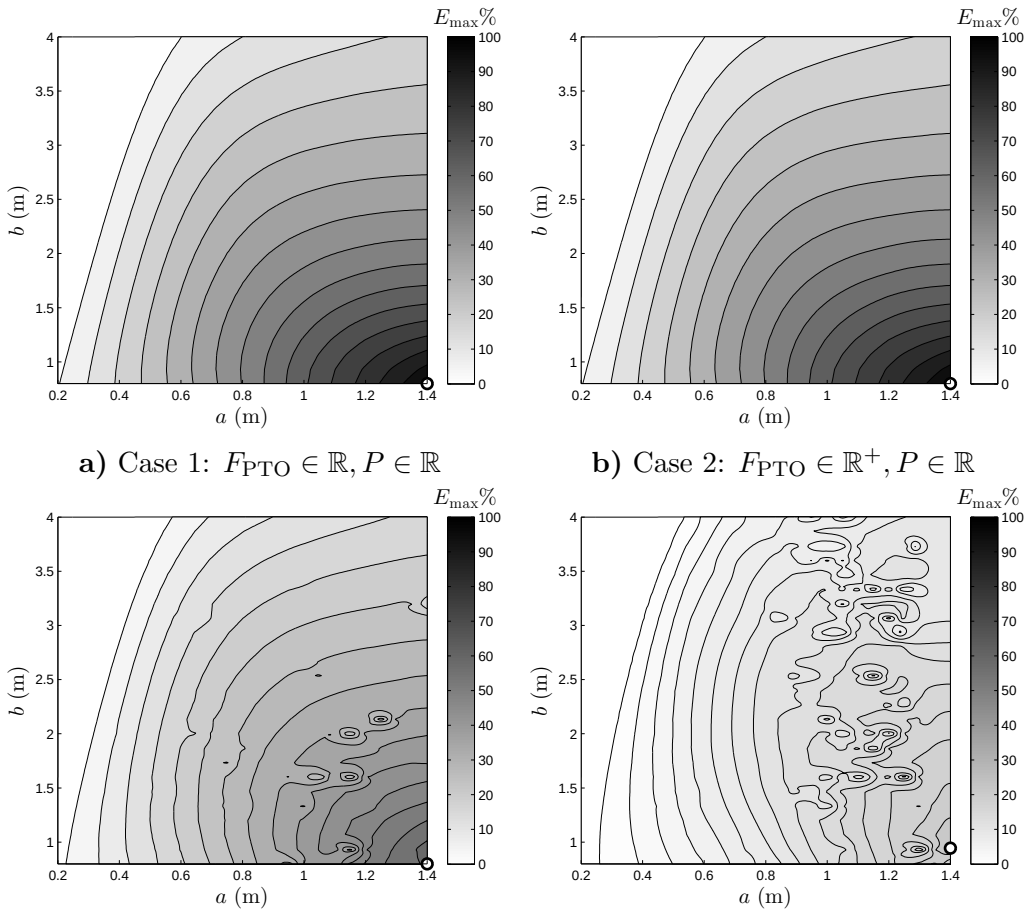

a) Case 1: $F_{\mathrm{PTO}} \in \mathbb{R}, P \in \mathbb{R}$ **b)** Case 2: $F_{\mathrm{PTO}} \in \mathbb{R}^+, P \in \mathbb{R}$

c) Case 3: $F_{\mathrm{PTO}} \in \mathbb{R}, P^+ \in \mathbb{R}$ **d)** Case 4: $F_{\mathrm{PTO}} \in \mathbb{R}^+, P^+ \in \mathbb{R}$

Figure 5.6 Energy results for all four cases in a regular wave ($E_{\max} = 3.37$ MJ and optimum located at $\circ$).

Table 5.2 Case results in a regular wave.

	Case 1	Case 2	Case 3	Case 4
a	1.4 m	1.4 m	1.4 m	1.4 m
b	0.8 m	0.8 m	0.8 m	0.933 m
R_{pen}	1×10^{-9}	1×10^{-9}	3×10^{-6}	3×10^{-6}
$\max\lvert z\rvert$	14.5 m	27.5 m	4.3 m	3.0 m
$\max\lvert \dot{z}\rvert$	11.4 m/s	11.4 m/s	6.3 m/s	3.3 m/s
$\max\lvert F_{\mathrm{PTO}}\rvert$	810.2 kN	1612.3 kN	230.9 kN	143.9 kN
$\overline{P}$	422.5 kW	422.5 kW	221.1 kW	85.5 kW

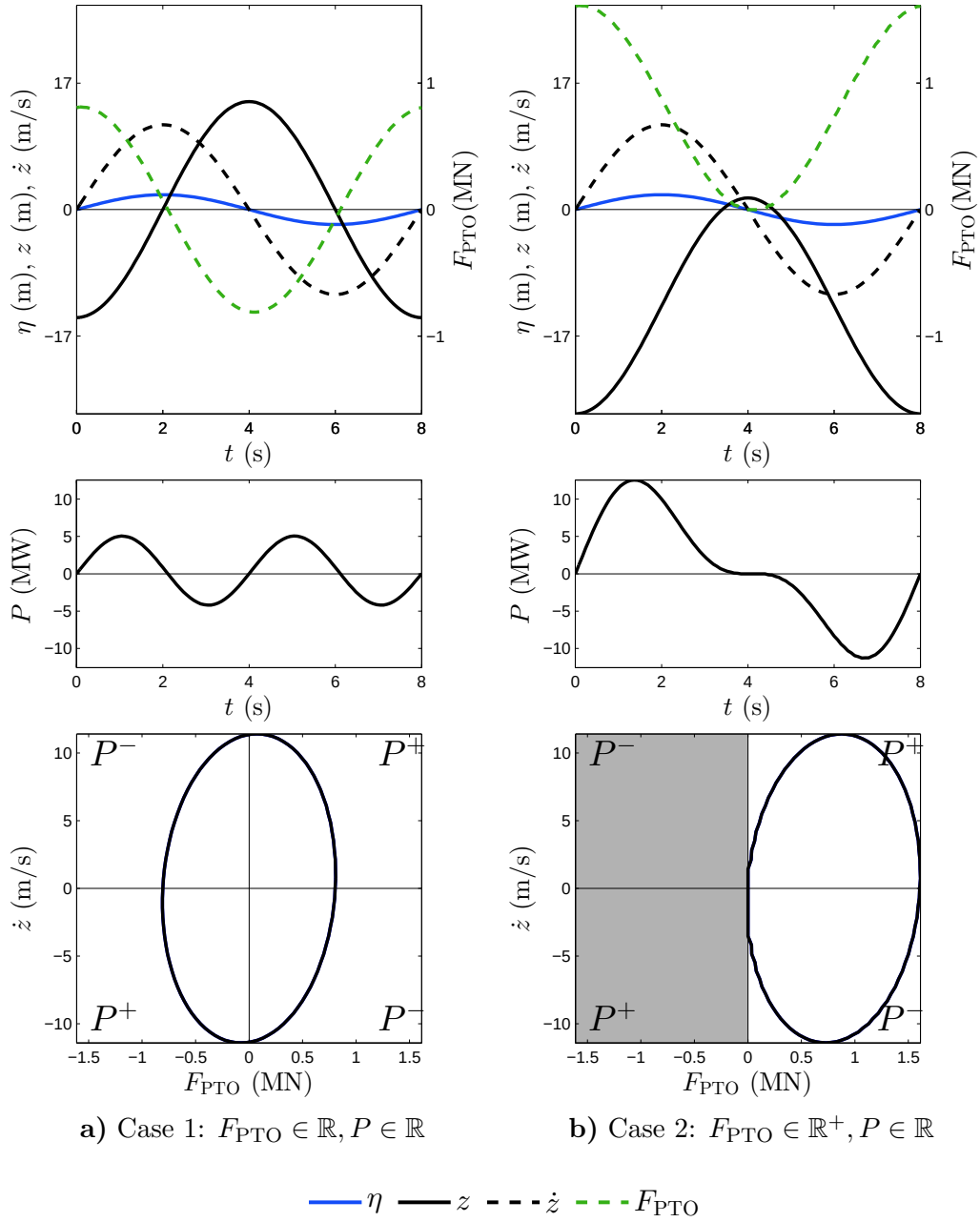

a) Case 1: $F_{\mathrm{PTO}} \in \mathbb{R}, P \in \mathbb{R}$ **b)** Case 2: $F_{\mathrm{PTO}} \in \mathbb{R}^+, P \in \mathbb{R}$

Figure 5.7 Optimal solutions for Cases 1 and 2 in a regular wave (grey shading indicates infeasible regions).

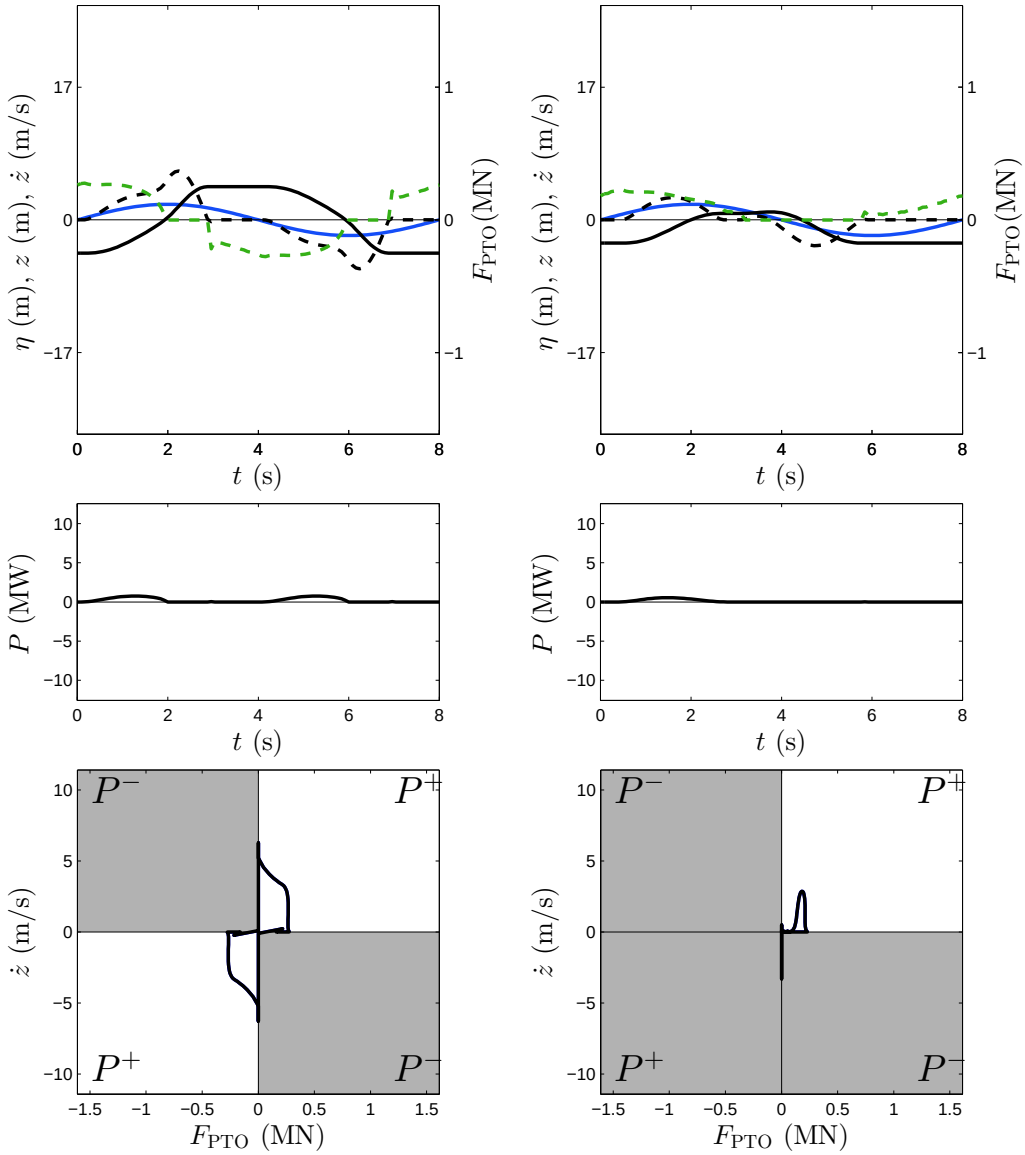

a) Case 3: $F_{\mathrm{PTO}} \in \mathbb{R}, P \in \mathbb{R}^+$ **b)** Case 4: $F_{\mathrm{PTO}} \in \mathbb{R}^+, P \in \mathbb{R}^+$

η z $\dot{z}$ F_{PTO}

Figure 5.8 Optimal solutions for Cases 3 and 4 in a regular wave (grey shading indicates infeasible regions).

energy is extracted for a much shorter time and at a lower rate. Once again, we note that neither latching nor declutching requirements were provided to the optimization algorithm—the behavior emerged naturally. Finally, the result with both the force and power constraints is shown in Fig. 5.8b. Larger periods of both latching and declutching are seen again. Only quadrant 1 is feasible but there is a special region where F_{PTO} such that the phase trajectory can extend in between quadrants 3 and 4. This is one reason behind the numerical difficulties experienced in Case 4.

Cases 1 and 2 were very dynamic; the absolute maximum velocity and position were unrealistically large. The power constrained cases had much slower dynamics, but this was at the cost of reduced energy production. Case 3 only produced 52% of the energy in Cases 1 and 2, while Case 4 produced only 20%.

5.2.2 Constrained Heaving Amplitude

Since the results in Section 5.2.1 were impractical for Cases 1 and 2, the heave amplitude was constrained (i.e., $|z| \leq 4$ m). Once again, parametric sweeps of (a, b) were performed for all four cases shown in Fig. 5.9. Adding more constraints (Case 4 has the most constraints) increased numerical difficulties, as evidenced by the numerical noise in Cases 3 and 4. The location of maximum energy extraction for each case is denoted by a white dot. Table 5.3 characterizes each of these solutions. The wave, states, and control along with instantaneous power and phase space are plotted for each of the four cases in Figs. 5.10 and 5.11.

Observing Fig. 5.11b, we see that the results from Case 4 are nearly the same as the unconstrained case. Some minor differences are most likely due to the final penalty parameter value. Once again, latching and declutching are present. The solutions are nearly the same since the heaving amplitude constraint was not violated in the previous study (i.e., $\max|z| = 3$ m). All the other cases did violate the constraint, so their motion needed to be reduced.

Cases 1 through 3 exhibited latching behavior in order to reduce the motion of the WEC. In Case 1, we see a slight amount of reactive power and symmetric, mostly harmonic velocity trajectories when extracting power. When compared to Case 3, the phase space must avoid quadrants 2 and 4; there-

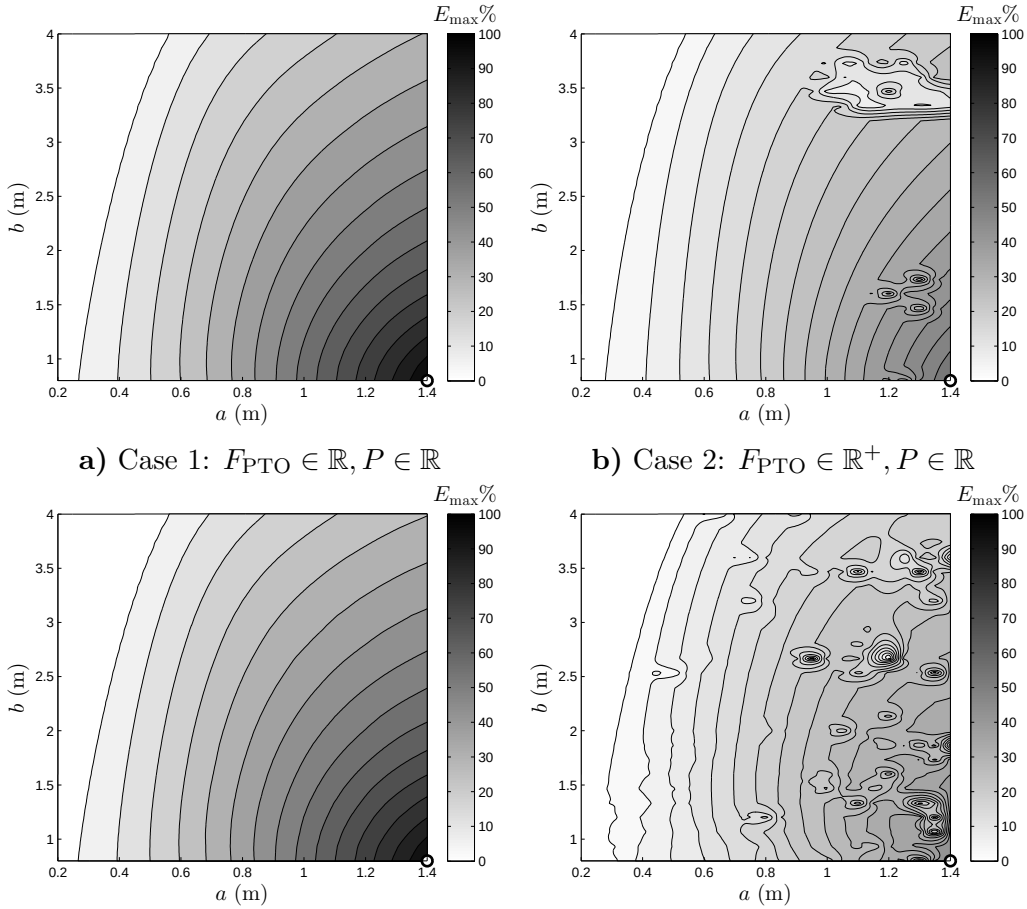

a) Case 1: $F_{\text{PTO}} \in \mathbb{R}, P \in \mathbb{R}$

b) Case 2: $F_{\text{PTO}} \in \mathbb{R}^+, P \in \mathbb{R}$

c) Case 3: $F_{\text{PTO}} \in \mathbb{R}, P \in \mathbb{R}^+$

d) Case 4: $F_{\text{PTO}} \in \mathbb{R}^+, P \in \mathbb{R}^+$

Figure 5.9 Energy results for all four cases in a regular wave with $|z| \leq 4$ m ($E_{\max} = 1.75$ MJ and optimum located at $\circ$).

Table 5.3 Case results in a regular wave with $|z| \leq 4$ m.

	Case 1	Case 2	Case 3	Case 4
a	1.4 m	1.4 m	1.4 m	1.4 m
b	0.8 m	0.8 m	0.8 m	0.8 m
R_{pen}	1×10^{-7}	5×10^{-7}	3×10^{-6}	1×10^{-5}
$\max\lvert z\rvert$	4.0 m	4.0 m	4.0 m	2.6 m
$\max\lvert \dot{z}\rvert$	4.9 m/s	3.8 m/s	5.5 m/s	2.9 m/s
$\max\lvert F_{\text{PTO}}\rvert$	328.9 kN	336.2 kN	276.7 kN	137.3 kN
$\overline{P}$	218.7 kW	122.6 kW	213.0 kW	61.7 kW

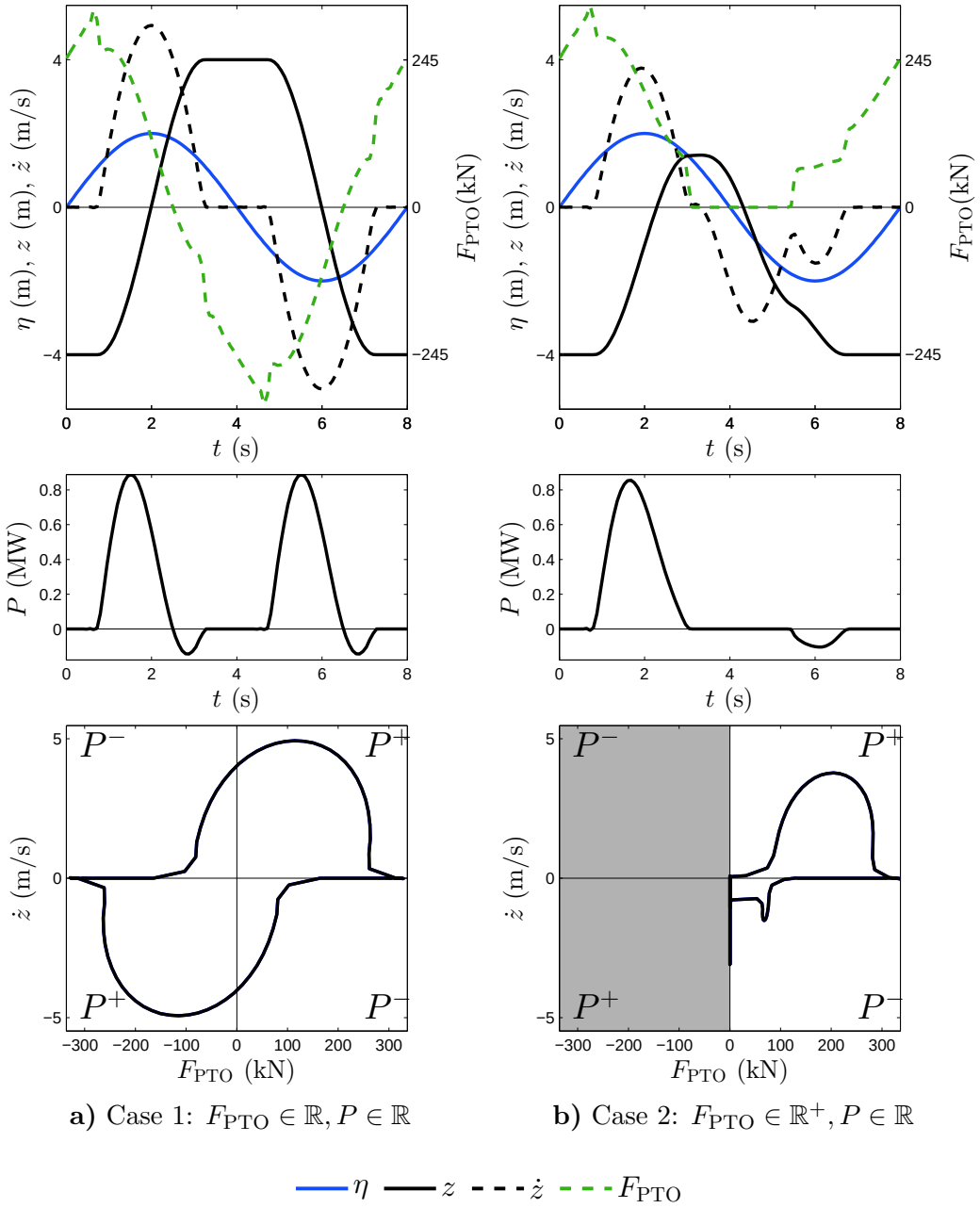

a) Case 1: $F_{\mathrm{PTO}} \in \mathbb{R}, P \in \mathbb{R}$ **b)** Case 2: $F_{\mathrm{PTO}} \in \mathbb{R}^+, P \in \mathbb{R}$

Figure 5.10 Optimal solutions for Cases 1 and 2 in a regular wave with $|z| \leq 4$ m (grey shading indicates infeasible regions).

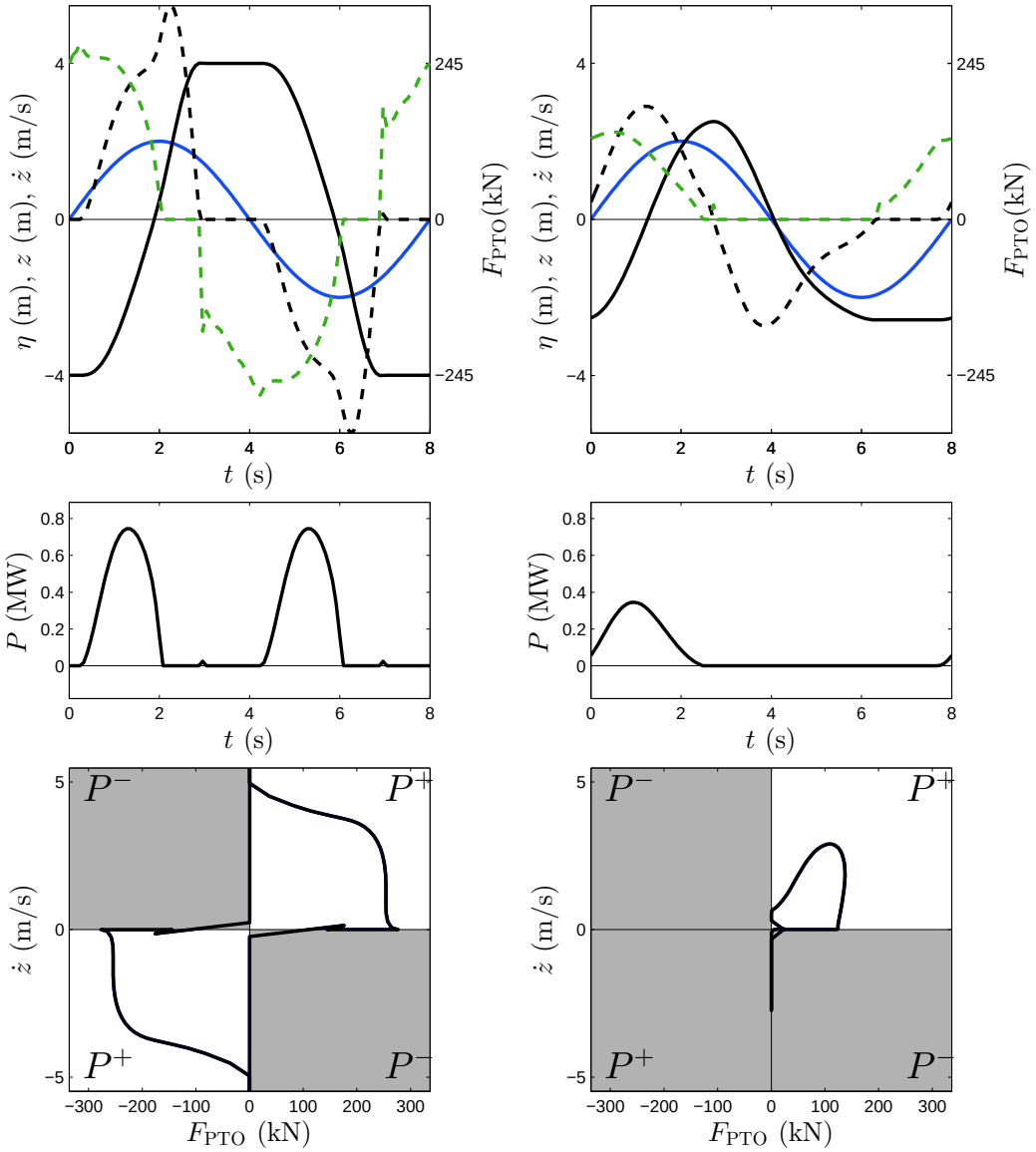

a) Case 3: $F_{\mathrm{PTO}} \in \mathbb{R}, P \in \mathbb{R}^+$ **b)** Case 4: $F_{\mathrm{PTO}} \in \mathbb{R}^+, P \in \mathbb{R}^+$

η z $\dot{z}$ F_{PTO}

Figure 5.11 Optimal solutions for Cases 3 and 4 in a regular wave with $|z| \leq 4$ m (grey shading indicates infeasible regions).

Table 5.4 Comparison of unconstrained and constrained average power results in a regular wave.

	Case 1	Case 2	Case 3	Case 4
Unconstrained	100%	100%	52%	20%
Constrained	52%	29%	50%	15%

fore, the velocity trajectories are no longer harmonic or symmetric but are still aligned with the extremums of the excitation force. Enforcing only the power constraint had a minor effect on the overall energy extraction. Case 3 was interesting because it performed the following sequence of strategies: latching, energy extraction, declutching, and reactive power. This is interesting because the extraction and reactive power trajectories were disjoint. It seems as if the reactive power helped position the excitation force and velocity during the extraction period.

In Table 5.4, the percentage of energy extracted relative to the maximum is shown. We notice that the power constraint degrades performance more in the unconstrained case. In addition, the force constraint did not degrade the energy extraction in the unconstrained study, but did severely in the constrained study, even more so than the power constraint. The force constraint in both studies produced one large "hump" of energy extraction. With the freedom to position the HC, the magnitude of this hump was severely limited. When both constraints are enforced, the energy results are poor. Therefore, if we can create a PTO design that does not require both of these constraints, a reasonable amount of energy production relative to the maximum is possible.

5.2.3 Final Penalty Parameter Values

Since Algorithm 1 was used to find the appropriate value for R_{pen}, we can observe the final values at each point in the plant design space. The final values for R_{pen} for the unconstrained and constrained studies are in Figs. 5.12 and 5.13.

For the unconstrained study, increasing a typically resulted in a small final value for R_{pen}. Larger values of a directly result in larger forces. Since the regularization procedure essentially limits the force if R_{pen} is too large, it is

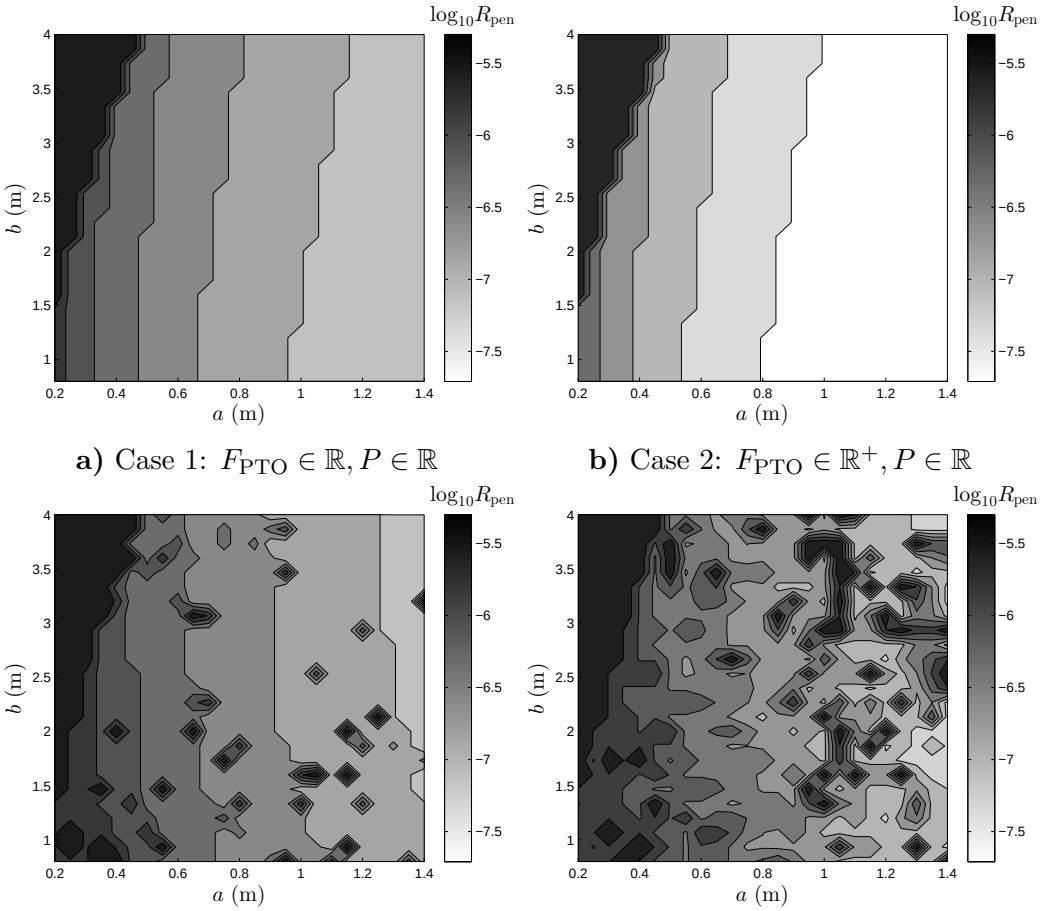

a) Case 1: $F_{\text{PTO}} \in \mathbb{R}, P \in \mathbb{R}$

b) Case 2: $F_{\text{PTO}} \in \mathbb{R}^+, P \in \mathbb{R}$

c) Case 3: $F_{\text{PTO}} \in \mathbb{R}, P \in \mathbb{R}^+$

d) Case 4: $F_{\text{PTO}} \in \mathbb{R}^+, P \in \mathbb{R}^+$

Figure 5.12 Final R_{pen} values for all four cases in a regular wave.

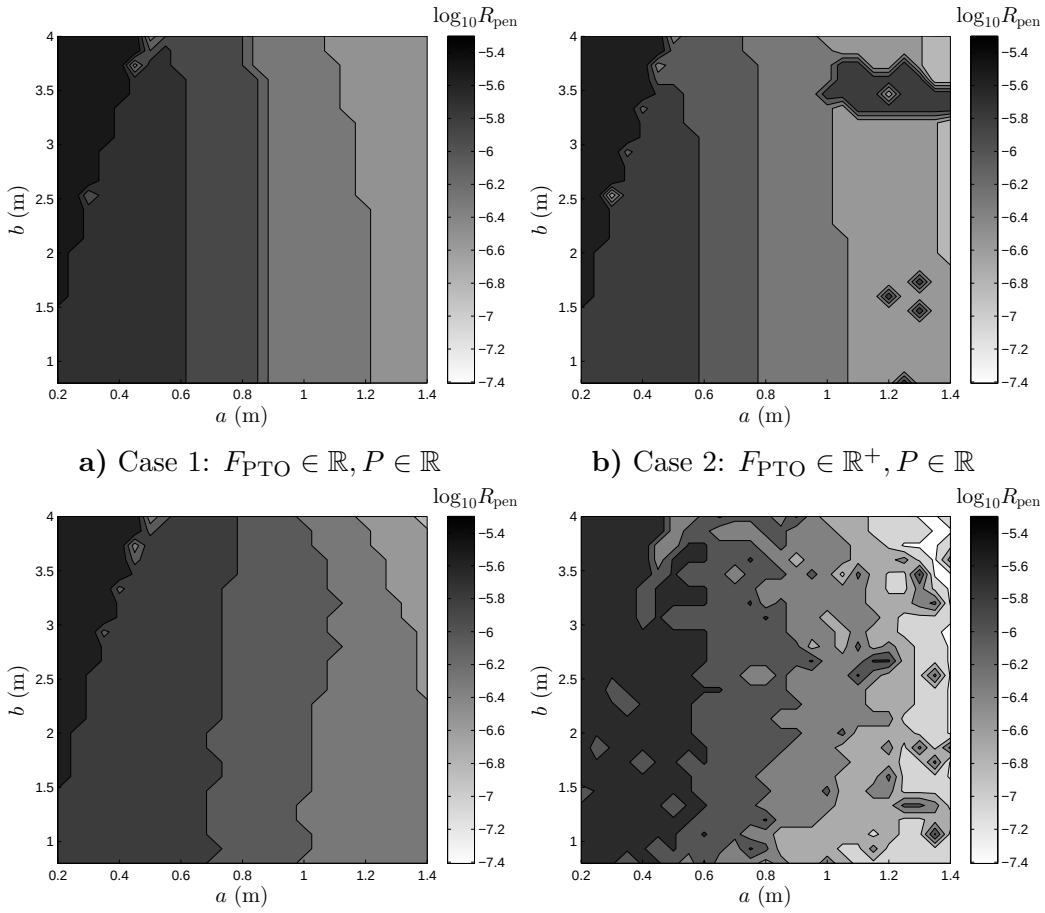

a) Case 1: $F_{\text{PTO}} \in \mathbb{R}, P \in \mathbb{R}$

b) Case 2: $F_{\text{PTO}} \in \mathbb{R}^+, P \in \mathbb{R}$

c) Case 3: $F_{\text{PTO}} \in \mathbb{R}, P \in \mathbb{R}^+$

d) Case 4: $F_{\text{PTO}} \in \mathbb{R}^+, P \in \mathbb{R}^+$

Figure 5.13 Final R_{pen} values for all four cases in a regular wave with $|z| \leq 4$ m.

natural to expect that larger optimal forces require a smaller final value for R_{pen}. This can directly be observed when comparing Cases 1 and 2 because they both have the same energy results. The forces required in Case 2 are much larger, so the final values of R_{pen} are smaller when compared to Case 1. Cases 3 and 4 experienced a significant amount of numerical sensitivity to the final value of R_{pen}, although the general trend was that equivalent points in the design space had larger final values of R_{pen} when compared to Cases 1 and 2.

For the constrained study, the results had similar trends. In general, the final values for R_{pen} in this study were larger than in the unconstrained study because the forces were generally lower.

5.2.4 Wave Period Sensitivity

Another sensitivity study was performed on the wave's period. This is similar to the 'Budal diagram' that explores the upper bounds on extractable energy available to a WEC [132]. This study can be seen in Figs. 5.14 and B.3 with the Case 1 assumptions ($a = 1$ m, $b = 2$ m). For the unconstrained case in Fig. 5.14a, the average power increases with T, similar to Eqn. (4.11). However, the resulting state trajectories are highly dynamic, i.e., both the heaving amplitude and velocity are quite large (see Fig. B.3a). Therefore, it is common to impose symmetric bounds on the heave amplitude to produce more realistic results.

The constrained amplitude results are shown in Fig. 5.14b. For small values of T, the results between the two formulations are the same because the maximum amplitude does not naturally exceed 4 m (see Fig. B.3b and note the increasingly step-like behavior of the position trajectory). After this point, energy production decreases as the wave period length increases. This result is consistent with the second upper power bound in the Budal diagram. This corresponds to when the WEC's swept volume (but not the wave energy available in the sea) is exploited as much as possible [132]. However, the HC still would leave the water during the regular wave period, motivating the use of the asymmetric position path constraint in Eqn. (4.39).

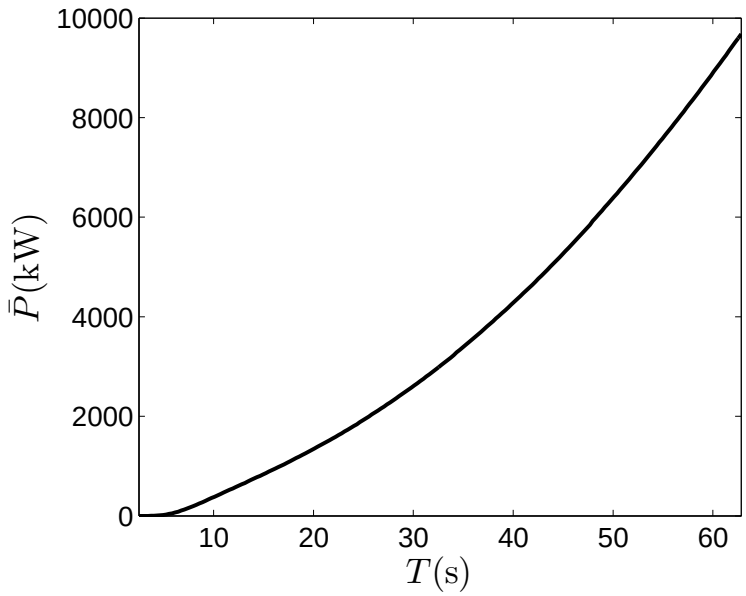

a) Unconstrained

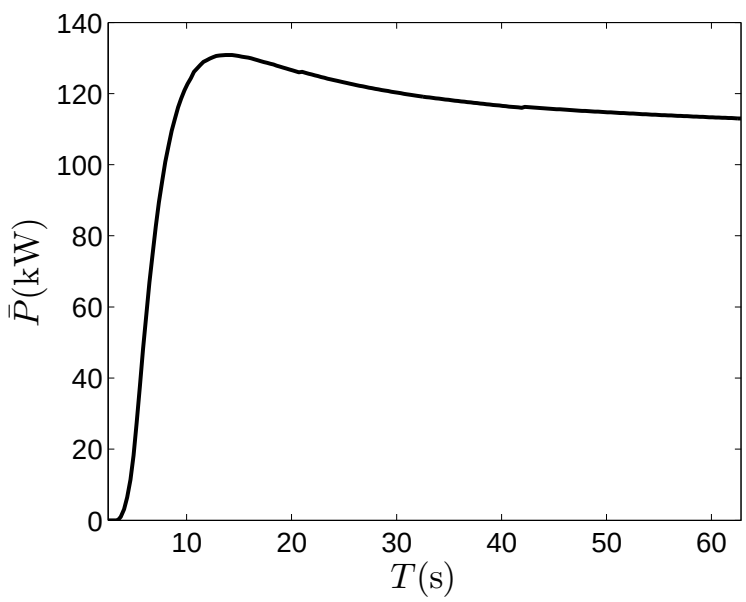

b) Constrained by $|z| \leq 4$ m

Figure 5.14 Sensitivity study on regular wave period length with both unconstrained and constrained heave amplitude.

5.2.5 Normalized Energy Results and Resonance

The energy results presented in Figs. 5.6 and 5.9 might not be aligned with the true design goal because an increasing HC radius results in more available energy since the capture width is larger. Therefore, we can normalize the energy values by dividing each point in the design space by $2a$ (i.e., making this modification directly on Figs. 5.6 and 5.9). These normalized results are presented in Fig. 5.15 for a select few cases. We note that the optimum locations are still located at the same positions. However in many cases for a fixed value of b, there is an optimal a that is in the interior of our design space.

To better under this observation, let us consider the resonance condition in Eqn. (4.35). Nondimensionalizing the added mass coefficient to $\mu(\omega) = m_r(\omega)/(\rho\pi a^2 b)$, the optimal draft can be calculated such that the HCWEC resonates with the incoming regular wave:

$$b = \frac{g}{\omega^2 \left(1 + \mu(\omega)\right)} \tag{5.2}$$

This is consistent with statements in Ref. [27, p. 185]. The maximum value $\mu(\omega)$ attains in our feasible design space is ≈ 0.94. The angular frequency these studies was $2\pi/T = 0.79$ rad/s. Therefore, the smallest possible b would be 8.2 m, which is outside our current feasible design space. However, the results are not trending toward large values of b, but smaller ones. Smaller b values indicate higher frequency (or lower period) devices. Why might this be the case? The resonance condition is a statement of when the intrinsic reactance vanishes, not when energy production is maximized. The excitation force depends on the plant design, i.e., a and b. In Fig. 4.5, we note the slender cylinders (i.e., $a \ll b$) result in smaller values of R_r while disk-like cylinders (i.e., $a \gg b$) result in larger values. The excitation force is proportional to the square root of R_r (see Eqn. (4.27)) so we favor larger excitation forces rather than resonance. The local optimums for fixed values of b might be an ideal trade-off between resonance and excitation force.

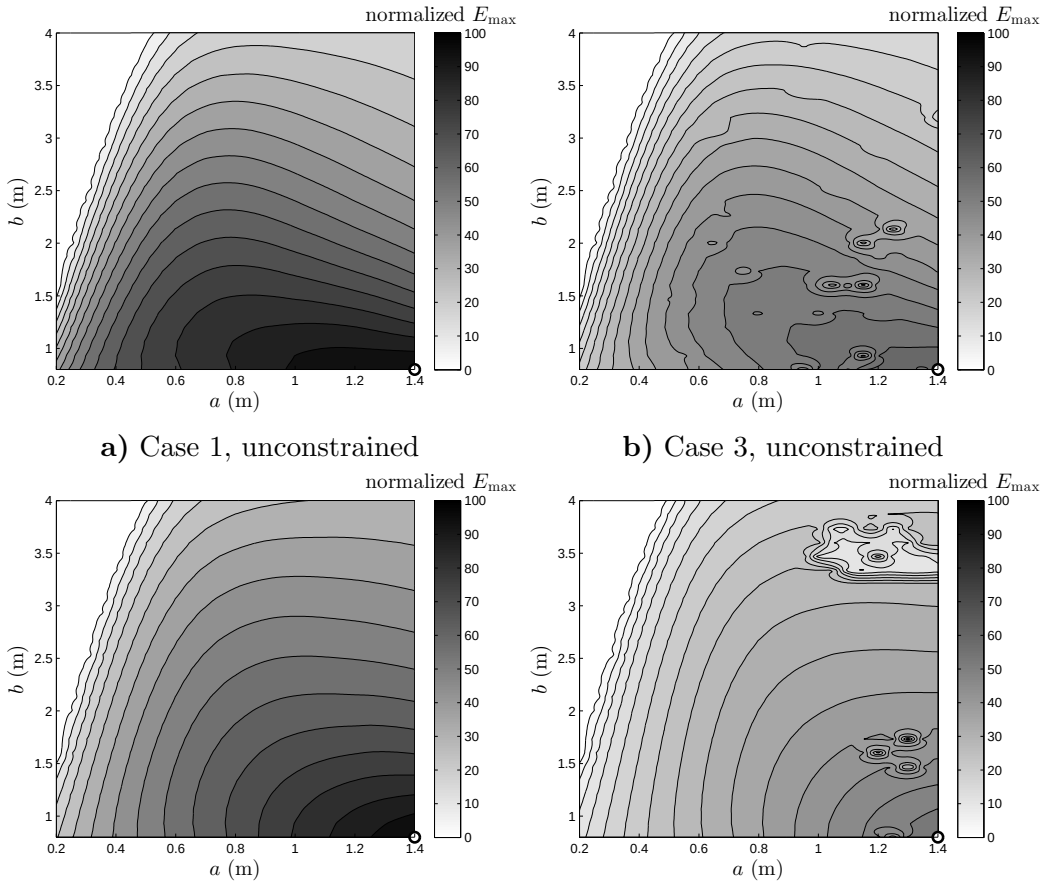

a) Case 1, unconstrained

b) Case 3, unconstrained

c) Case 1, $|z| \leq 4$ m

d) Case 2, $|z| \leq 4$ m

Figure 5.15 Energy results normalized by the HCWEC's radius for a variety of cases (optimum located at ∘).

5.3 Irregular Waves

This section will discuss optimal energy extraction in irregular waves. All studies use GPOPS-I[3] to formulate the NLP, which employs the pseudospectral method with LGR points and an *hp*-adaptive mesh refinement approach [63]. This software package also uses SNOPT® to solve the underlying sparse optimization problem. The complete WEC design problem including the slamming constraint was considered. Because all cases in regular waves tended towards the same plant design ($a = 1.4$ m and $b = 0.8$ m), this was assumed to be the plant design. The initial guess for the states and control was a completely declutched WEC (i.e., $F_{\text{PTO}} \equiv 0$) obtained through a for-

[3]Current version available for licensing at `http://www.gpops2.com/`

Table 5.5 Parameters for irregular wave studies.

Parameter	Value	Parameter	Value
$H_{1/3}$	4 m	seed	10000
T_p	8 s	t_f	62.832 s
h	10 m	`setup.derivatives`	complex
$F_{\text{PTO,max}}$	10^8 N	`setup.mesh.tolerance`	10^{-5}
$\dot{z}_{\text{max}}$	10 m/s		

Table 5.6 Case results in an irregular wave.

	Case 1	Case 2	Case 3	Case 4
R_{pen}	1×10^{-6}	3×10^{-6}	5×10^{-6}	4×10^{-6}
$\max\lvert z\rvert$	9.2 m	5.3 m	3.4 m	3.5 m
$\max\lvert\dot{z}\rvert$	6.5 m/s	4.7 m/s	3.4 m/s	3.2 m/s
$\max\lvert F_{\text{PTO}}\rvert$	551.6 kN	278.7 kN	185.9 kN	210.1 kN
$\overline{P}$	85.1 kW	44.6 kW	33.8 kW	25.4 kW
$\hat{\mathcal{L}}$	-3.7×10^6	-1.6×10^6	-5.0×10^5	-1.5×10^5
$\lvert\dot{z}\rvert \leq 10^{-3}$	0%	0%	23%	33%
$\lvert F_{\text{PTO}}\rvert \leq 10^{-3}$	0%	36%	23%	42%

ward simulation of the derivative function. In addition, the sparsity pattern was given manually. Some additional parameters used are listed in Table 5.5. Poor results occurred if the optimization algorithm terminated due to reaching the maximum iterations because the next mesh refinement iteration had a poor solution to generate the new mesh.

5.3.1 Irregular Wave Cases

The optimal states, control, and power trajectories for Cases 1 to 4 are illustrated in Figs. 5.16 to 5.19. Finally, the results are summarized in Table 5.6. In Case 1 in Fig. 5.16, we see strong levels of active control; the WEC is nearly pulled to the bottom twice. This maneuver requires a lot of reactive power, but results in large positive power spikes and typically occurs right before the wave increases in elevation. The force trajectory was on the positive side. This differs from results in a regular wave for Case 1, which was symmetric. The solution seems to indicate that extremums of the excitation

force and velocity should be in phase (the reactive control condition) but was not fully realized, perhaps due to the various constraints imposed. Overall, the solution focused on extracting the most energy during the largest variations in η. For Case 2 in Fig. 5.17, the resulting solution was similar to Case 1 except the magnitudes of z and $\dot{z}$ were smaller. PTO was declutched for 36% of the entire time horizon. Since a negative PTO force could not assist in placing the WEC in the proper position for maximum energy extraction, the overall dynamics were less intense.

Cases 3 and 4 were challenging to solve. The drop-off shown in Fig. 5.4 was hard to find and results slightly away from the ideal value of R_{pen} had poor energy production. The values of R_{pen} selected still have some unrealistic and nonoptimal PTO force spikes. Case 3 in Fig. 5.18 showed a fair amount latching, which might be surprising because latching requires unique control trajectories. Declutching was also seen and 46% of the entire solution was in either of these states. The magnitude of the power trajectory is much smaller than when the power constraint was not enforced; however, the energy production was only 24% less than Case 2. Case 4 in Fig. 5.19 spent 75% of the time in either latching or declutching. The amount of time latched was more than Case 3, which was the opposite from the results based on regular waves.

All four cases tried to align the excitation force and velocity as best as they could under their various constraints. Similar to the unconstrained results in regular waves, the relative energy results were:

$$E_1 > E_2 > E_3 > E_4 \tag{5.3}$$

Also, the maximum velocity decreased with decreasing energy production. The phase spaces of the objective function are in Figs. B.4 and B.5. The general trajectories are similar to their regular wave counterparts. Some points may stray into the infeasible regions either due to the numerical issues or the fact that the path constraints are not checked in between the collocated points. Finally, a visualization of the position path constraint ($z - \eta \leq b$) is shown in Fig. B.6. Note that in all four cases, this constraint was active during specific parts of the time horizon. Case 1 exhibited extended periods of this constraint being active.

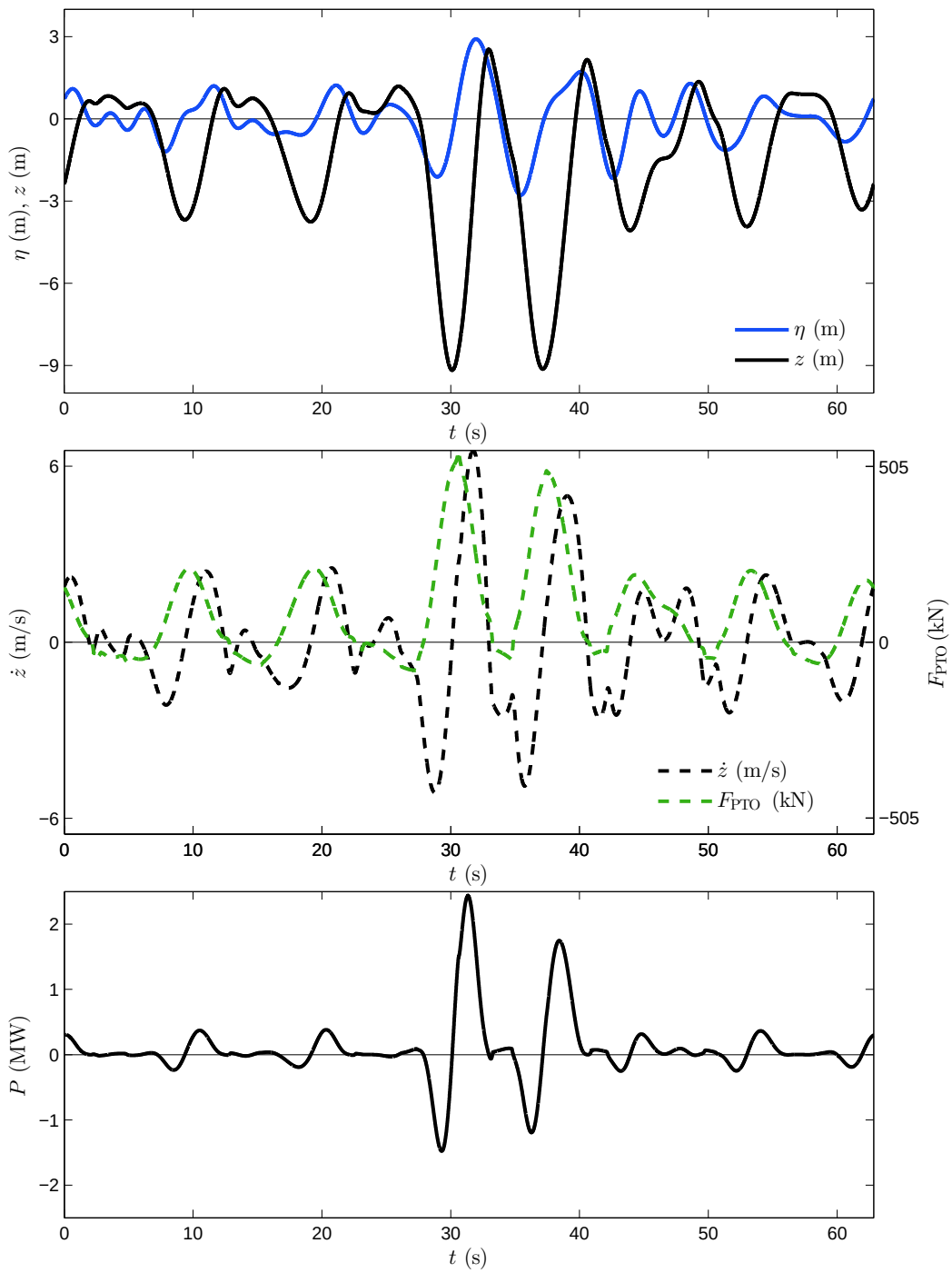

Figure 5.16 Optimal solution for Case 1: $F_{\mathrm{PTO}} \in \mathbb{R}, P \in \mathbb{R}$ in an irregular wave.

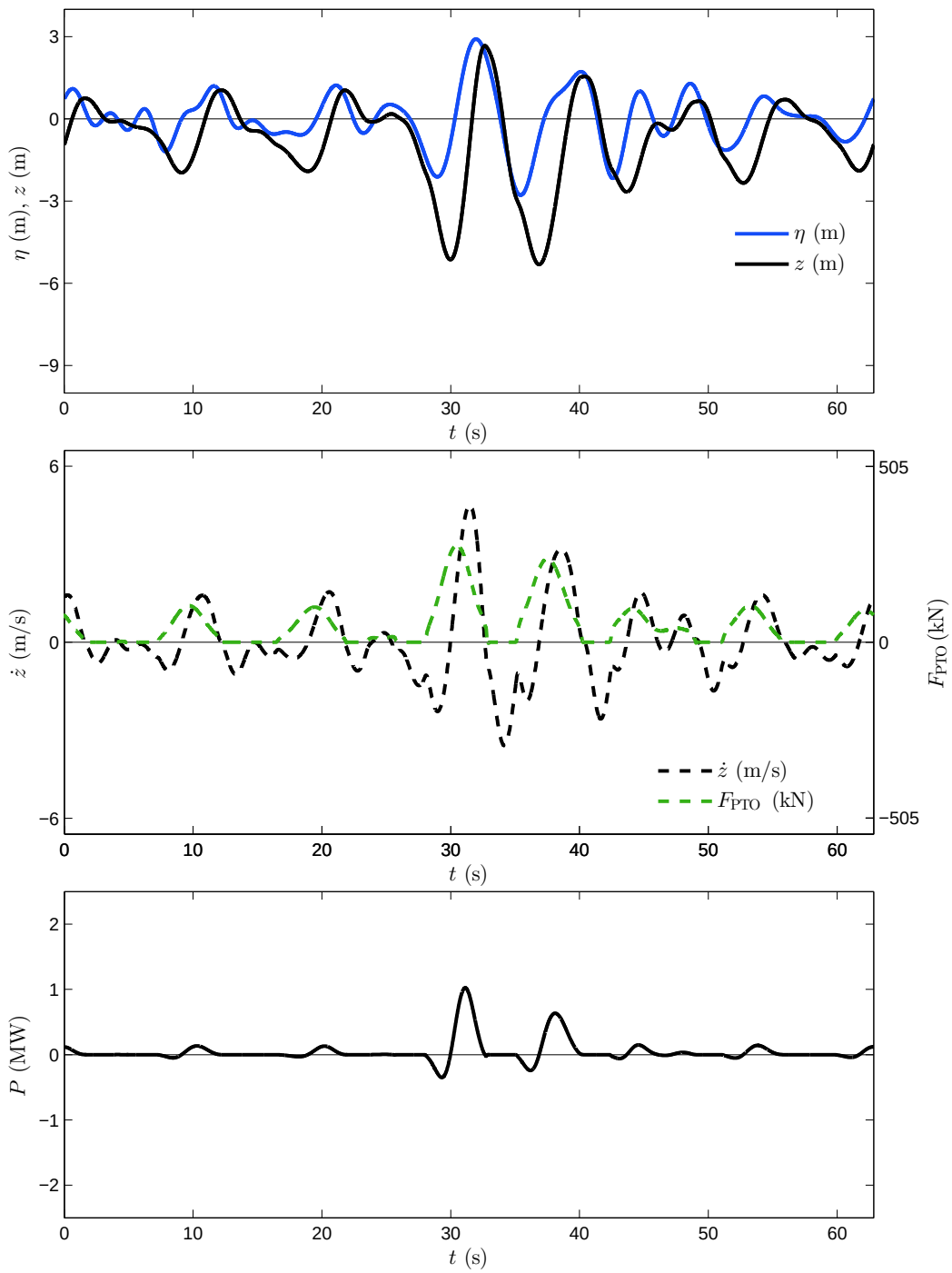

Figure 5.17 Optimal solution for Case 2: $F_{\mathrm{PTO}} \in \mathbb{R}^{+}, P \in \mathbb{R}$ in an irregular wave.

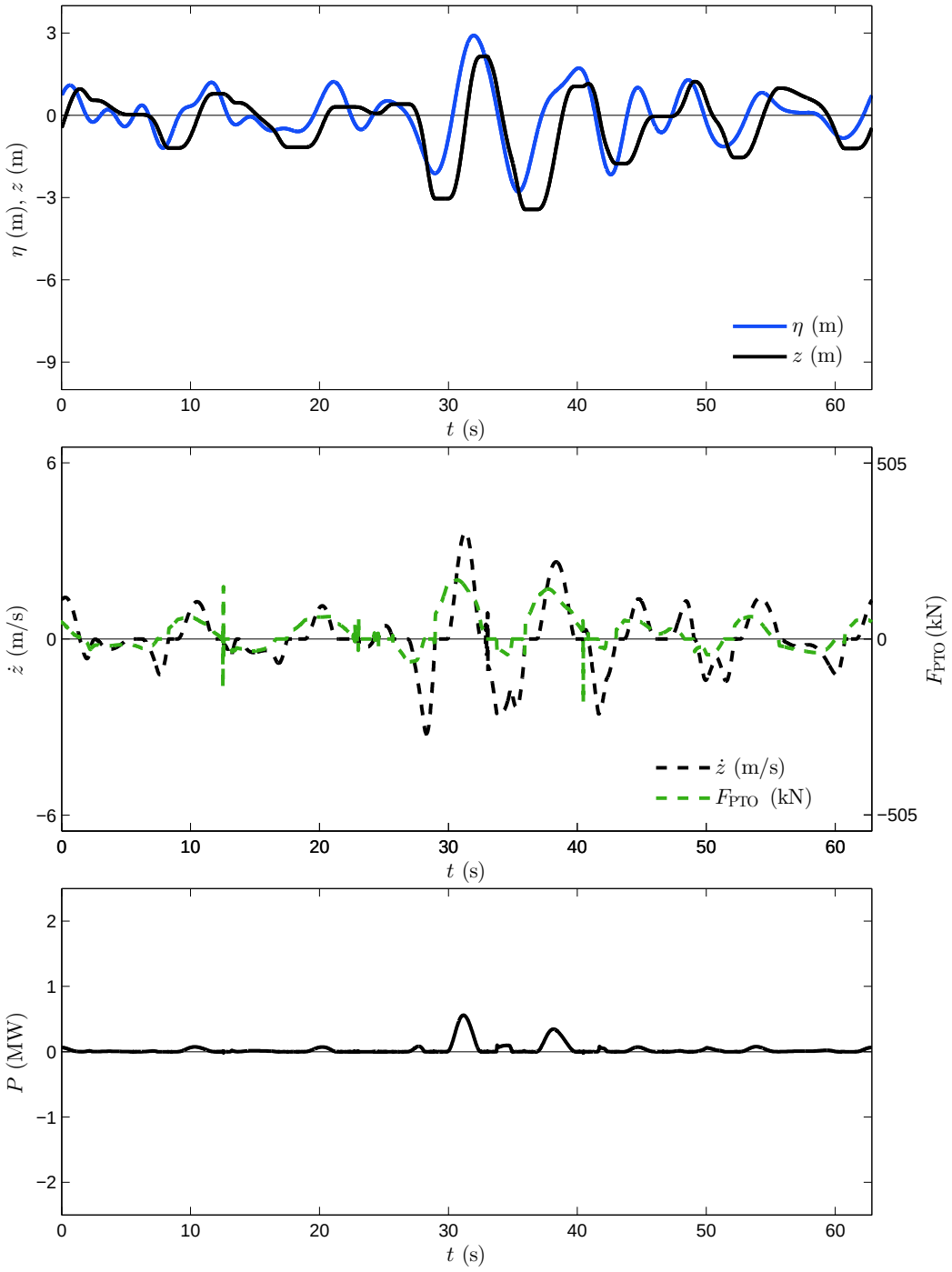

Figure 5.18 Optimal solution for Case 3: $F_{\mathrm{PTO}} \in \mathbb{R}, P \in \mathbb{R}^{+}$ in an irregular wave.

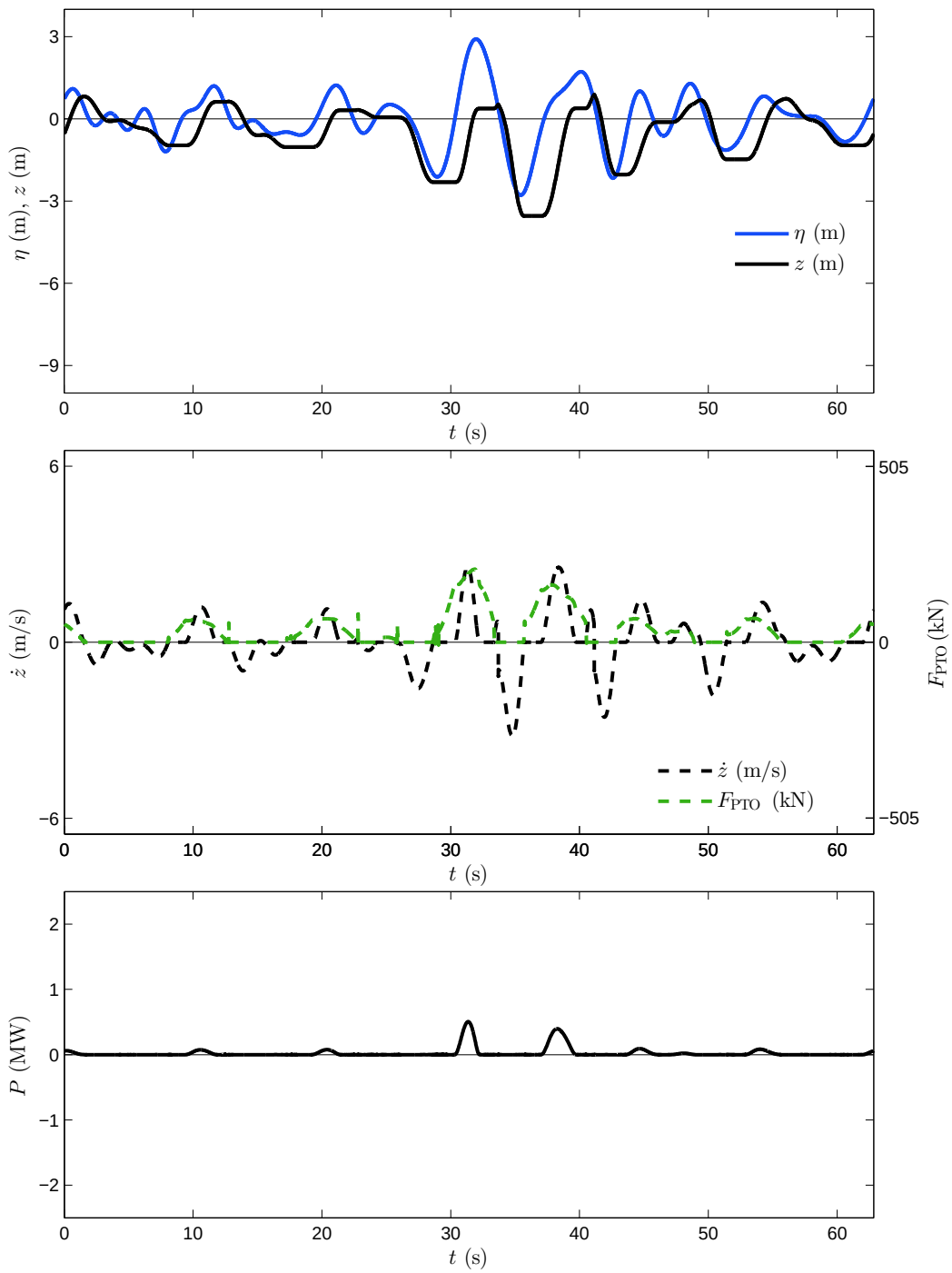

Figure 5.19 Optimal solution for Case 4: $F_{\mathrm{PTO}} \in \mathbb{R}^+, P \in \mathbb{R}^+$ in an irregular wave.

5.3.2 Maximum Instantaneous Power Bound Study

A WEC PTO must handle the largest value of the instantaneous power that may occur, adding to system expense, and potentially sacrificing its cost to production ratio. A power constraint (i.e., $|P| \leq C_{\max}$), $C_{\max}$ is the maximum allowed power) was added to Case 1 to investigate this practical design issue. This bound was varied from 200 kW down to 10 kW. The results are shown in Fig. 5.20 with R_{pen} increased to 10^{-5} to produce intuitive solutions for all values of $C_{\max}$. As expected, energy extraction decreases with $C_{\max}$. Increasing beyond 135 kW does not improve energy performance noticeably. In fact, when the maximum power is limited to $C_{\max} = 53$ kW, the energy production is still 80% of the maximum, potentially improving the energy/cost ratio. To illustrate system behavior more clearly, the power trajectory is plotted for a few select values of $C_{\max}$ in Fig. 5.21. As the maximum power is reduced, flat spots appear at the power bound. The width of these flat spots increases with decreasing $C_{\max}$, allowing the WEC to produce more energy than if the power trajectory for the unconstrained case was simply "cut" at the bound. In addition to reducing PTO power requirements, introducing the power bound results in a more consistent power level, which is desirable for grid integration.

One way to visualize these constrained solutions is to once again observe the phase space of the objective function. We can draw curves that represent constant power with $C_{\max} = \dot{z}F_{\text{PTO}}$, which forms a rectangular hyperbola when plotted. This is plotted for two different values of $C_{\max}$ in Fig. 5.22. Note the large portions that conform to the maximum power lines. This study is an excellent example of the complex constraints that can be imposed when using DT.

This completes the numeric studies on WEC design. Dynamic system design optimization utilizing direct transcription identified both control and plant design strategies to maximize energy production and produce realistic WECs. Some of these strategies were already found in the literature but in this work, a single approach was applied to identify them and is capable for more detailed studies in the future.

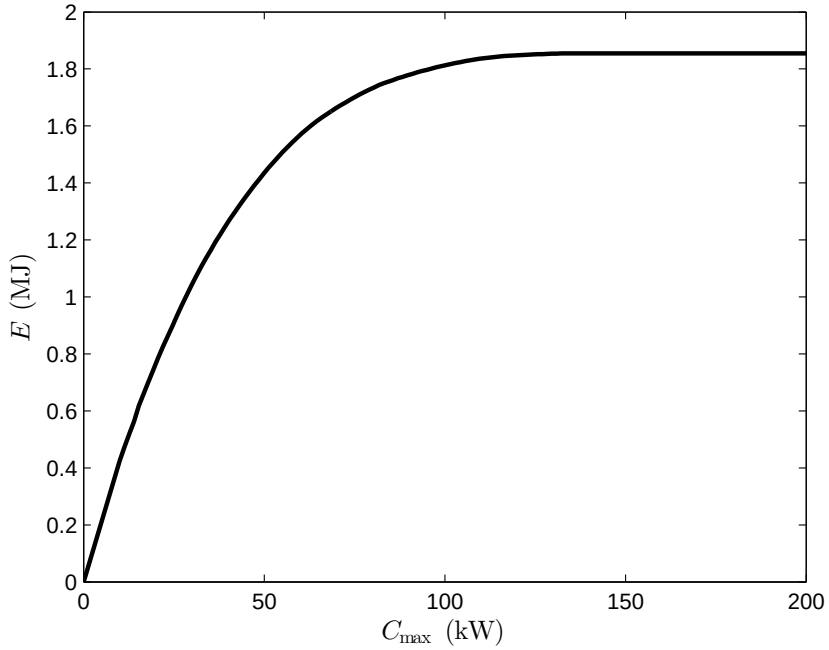

Figure 5.20 Energy extraction vs. $C_{\max}$ for Case 1.

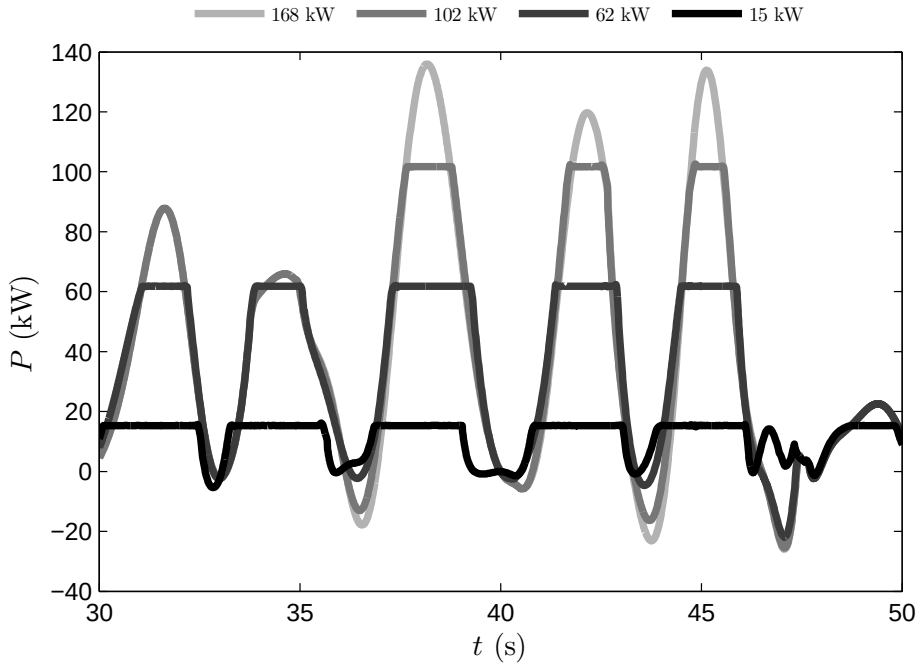

Figure 5.21 Power trajectory for various levels of $C_{\max}$ for Case 1.

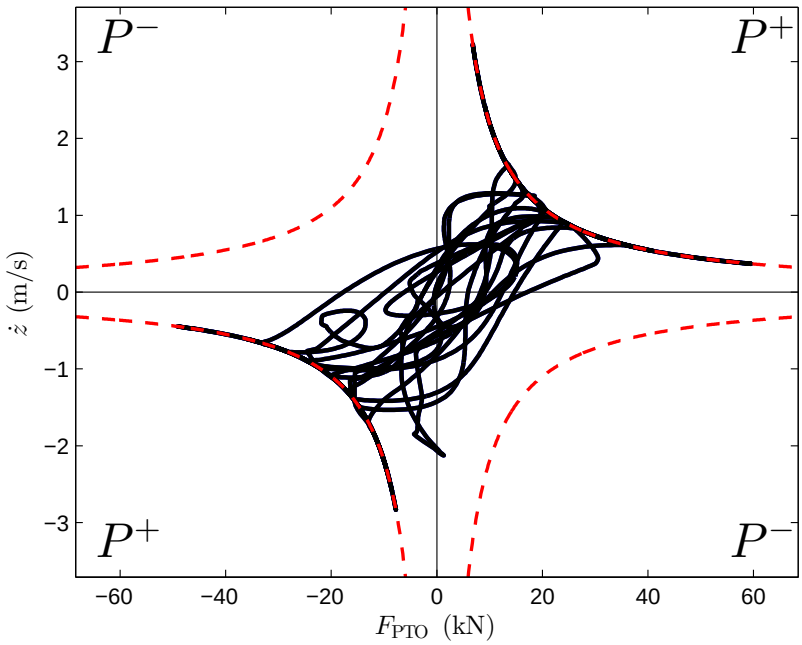

a) $C_{\max} = 22$ kW

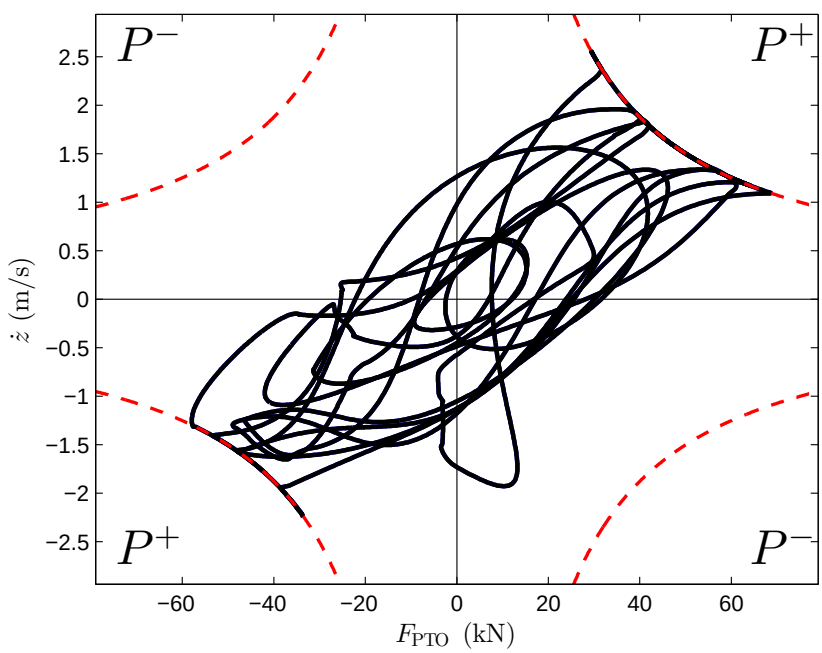

b) $C_{\max} = 75$ kW

Figure 5.22 Phase space of the objective for two levels of maximum power (red dotted lines indicate maximum power curve).

Chapter 6

Conclusion

6.1 Thesis Summary

This thesis focused on three primary topics: dynamic system design optimization, direct transcription, and wave energy converter design. The WEC design problem served as an excellent example of the applicability of the first two topics on a challenging dynamic system design problem.

Dynamic System Design Optimization — An essential ingredient in an ODSD problem is the natural inclusion of the dynamics. The dynamics of the system commonly depend on both the physical and control design elements; therefore, only a formulation that directly considers the interaction between the two can produce the optimal system dynamics. An ODSD formulation is a general methodology for properly formulating this type of problem. Many different types of objectives and constraints can be included naturally. However, this can be a challenging problem to solve in particular because DAEs need to be solved efficiently. Indirect methods for optimal control were denoted "undesirable" since their formulations contain multiple BVPs, numerically sensitive costate calculations, and an inability to efficiently handle inequality constraints. Additionally, sequential system design is always undesirable since it does not account for the coupling between the plant and control designs, resulting in suboptimal system designs. Simultaneous and nested co-design utilizing DT was identified as the most promising solution approaches.

Direct Transcription — This class of methods enables us to perform simultaneous analysis and design of the dynamics. This is accomplished by parametrizing both the state and control trajectories and adding a large number of equality constraints that ensure feasible dynamics. Two main approaches were identified: local collocation (or time-marching methods) and

global collocation (or pseudospectral methods). In addition to favorable convergence properties and the ability to handle unstable DAEs, DT can be used on singular optimal control problems and for early-stage design.

Wave Energy Converter Design — The numerical studies on the WEC design problem provided a number of insights. First, disk-like cylinders were preferred (i.e., $a \gg b$). This was attributed to the increase in excitation force. Typically, WECs are designed to resonate with the incoming wave but this assumes that the excitation force in independent of the plant design. Second, a number of previous optimal WEC control strategies were identified in the results. In a regular wave without any constraints, the excitation force and optimal velocity were exactly in phase, which is the reactive control condition. However, the unconstrained solutions were highly dynamic and required large amounts of reactive power. Other identified control strategies included latching and declutching. It is important to note that these strategies emerged naturally, not as part of the design formulations, but instead because of DT's flexibility.

A number of cases were examined to explore the design tradeoffs that commonly are experienced when designing a WEC PTO including asymmetric force and power constraints. Case 1 always extracted the most energy, although Case 2 extracted the same amount when only the force constraint was imposed. Generally, the power constraint degraded performance more than the force constraint in both regular and irregular ocean waves. However, imposing a constraint on the heaving amplitude reversed this observation. Imposing both force and power constraints produce extremely poor energy results. Therefore, if we can create a PTO design that does not require both of these constraints, a reasonable amount of energy production relative to the maximum is still possible. The final study was on the sensitivity of maximum instantaneous power. As expected, energy extraction decreases as we decrease this bound. However, we can still extract a substantial percentage of the maximum energy while limiting actuator peak power (and hence system expense). This study was an excellent example of the complex constraints that can be imposed when using DT.

6.2 Future Work

A number of future work items were identified that have the potential to improve the design of WECs and more general dynamic engineering systems:

(1) Validation of the proposed effectiveness of problem formulations for ODSD in Table 2.1 through the enumeration of all possible combinations.

(2) Further investigation into the applicability of local and global collocation methods on co-design problems especially problems with highly nonlinear plant constraints.

(3) Further investigation into the applicability of local and global collocation methods on singular optimal control problems and potential methods to improve their solutions.

(4) The development of a methodology to accurately transfer identified open-loop control solutions to realistic control systems including the physical components and closed-loop feedback laws.

(5) A fair comparison between the numerical results in this thesis to previously identified optimal solutions for WEC design.

(6) More detailed WEC design studies which could include accurate in-the-loop calculations of the radiation impedance for other topologies (i.e., not limited to a heaving cylinder), realistic PTO architectures still utilizing open-loop control to identify the system performance limits, and optimal design under a variety of sea states.

Appendix A

Problem Structure and Sparsity Pattern for the WEC Design Problem

In this section, the general problem structure and sparsity pattern of the WEC design problem using the trapezoidal rule with equidistant points for both the defect constraints and numerical quadrature is the explained. In addition, the plant design and time horizon will be held fixed so the defect constraints are linear. This formulation lends itself to nested co-design since the plant design is held fixed while solving the OCSD subproblem. The position constraint in Eqn. (4.39) is not included in this formulation but would also be a linear constraint.

If the above assumptions and numerical methods are used, the WEC design problem can be represented as a quadratically constrained quadratic program (QCQP) [137, pp. 152-153]:

$$\min_{\mathbf{x}} \quad \frac{1}{2}\mathbf{x}^T\mathbf{H}\mathbf{x} + \mathbf{G}^T\mathbf{x} \tag{A.1a}$$

subject to:

$$\mathbf{A}\mathbf{x} = \mathbf{b} \tag{A.1b}$$

$$\mathbf{x}^T\mathbf{P}_i\mathbf{x} + \mathbf{q}_i^T\mathbf{x} + r_i \leq \mathbf{0} \quad \{i \mid i \in \mathbb{N}, i \leq n_q\} \tag{A.1c}$$

where $\mathbf{H}$, $\mathbf{G}$, $\mathbf{A}$, $\mathbf{b}$, $\mathbf{P}_i$, $\mathbf{q}_i$, and r_i are constant and $\mathbf{H}$ is symmetric. If Eqn. (A.1c) is not present, the problem is called a quadratic program (QP). This leads to especially efficient solution [137, pp. 152-153]. Without the power constraint (Cases 1 and 2), the resulting problem can be formulated as a QP. With the additional power constraint (Cases 3 and 4), the WEC design problem can be formulated as a QCQP.

A.1 Hessian Calculation

We will start by defining the quadratic objective function. Recall the composite trapezoidal rule on a uniform grid is given in Eqn. (3.24). Note that the regularized objective function in Eqn. (4.38) contains only quadratic terms (i.e., the second partial derivatives will be constant). Therefore, $\mathbf{G}$ does not exist for this problem. The Hessian for the discrete ODSD problem was defined in Eqn. (3.35), now modified to only include the optimization variables present and no Mayer term:

$$\mathbf{H} = \nabla_{\mathbf{xx}}\psi = \begin{bmatrix} \frac{\partial^2\psi}{\partial\boldsymbol{\xi}^2} & \frac{\partial^2\psi}{\partial\boldsymbol{\xi}\partial\mathbf{u}} \\ \frac{\partial^2\psi}{\partial\boldsymbol{\xi}\partial\mathbf{u}} & \frac{\partial^2\psi}{\partial\mathbf{u}^2} \end{bmatrix} \tag{A.2}$$

Now expanding with $n_\xi = 2$ and $n_u = 1$ and replacing $\boldsymbol{\xi}$ and $\mathbf{u}$ with the proper variable names:

$$\mathbf{H} = \begin{bmatrix} \frac{\partial^2\psi}{\partial z^2} & \frac{\partial^2\psi}{\partial z\partial\dot{z}} & \frac{\partial^2\psi}{\partial z\partial F_{\mathrm{PTO}}} \\ \frac{\partial^2\psi}{\partial z\partial\dot{z}} & \frac{\partial^2\psi}{\partial\dot{z}^2} & \frac{\partial^2\psi}{\partial\dot{z}\partial F_{\mathrm{PTO}}} \\ \frac{\partial^2\psi}{\partial z\partial F_{\mathrm{PTO}}} & \frac{\partial^2\psi}{\partial\dot{z}\partial F_{\mathrm{PTO}}} & \frac{\partial^2\psi}{\partial F_{\mathrm{PTO}}^2} \end{bmatrix} \tag{A.3}$$

We now find the entries of the Hessian that are obviously zero since they do not appear in the continuous form of the objective:

$$\mathbf{H} = \begin{bmatrix} \mathbf{0} & \mathbf{0} & \mathbf{0} \\ \mathbf{0} & \mathbf{0} & \frac{\partial^2\psi}{\partial\dot{z}\partial F_{\mathrm{PTO}}} \\ \mathbf{0} & \frac{\partial^2\psi}{\partial\dot{z}\partial F_{\mathrm{PTO}}} & \frac{\partial^2\psi}{\partial F_{\mathrm{PTO}}^2} \end{bmatrix} \tag{A.4}$$

Finally, we can determine the entries. The composite trapezoidal will only have block diagonal entries and will be symmetric:

$$\frac{\partial^2\psi}{\partial\dot{z}[t_k]\partial F_{\mathrm{PTO}}[t_k]} = -Q[t_k]h \tag{A.5a}$$

$$\frac{\partial^2\psi}{\partial F_{\mathrm{PTO}}^2[t_k]} = Q[t_k]R_{\mathrm{pen}}h \tag{A.5b}$$

$$\text{where:} \quad Q[t_k] = \begin{cases} \frac{1}{2} & \text{if } k = 0 \text{ or } n_t \\ 1 & \text{otherwise} \end{cases} \tag{A.5c}$$

A.2 Linear Constraint Calculation

Recall the constraint Jacobian in Eqn. (3.36). The linear constraints in the problem are the dynamic constraints in Eqn. (4.33) and the periodic constraint in Eqn. (4.42) (with an additional periodic control constraint) since their calculation only depends linearly on the states and control. The modified constraint Jacobian only including the optimization variables present and no path constraints is:

$$\nabla_{\mathbf{x}} \begin{bmatrix} \boldsymbol{\phi} \\ \boldsymbol{\zeta} \end{bmatrix} = \begin{bmatrix} \frac{\partial \boldsymbol{\phi}}{\partial \boldsymbol{\xi}} & \frac{\partial \boldsymbol{\phi}}{\partial \mathbf{u}} \\ \frac{\partial \boldsymbol{\zeta}}{\partial \boldsymbol{\xi}} & \frac{\partial \boldsymbol{\zeta}}{\partial \mathbf{u}} \end{bmatrix} \tag{A.6}$$

Now expanding with $n_\xi = 2$ and $n_u = 1$ and replacing $\boldsymbol{\xi}$ and $\mathbf{u}$ with the proper variable names:

$$\nabla_{\mathbf{x}} \begin{bmatrix} \boldsymbol{\phi} \\ \boldsymbol{\zeta} \end{bmatrix} = \begin{bmatrix} \frac{\partial \boldsymbol{\phi}_z}{\partial z} & \frac{\partial \boldsymbol{\phi}_z}{\partial \dot{z}} & \frac{\partial \boldsymbol{\phi}_z}{\partial F_{\mathrm{PTO}}} \\ \frac{\partial \boldsymbol{\phi}_{\dot{z}}}{\partial z} & \frac{\partial \boldsymbol{\phi}_{\dot{z}}}{\partial \dot{z}} & \frac{\partial \boldsymbol{\phi}_{\dot{z}}}{\partial F_{\mathrm{PTO}}} \\ \frac{\partial \boldsymbol{\phi}_{F_{\mathrm{PTO}}}}{\partial z} & \frac{\partial \boldsymbol{\phi}_{F_{\mathrm{PTO}}}}{\partial \dot{z}} & \frac{\partial \boldsymbol{\phi}_{F_{\mathrm{PTO}}}}{\partial F_{\mathrm{PTO}}} \\ \frac{\partial \boldsymbol{\zeta}_z}{\partial z} & \frac{\partial \boldsymbol{\zeta}_z}{\partial \dot{z}} & \frac{\partial \boldsymbol{\zeta}_z}{\partial F_{\mathrm{PTO}}} \\ \frac{\partial \boldsymbol{\zeta}_{\dot{z}}}{\partial z} & \frac{\partial \boldsymbol{\zeta}_{\dot{z}}}{\partial \dot{z}} & \frac{\partial \boldsymbol{\zeta}_{\dot{z}}}{\partial F_{\mathrm{PTO}}} \end{bmatrix} \tag{A.7}$$

We now find the entries of this constraint Jacobian that are obviously zero since they do not appear in the continuous form of the constraints:

$$\nabla_{\mathbf{x}} \begin{bmatrix} \boldsymbol{\phi} \\ \boldsymbol{\zeta} \end{bmatrix} = \begin{bmatrix} \frac{\partial \boldsymbol{\phi}_z}{\partial z} & \mathbf{0} & \mathbf{0} \\ \mathbf{0} & \frac{\partial \boldsymbol{\phi}_{\dot{z}}}{\partial \dot{z}} & \mathbf{0} \\ \mathbf{0} & \mathbf{0} & \frac{\partial \boldsymbol{\phi}_{F_{\mathrm{PTO}}}}{\partial F_{\mathrm{PTO}}} \\ \frac{\partial \boldsymbol{\zeta}_z}{\partial z} & \frac{\partial \boldsymbol{\zeta}_z}{\partial \dot{z}} & \mathbf{0} \\ \frac{\partial \boldsymbol{\zeta}_{\dot{z}}}{\partial z} & \frac{\partial \boldsymbol{\zeta}_{\dot{z}}}{\partial \dot{z}} & \frac{\partial \boldsymbol{\zeta}_{\dot{z}}}{\partial F_{\mathrm{PTO}}} \end{bmatrix} \tag{A.8}$$

Finally, we can determine the entries. The discretized boundary constraints

only require a single linear constraint:

$$\frac{\partial \boldsymbol{\phi}_z}{\partial z[t_k]} = Q[t_k] \tag{A.9a}$$

$$\frac{\partial \boldsymbol{\phi}_{\dot{z}}}{\partial \dot{z}[t_k]} = Q[t_k] \tag{A.9b}$$

$$\frac{\partial \boldsymbol{\phi}_{F_{\mathrm{PTO}}}}{\partial F_{\mathrm{PTO}}[t_k]} = Q[t_k] \tag{A.9c}$$

$$\text{where:} \quad Q[t_k] = \begin{cases} 1 & \text{if } k = 0 \\ -1 & \text{if } k = n_t \\ 0 & \text{otherwise} \end{cases} \tag{A.9d}$$

We will need $n_t \times n_\xi$ linear constraints to represent the defect constraints:

$$\frac{\partial \boldsymbol{\zeta}_z[t_k]}{\partial z[t_k]} = 1 \tag{A.10a}$$

$$\frac{\partial \boldsymbol{\zeta}_z[t_k]}{\partial z[t_{k-1}]} = -1 \tag{A.10b}$$

$$\frac{\partial \boldsymbol{\zeta}_z[t_k]}{\partial \dot{z}[t_k]} = \frac{\partial \boldsymbol{\zeta}_z[t_k]}{\partial \dot{z}[t_{k-1}]} = -\frac{h}{2} \tag{A.10c}$$

$$\frac{\partial \boldsymbol{\zeta}_{\dot{z}}[t_k]}{\partial z[t_k]} = \frac{\partial \boldsymbol{\zeta}_{\dot{z}}[t_k]}{\partial z[t_{k-1}]} = \frac{h k_b}{2\left(m + \overline{m}_r\right)} \tag{A.10d}$$

$$\frac{\partial \boldsymbol{\zeta}_{\dot{z}}[t_k]}{\partial \dot{z}[t_k]} = \frac{h\left(\overline{R}_r + R_v\right)}{2\left(m + \overline{m}_r\right)} + 1 \tag{A.10e}$$

$$\frac{\partial \boldsymbol{\zeta}_{\dot{z}}[t_k]}{\partial \dot{z}[t_{k-1}]} = \frac{h\left(\overline{R}_r + R_v\right)}{2\left(m + \overline{m}_r\right)} - 1 \tag{A.10f}$$

$$\frac{\partial \boldsymbol{\zeta}_{\dot{z}}[t_k]}{\partial F_{\mathrm{PTO}}[t_k]} = \frac{\partial \boldsymbol{\zeta}_{\dot{z}}[t_k]}{\partial F_{\mathrm{PTO}}[t_{k-1}]} = \frac{h}{2\left(m + \overline{m}_r\right)} \tag{A.10g}$$

However, these equations do not fully define the original defect constraints. One of the forces acting on the WEC is state independent: the excitation force. Since this force is a constant at a specific value of t_k, it can readily be included in $\mathbf{b}$:

$$\mathbf{b} = \begin{bmatrix} \mathbf{0}_{(3+n_t)\times 1} \\ \mathbf{Q} \end{bmatrix} \tag{A.11a}$$

$$\text{where:} \quad Q_k = \frac{h}{2\left(m + \overline{m}_r\right)}\left(F_e[t_{k-1}] + F_e[t_k]\right) \tag{A.11b}$$

Therefore, the linear constraints in the WEC design problem are defined by:

$$\nabla_{\mathbf{x}} \begin{bmatrix} \boldsymbol{\phi} \\ \boldsymbol{\zeta} \end{bmatrix} \mathbf{x} = \mathbf{b} \tag{A.12}$$

A.3 Quadratic Constraint Calculation

Once again recall the constraint Jacobian in Eqn. (3.36) but now consider the second partial derivatives (similar to the Hessian calculation). The nonlinear (but quadratic) constraint is the power constraint defined in Eqn. (4.40) since the constraint function only depends quadratically on the states and control. This also implies that $\mathbf{q}$ and r are zero for this constraint. The modified first derivative of the constraint Jacobian only including the optimization variables present and no dynamic and boundary constraints is:

$$\nabla_{\mathbf{xx}} \mathbf{C} = \begin{bmatrix} \frac{\partial \mathbf{C}}{\partial \boldsymbol{\xi}^2} & \frac{\partial \mathbf{C}}{\partial \boldsymbol{\xi} \partial \mathbf{u}} \\ \frac{\partial \mathbf{C}}{\partial \boldsymbol{\xi} \partial \mathbf{u}} & \frac{\partial \mathbf{C}}{\partial \mathbf{u}^2} \end{bmatrix} \tag{A.13}$$

Now expanding with $n_\xi = 2$ and $n_u = 1$ and replacing $\boldsymbol{\xi}$ and $\mathbf{u}$ with the proper variable names:

$$\nabla_{\mathbf{xx}} \mathbf{C}_1 = \begin{bmatrix} \frac{\partial^2 \mathbf{C}_1}{\partial z^2} & \frac{\partial^2 \mathbf{C}_1}{\partial z \partial \dot{z}} & \frac{\partial^2 \mathbf{C}_1}{\partial z \partial F_{\mathrm{PTO}}} \\ \frac{\partial^2 \mathbf{C}_1}{\partial z \partial \dot{z}} & \frac{\partial^2 \mathbf{C}_1}{\partial \dot{z}^2} & \frac{\partial^2 \mathbf{C}_1}{\partial \dot{z} \partial F_{\mathrm{PTO}}} \\ \frac{\partial^2 \mathbf{C}_1}{\partial z \partial F_{\mathrm{PTO}}} & \frac{\partial^2 \mathbf{C}_1}{\partial \dot{z} \partial F_{\mathrm{PTO}}} & \frac{\partial^2 \mathbf{C}_1}{\partial F_{\mathrm{PTO}}^2} \end{bmatrix} \tag{A.14}$$

We now find the entries of this matrix that are obviously zero since they do not appear in the continuous form of the constraints:

$$\nabla_{\mathbf{xx}} \mathbf{C}_1 = \begin{bmatrix} \mathbf{0} & \mathbf{0} & \mathbf{0} \\ \mathbf{0} & \mathbf{0} & \frac{\partial^2 \mathbf{C}_1}{\partial \dot{z} \partial F_{\mathrm{PTO}}} \\ \mathbf{0} & \frac{\partial^2 \mathbf{C}_1}{\partial \dot{z} \partial F_{\mathrm{PTO}}} & \mathbf{0} \end{bmatrix} \tag{A.15}$$

Finally, we can determine the entries. The second partial derivatives will be

-1 on the block diagonal and 0 elsewhere. Therefore, we can write:

$$\nabla_{\mathbf{xx}}\mathbf{C}_1 = \begin{bmatrix} \mathbf{0} & \mathbf{0} & \mathbf{0} \\ \mathbf{0} & \mathbf{0} & -\mathbf{I} \\ \mathbf{0} & -\mathbf{I} & \mathbf{0} \end{bmatrix} \tag{A.16}$$

where $\mathbf{I}$ an identity matrix of size $(n_t + 1) \times (n_t + 1)$. In conclusion, the quadratic power constraint can be expressed as:

$$\frac{1}{2}\mathbf{x}^T \nabla_{\mathbf{xx}}\mathbf{C}_1\mathbf{x} \leq \mathbf{0} \tag{A.17}$$

which is consistent with the QCQP formulation. As stated in Sec. 3.3.2, modern NLP algorithms typically only use the constraint Jacobian:

$$\nabla_{\mathbf{x}}\mathbf{C}_1 = \begin{bmatrix} \frac{\partial \mathbf{C}_1}{\partial z} & \frac{\partial \mathbf{C}_1}{\partial \dot{z}} & \frac{\partial \mathbf{C}_1}{\partial F_{\mathrm{PTO}}} \end{bmatrix} \tag{A.18a}$$

$$= \begin{bmatrix} \mathbf{0} & \frac{\partial \mathbf{C}_1}{\partial \dot{z}} & \frac{\partial \mathbf{C}_1}{\partial F_{\mathrm{PTO}}} \end{bmatrix} \tag{A.18b}$$

with the nonzero entries defined as:

$$\frac{\partial C_1[t_k]}{\partial \dot{z}[t_k]} = -F_{\mathrm{PTO}}[t_k] \tag{A.19a}$$

$$\frac{\partial C_1[t_k]}{\partial F_{\mathrm{PTO}}[t_k]} = -\dot{z}[t_k] \tag{A.19b}$$

A.4 Creating Sparse Matrices in MATLAB®

There are a number of ways to construct the sparse matrices defined in the previous sections. First, let us review some of the useful MATLAB® functions:

sparse — `S = sparse(i,j,s,m,n,nzmax)` uses vectors `i`, `j`, and `s` to generate an `m×n` sparse matrix such that `S(i(k),j(k))= s(k)`, with space allocated for `nzmax` nonzeros.[1]

spalloc — `S = spalloc(m,n,nzmax)` creates an all zero sparse matrix `S` of size `m×n` with room to hold `nzmax` nonzeros. `spalloc(m,n,nzmax)` is shorthand for `sparse([],[],[],m,n,nzmax)`.[2]

[1] http://www.mathworks.com/help/matlab/ref/sparse.html
[2] http://www.mathworks.com/help/matlab/ref/spalloc.html

spdiags — `A = spdiags(B,d,m,n)` creates an `m`×`n` sparse matrix by taking the columns of `B` and placing them along the diagonals specified by `d`.[3]

spy — `spy(S)` plots the sparsity pattern of any matrix `S`.[4]

Three different methods for constructing the sparse matrices will be discussed: index method, row method, and diagonal method. Each method is ideal for the specific matrix the needs to be constructed.

Index method — This method is the most intuitive to implement. Indexing loops are used to assign single elements in the matrix. This method is the least efficient but is suitable for matrices that only need to be calculated once. In Section A.1, the Hessian is constant. Also, Eqn. (A.5c) specifies coefficients based on the index value. Therefore, the index method is well suited to calculate this Hessian. MATLAB® code for calculating the Hessian described in Eqns. (A.4) and (A.5) is shown in Fig. A.1. The sparsity pattern for $\mathbf{H}$ with $n_t = 7$ is shown in Fig. A.2. Note the diagonal matrices created by the composite trapezoidal rule.

Row method — This approach defines many entries (typically an entire row) in the sparse matrix with a single index call. Sparse row vectors of variable size are used to place the elements into their correct locations at each index call. This is ideal for sparse matrices that contain similar rows. The linear defect constraints created by the trapezoidal rule fit this description. Since more elements are placed in a single index call, it is more efficient than the index method but has increased complexity. MATLAB® code for calculating the linear constraints described in Eqns. (A.8), (A.9), and (A.10) is shown in Fig. A.3. The sparsity pattern of $\mathbf{A}$ with $n_t = 7$ is shown in Fig. A.4. Note the zigzag diagonal pattern created by the trapezoidal rule.

Diagonal method — If the sparse matrix has only diagonal elements, then the `spdiags` function can be efficiently used to create the matrix. Path constraints and the Hessian are of this form. The Hessian however requires some additional calculation to create the input vector that defines the diagonal entries of the matrix. Path constraints, on the other hand, depend on the easily extracted discretized state and control vectors. MATLAB® code for calculating the constraint Jacobian for the power path constraint described

[3] `http://www.mathworks.com/help/matlab/ref/spdiags.html`
[4] `http://www.mathworks.com/help/matlab/ref/spy.html`

```
function H = Hessian(p)
    % parameters
    R = p.Rpen; h = p.h; nt = p.nt;
    % full length
    N = nt+1;
    % initialize Hessian
    H = spalloc(3*N,3*N,3*N);

    % dudu
    H(2*N+1,2*N+1) = 1/2*R*h;
    for i = 2:nt
        H(2*N+i,2*N+i) = R*h;
    end
    H(3*N,3*N) = 1/2*R*h;

    % dudv
    H(N+1,2*N+1) = -1/2*h;
    for i = 2:nt
        H(N+i,i+2*N) = -h;
    end
    H(2*N,3*N) = -1/2*h;

    % dvdu
    H(2*N+1,N+1) = -1/2*h;
    for i = 2:nt
        H(i+2*N,N+i) = -h;
    end
    H(3*N,2*N) = -1/2*h;
end
```

Figure A.1 MATLAB® code for Hessian calculation using the index method.

in Eqns. (A.18) and (A.19) is shown in Fig. A.5. The sparsity pattern for $\mathbf{H}$ with $n_t = 7$ is shown in Fig. A.6. Note the block diagonal matrices created by the discretized path constraint.

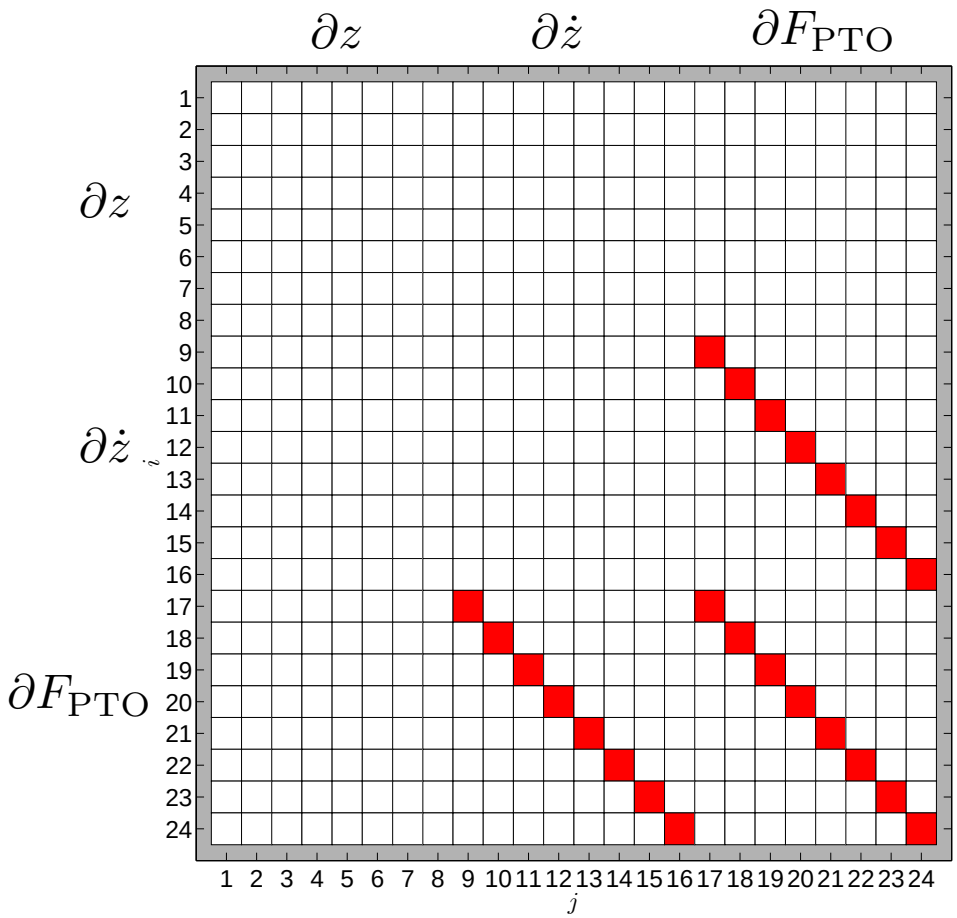

Figure A.2 Hessian sparsity pattern for WEC design problem using trapezoidal quadrature (red indicates nonzero element).

```
function [A,B] = LinearConstraints(p)
    % parameters
    nt = p.nt; ns = p.ns;
    % full length
    N = nt+1;
    % initialize equality constraint matrix A and vector B
    A = spalloc(2*N+1,3*N,6*N*3);
    B = spalloc(2*N+1,1,(ns-1)*N+1);

    % periodic constraint: states
    A(1:ns,:) = [ [1;0] spalloc(ns,N-2,0) [-1;0] ...
        [0;1] spalloc(ns,N-2,0) [0;-1] spalloc(ns,N,0)];
    B(1:ns,1) = [0;0];

    % periodic constraint: control
    A(ns+1,:) = [spalloc(1,2*N,0) 1 spalloc(1,N-2,0) -1];
    B(ns+1,1) = 0;

    % defect constraints: state 1, position
    for i = 1:(N-1)
       A(i+ns+1,:) = [spalloc(1,i-1,0) -1 1 spalloc(1,N-2,0) ...
           -p.h/2 -p.h/2 spalloc(1,2*N-i-1,0)];
    end

    % defect constraints: state 2, velocity
    for i = 1:(N-1)
        A(i+ns+N,:) = [...
            spalloc(1,i-1,0)...
            (p.h*p.k)/(2*p.m)... % z(k)
            (p.h*p.k)/(2*p.m)... % z(k+1)
            spalloc(1,N-2,0)...
            ((p.h*p.b)/(2*p.m)-1)... % v(k)
            ((p.h*p.b)/(2*p.m)+1)... % v(k+1)
            spalloc(1,N-i-1,0)...
            spalloc(1,i-1,0)...
            p.h/(2*p.m)... % u(k)
            p.h/(2*p.m)... % u(k+1)
            spalloc(1,N-i-1,0)];
        B(i+ns+N,:) = p.h/(2*p.m)*(p.Fe(i) + p.Fe(i+1));
    end
end
```

Figure A.3 MATLAB® code for linear constraint calculation using the row method.

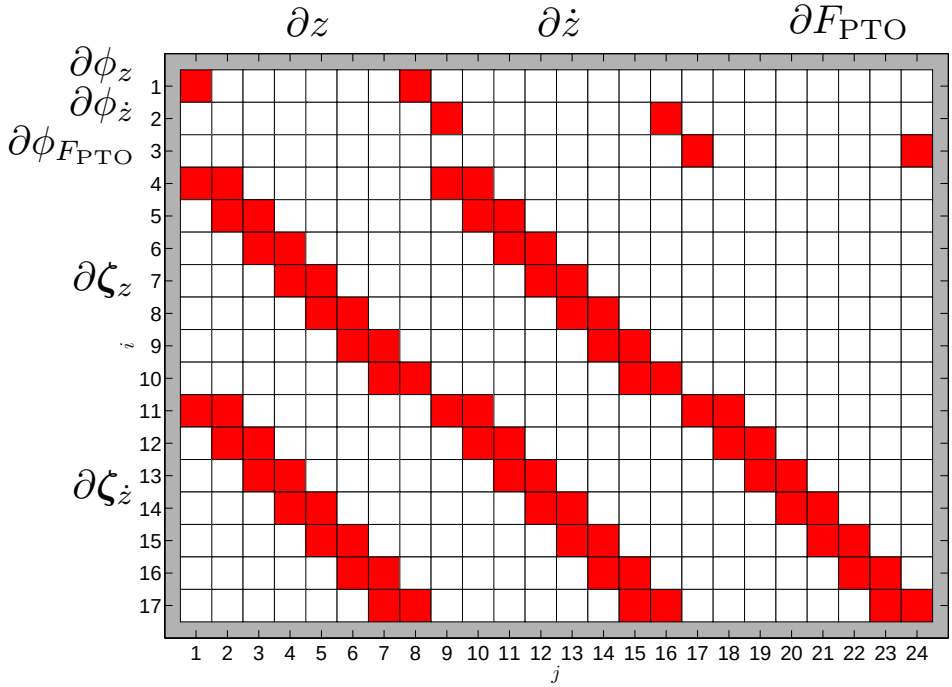

Figure A.4 Linear constraint matrix **A** sparsity pattern for WEC design problem using the trapezoidal rule (red indicates nonzero element).

```
function J = JacobianNonlinear(x,p)
    % full length
    N = p.nt + 1;
    % nonlinear constraint: power
    J = [spalloc(N,N,N)...
        spdiags(-x(2*N+1:3*N),0,N,N)...
        spdiags(-x(N+1:2*N),0,N,N)];
end
```

Figure A.5 MATLAB® code for constraint Jacobian calculation using the diagonal method.

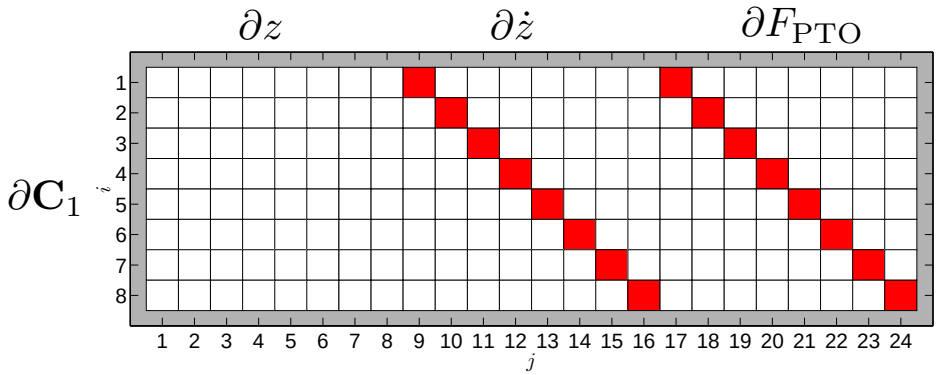

Figure A.6 Nonlinear constraint Jacobian sparsity pattern for WEC design problem (red indicates nonzero element).

Appendix B

Additional Figures

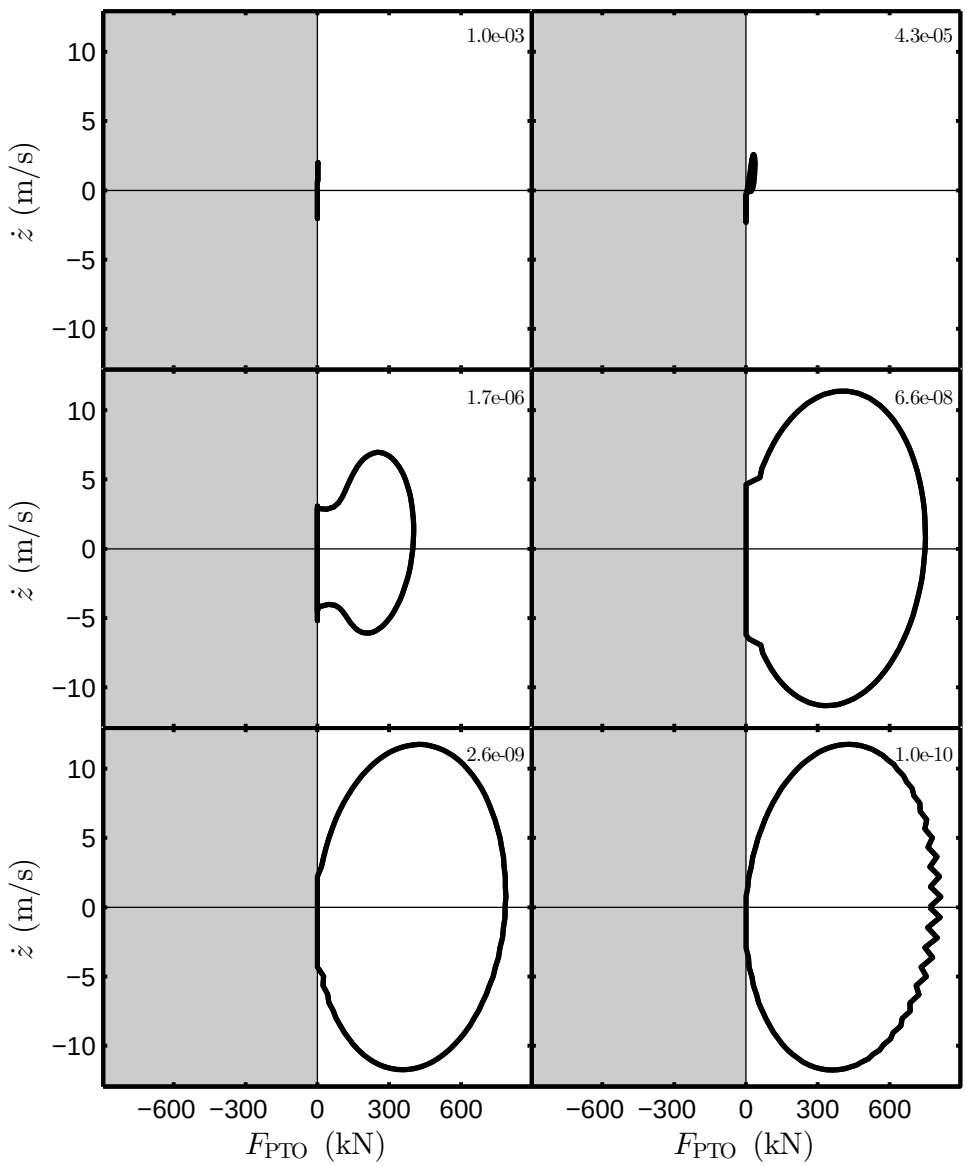

Figure B.1 The effect of R_{pen} on the phase space of the objective function for Case 2 (note that the R_{pen} values are in the northeast corners, grey shading indicates infeasible regions).

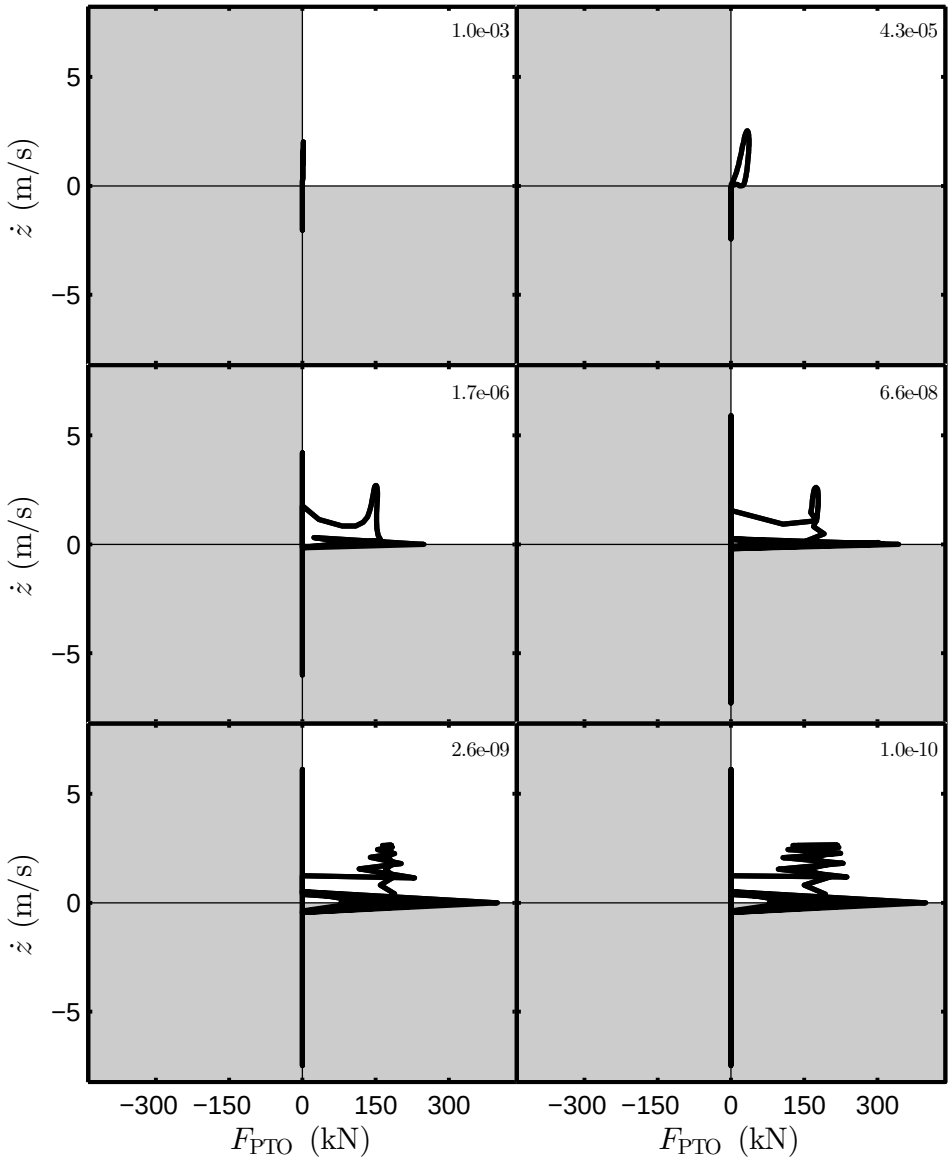

Figure B.2 The effect of R_{pen} on the phase space of the objective function for Case 4 (note that the R_{pen} values are in the northeast corners, grey shading indicates infeasible regions).

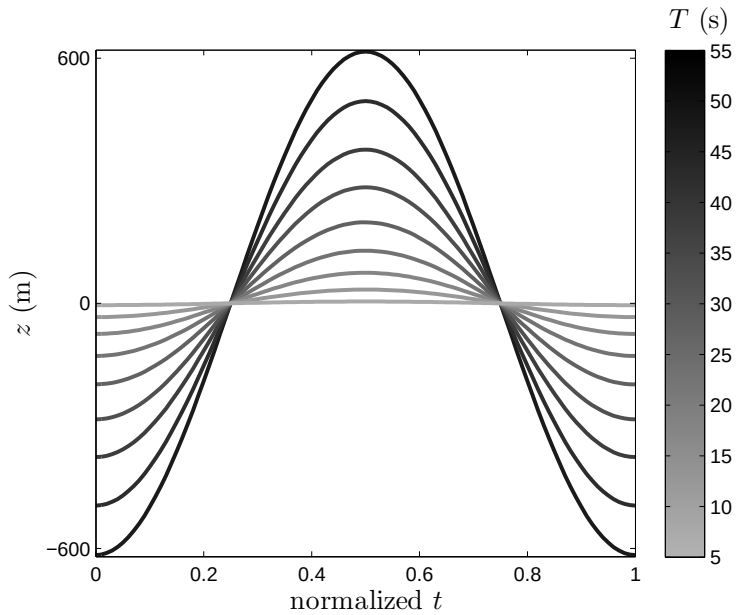

a) Unconstrained

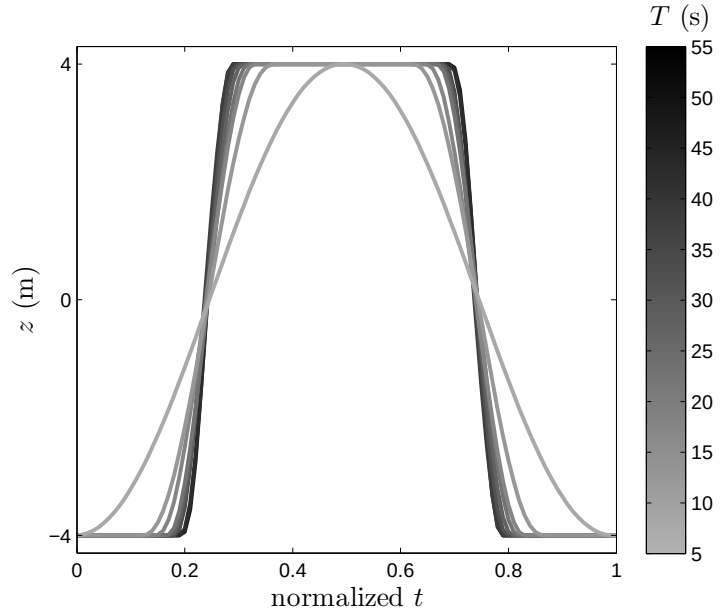

b) Constrained by $|z| \leq 4$ m

Figure B.3 Position trajectories for various values of the regular wave period with both unconstrained and constrained heave amplitude.

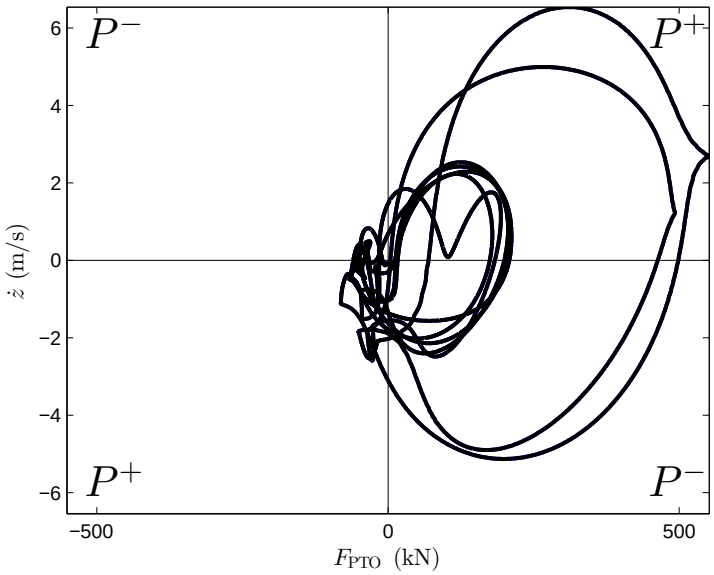

a) Case 1: $F_{\mathrm{PTO}} \in \mathbb{R}, P \in \mathbb{R}$

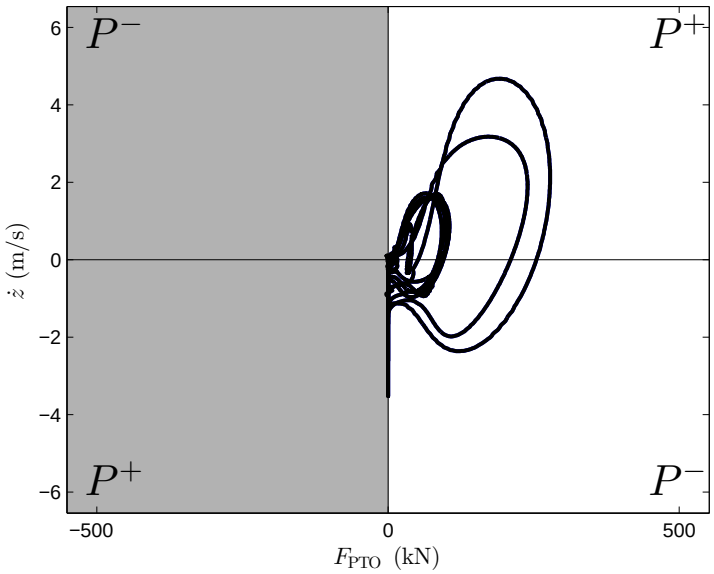

b) Case 2: $F_{\mathrm{PTO}} \in \mathbb{R}^+, P \in \mathbb{R}$

Figure B.4 Phase space of the objective function for Cases 1 and 2 in an irregular wave (grey shading indicates infeasible regions).

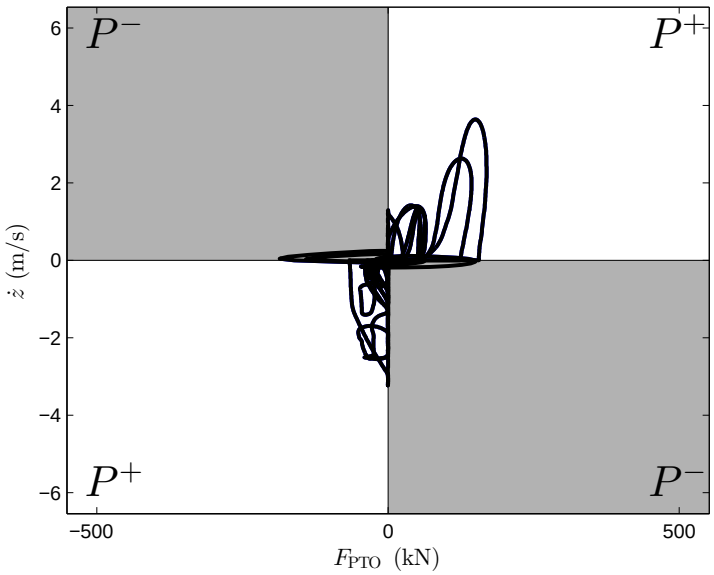

a) Case 3: $F_{\mathrm{PTO}} \in \mathbb{R}, P \in \mathbb{R}^+$

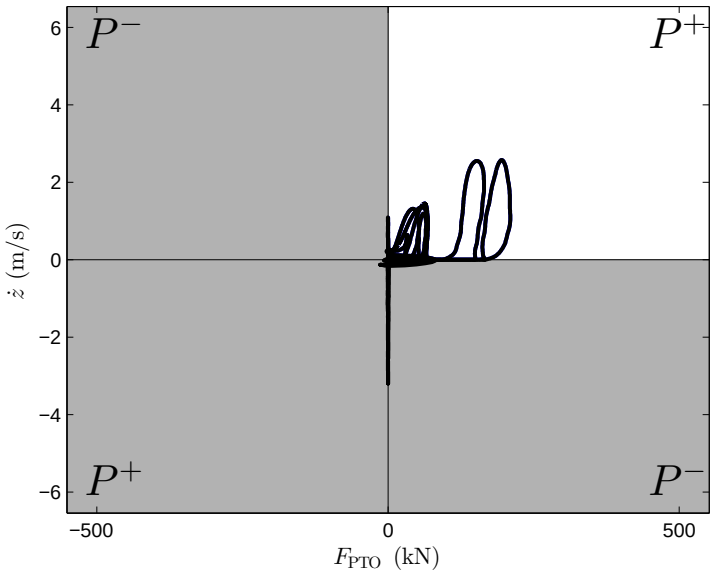

b) Case 4: $F_{\mathrm{PTO}} \in \mathbb{R}^+, P \in \mathbb{R}^+$

Figure B.5 Phase space of the objective function for Cases 3 and 4 in an irregular wave (grey shading indicates infeasible regions).

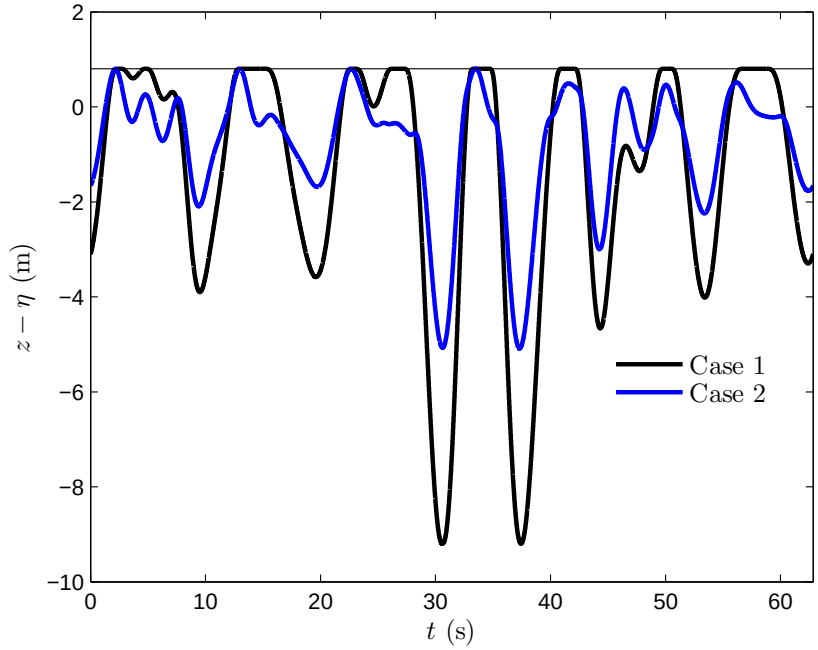

a)

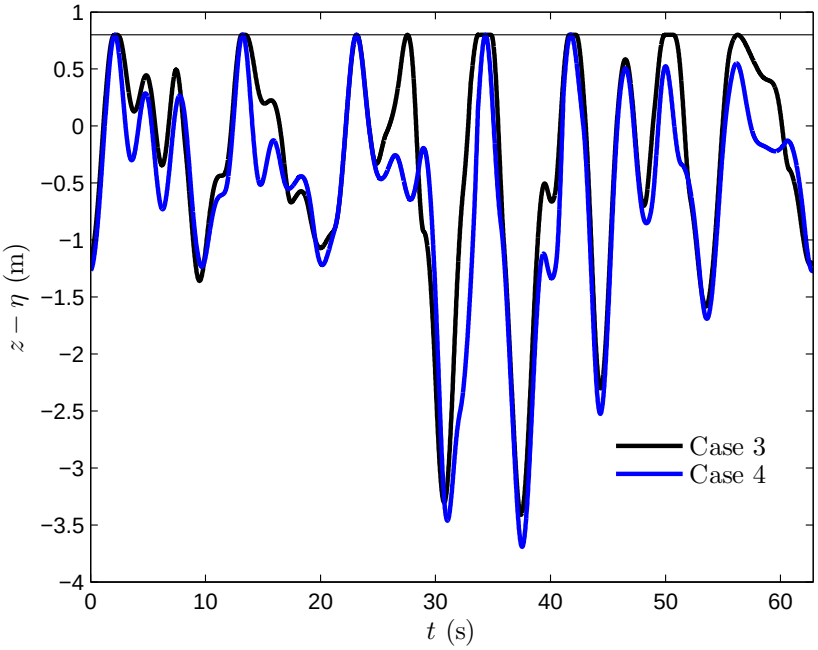

b)

Figure B.6 Visualization of the slamming path constraint ($z - \eta \leq b$) for all four cases in an irregular wave (horizontal line indicates the maximum allowed value of this constraint).

Bibliography

[1] Danielsson, O. "Wave Energy Conversion: Linear Synchronous Permanent Magnet Generator." Ph.D. Dissertation. Uppsala University: Uppsala, Sweden, Dec. 2006.
URL: http://urn.kb.se/resolve?urn=urn:nbn:se:uu:diva-7194

[2] Hirsch, R L, R Bezdek, and R Wendling. *Peaking of World Oil Production: Impacts, Mitigation, & Risk Management*. Tech. rep. Science Applications International Corporation/U.S. Department of Energy, National Energy Technology Laboratory, Feb. 2005.

[3] Odell, P R. *Why Carbon Fuels Will Dominate the 21st Centurys Global Energy Economy,* 1st edition, Multi-Science Publishing Co. 2004.
ISBN: 0906522226

[4] Mann, M E, R S Bradley, and M K Hughes. "Global-scale Temperature Patterns and Climate Forcing Over the Past Six Centuries." *Nature*, NPG. ***392***, Apr. 1998, pp. 779–787.
DOI: 10.1038/33859

[5] Backer, G D. "Hydrodynamic Design Optimization of Wave Energy Converters Consisting of Heaving Point Absorbers." Ph.D. Dissertation. Ghent University: Ghent, Belgium, Dec. 2009.
URL: http://hdl.handle.net/1854/LU-1006160

[6] Murray, R. *Review and Analysis of Ocean Energy Systems Development and Supporting Policies*. Tech. rep. International Energy Agency, June 2006.

[7] Thorpe, T W. "An Overview of Wave Energy Technologies: Status, Performance, and Costs." *Proceedings of the IME 1999 Wave Power: Moving Towards Commercial Viability*, London, UK, Nov. 1999.
URL: http://waveberg.com/pdfs/overview.pdf

[8] Clément, A et al. "Wave Energy in Europe: Current Status and Perspectives." *Renewable and Sustainable Energy Reviews*, Elsevier. ***6*** (5), Oct. 2002, pp. 405–431.
DOI: 10.1016/S1364-0321(02)00009-6

[9] Leijon, M, H Bernhoff, M Berg, and O Ågren. "Economical Considerations of Renewable Electric Energy Production–Especially Development of Wave Energy." *Renewable Energy*, Elsevier. ***28*** (8), July 2003, pp. 1201–1209.
DOI: 10.1016/S0960-1481(02)00157-X

[10] Pelc, R and R M Fujita. "Renewable Energy from the Ocean." *Marine Policy*, Elsevier. ***26*** (6), Nov. 2002, pp. 471–479.
doi: 10.1016/S0308-597X(02)00045-3

[11] Previsic, M et al. *The Future Potential of Wave Power in the United States*. Tech. rep. RE Vision Consulting for the US Department of Energy, Aug. 2012.
URL: http://re-vision.net/documents/The%20Future%20of%20Wave%20Power%20MP%209-20-12.pdf.

[12] Robinson, M. *Ocean Energy Technology Development*. Presentation NREL/PR-500-40461. National Renewable Energy Laboratory, Oct. 2006.
URL: http://www.nrel.gov/docs/gen/fy07/40461.pdf.

[13] Bedard, R. *Final Summary Report–Project Definition Study–Offshore Wave Power Feasibility Demonstration Project*. Tech rep. E2I EPRI Global WP 009 – US Rev 2. Electric Power Research Institute Inc., Sept. 2005.
URL: http://oceanenergy.epri.com/attachments/wave/reports/009_Final_Report_RB_Rev_2_092205.pdf.

[14] McCormick, M E. *Ocean Wave Energy Conversion,* 2nd edition, Dover Publications, 2007.
isbn: 9780468462455

[15] Guerber, E. "Modélisation Numérique des Interactions Non-Linéaires entre Vagues et Structures Immergées, Appliquée à la Simulation de Systémes Houlomoteurs." Ph.D. Dissertation. Université Paris-Est: Paris, France, Oct. 2011.

[16] Falnes, J and K Budal. "Wave Power Conversion by Point Absorbers." *Norwegian Maritime Research*. ***6*** (4), 1978, pp. 2–11.

[17] Budal, K and J Falnes. "A Resonant Point Absorber of Ocean-Wave Power." *Nature*, NPG. ***256***, Aug. 1975, pp. 478–479.
doi: 10.1038/256478a0

[18] Hals, J. "Modelling and Phase Control of Wave-Energy Converters." Ph.D. Dissertation. Norwegian University of ScienceTechnology: Trondheim, Norway, May 2010.
URL: http://urn.kb.se/resolve?urn=urn:nbn:no:ntnu:diva-11952

[19] Drew, B, A R Plummer, and M N Sahinkaya. "A Review of Wave Energy Converter Technology." *Proceedings of the Institution of Mechanical Engineers, Part A: Journal of Power and Energy*, SAGE. ***223*** (8), Dec. 2009, pp. 887–902.
doi: 10.1243/09576509JPE782

[20] Eriksson, M. "Modelling and Experimental Verification of Direct Drive Wave Energy Conversion: Buoy-Generator Dynamics." Ph.D. Dissertation. Uppsala University: Uppsala, Sweden, May 2007.
URL: http://urn.kb.se/resolve?urn=urn:nbn:se:uu:diva-7785

[21] Falnes, J. "A Review of Wave-Energy Extraction." *Marine Structures*, Elsevier. ***20*** (4), Oct. 2007, pp. 185–201.
doi: 10.1016/j.marstruc.2007.09.001

[22] Ocean Power Technologies. *Mark 4 - The Powertower*. Feb. 3, 2013.
URL: http://www.oceanpowertechnologies.com/mark4.html.

[23] Taghipour, R and T Moan. "Efficient Frequency-Domain Analysis of Dynamic Response for the Multi-Body Wave Energy Converter in Multi-Directional Waves." *Proceedings of the ISOPE 2008 International Offshore and Polar Engineering Conference*, Vancouver, Canada, July 2008, pp. 357–365.

[24] Bjerrum, A. "The Wave Star Energy Concept." *Proceedings of the 2008 International Conference on Ocean Energy*, Brest, France, Oct. 2008.

[25] Pizer, D J, C H Retzler, and R W Yemm. "The OPD Pelamis. Experimental and Numerical Results from the Hydrodynamic Work Program." *Proceedings of the EWTEC 2000 European Wave Energy Conference*, Aalborg, Denmark, Dec. 2000, pp. 227–234.

[26] Salter, S H. "Wave Power." *Nature*, NPG. ***249***, June 1974, pp. 720–724.
doi: 10.1038/249720a0

[27] Falnes, J. *Ocean Waves and Oscillating Systems,* 1st edition, Cambridge University Press, 2002.
doi: 10.1017/CBO9780511754630

[28] Clément, A H and A Babarit. "Discrete Control of Resonant Wave Energy Devices." *Philosophical Transactions of the Royal Society A*, Royal Society Publishing. ***370*** (1959), Jan. 2012, pp. 288–314.
doi: 10.1098/rsta.2011.0132

[29] Herber, D R and J T Allison. "Wave Energy Extraction Maximization in Irregular Ocean Waves Using Pseudospectral Methods." *Proceedings of the ASME 2013 International Design Engineering Technical Conferences*, No. DETC2013-12600, Portland, OR, USA, Aug. 2013.
doi: 10.1115/DETC2013-12600

[30] Falcão, A D d O. "Phase Control through Load Control of Oscillating-Body Wave Energy Converters with Hydraulic PTO System." *Ocean Engineering*, Elsevier. ***35*** (3–4), Mar. 2008, pp. 358–366.
doi: 10.1016/j.oceaneng.2007.10.005

[31] Tedeschi, E, M Molinas, M Carraro, and P Mattavelli. "Analysis of Power Extraction from Irregular Waves by All-Electric Power Take Off." *Proceedings of the IEEE 2010 Energy Conversion Congress and Exposition*, Atlanta, GA, USA, Sept. 2010, pp. 2370–2377.
doi: 10.1109/ECCE.2010.5617893

[32] Ivanova, I A, H Bernhoff, O Ågren, and M Leijon. "Simulated Generator for Wave Energy Extraction in Deep Water." *Ocean Engineering*, Elsevier. ***32*** (14–15), Oct. 2005, pp. 1664–1678.
DOI: 10.1016/j.oceaneng.2005.02.006

[33] Santana, A G, D E M Andrade, and A d l V Jaén. "Control of Hydrodynamic Parameters of Wave Energy Point Absorbers using Linear Generators and VSC-based Power Converters Connected to the Grid." *Proceedings of the EA4EPQ 2010 International Conference on Renewable Energies and Power Quality*, No. 291, Granada, Spain, Mar. 2010.
URL: http://www.icrepq.com/icrepq'10/291-Garcia.pdf

[34] Niu, X. *Modeling and Design Analysis of a Permanent Magnet Linear Synchronous Generator*. Tech. rep. UIUC-ESDL-2013-01. Engineering System Design Lab, Aug. 2013.
URL: http://hdl.handle.net/2142/47069.

[35] Abraham, E and E C Kerrigan. "Optimal Active Control and Optimization of a Wave Energy Converter." *Transactions on Sustainable Energy*, IEEE. ***4*** (2), Apr. 2013, pp. 324–332.
DOI: 10.1109/TSTE.2012.2224392

[36] Allison, J T, A Kaitharath, and D R Herber. "Wave Energy Extraction Maximization Using Direct Transcription." *Proceedings of the ASME 2011 International Mechanical Engineering Congress & Exposition*, No. IMECE2012-86619, Houston, TX, USA, Nov. 2012.
DOI: 10.1115/IMECE2012-86619

[37] Cramer, E J, J E Deniss Jr, P D Frank, R M Lewis, and G R Shubin. "Problem Formulation for Multidisciplinary Optimization." *Journal on Optimization*, SIAM. ***4*** (4), Aug. 1994, pp. 754776.
DOI: 10.1137/0804044

[38] Hals, J, J Falnes, and T Moan. "Constrained Optimal Control of a Heaving Buoy Wave-Energy Converter." *Journal of Offshore Mechanics and Arctic Engineering*, ASME. ***133*** (1), Nov. 2011, pp. 011401.
DOI: 10.1115/1.4001431

[39] Ernst, S G. "A Novel Linear Generator for Wave Energy Applications." M.S. Thesis. Oregon State University: Corvallis, OR, USA, May 2009.
URL: http://hdl.handle.net/1957/11781

[40] Allison, J T and D R Herber. "Multidisciplinary Design Optimization of Dynamic Engineering Systems." *AIAA Journal*. ***52*** (4), Apr. 2014, pp. 691–710.
DOI: 10.2514/1.J052182

[41] Li, Q, W J Zhang, and L Chen. "Design for Control—A Concurrent Engineering Approach for Mechatronic Systems Design." *Transactions on Mechatronics*, IEEE/ASME. ***6*** (2), June 2001, pp. 161–169.
DOI: 10.1109/3516.928731

[42] Fathy, H K, J A Reyer, P Y Papalambros, and A G Ulsoy. "On the Coupling between the Plant and Controller Optimization Problems." *Proceedings of the IEEE 2001 American Control Conference*, Arlington, VA, USA, June 2001, pp. 1864–1869.
DOI: 10.1109/ACC.2001.946008

[43] Reyer, J A, H K Fathy, P Y Papalambros, and A G Ulsoy. "Comparison of Combined Embodiment Design and Control Optimization Strategies using Optimality Conditions." *Proceedings of the ASME 2001 Design Engineering Technical Conferences*, No. DETC 2001/DAC-21119, Pittsburgh, PA, USA, Sept. 2001, pp. 1023–1032.

[44] Fathy, H K, P Y Papalambros, A G Ulsoy, and D Hrovat. "Nested Plant/Controller Optimization with Application to Combined Passive/Active Automotive Suspensions." *Proceedings of the IEEE 2003 American Control Conference*, Denver, CO, USA, June 2003, pp. 3375–3380.
DOI: 10.1109/ACC.2003.1244053

[45] Peters, D L, P Y Papalambros, and A G Ulsoy. "On Measures of Coupling Between the Artifact and Controller Optimal Design Problems." *Proceedings of the ASME 2009 International Design Engineering Technical Conferences*, No. DETC2009-86868, San Diego, CA, USA, Sept. 2009, pp. 1363–1372.
DOI: 10.1115/DETC2009-86868

[46] Allison, J T and S Nazari. "Combined Plant and Controller Design Using Decomposition-Based Design Optimization and the Minimum Principle." *Proceedings of the ASME 2010 International Design Engineering Technical Conferences*, No. DETC2010-28887, Montreal, Quebec, Canada, Aug. 2010, pp. 765–774.
DOI: 10.1115/DETC2010-28887

[47] Allison, J T, T Guo, and Z Han. "Co-Design of an Active Suspension Using Simultaneous Dynamic Optimization." *Journal of Mechanical Design*, ASME.
DOI: 10.1115/1.4027335

[48] Allison, J T. "Engineering System Co-Design with Limited Plant Redesign." *Engineering Optimization*, Taylor & Francis. ***46*** (2), 2014, pp. 200–217.
DOI: 10.1080/0305215X.2013.764999

[49] Allison, J T. "Plant-Limited Co-Design of an Energy-Efficient Counterbalanced Robotic Manipulator." *Journal of Mechanical Design*, ASME. ***135*** (10), Oct. 2013, pp. 101003.
DOI: 10.1115/1.4024978

[50] Biegler, L T. "An Overview of Simultaneous Strategies for Dynamic Optimization." *Chemical Engineering and Processing: Process Intensification*, Elsevier. ***46*** (11), Nov. 2007, pp. 1043–1053.
DOI: 10.1016/j.cep.2006.06.021

[51] Biegler, L T. *Nonlinear Programming: Concepts, Algorithms, and Applications to Chemical Processes,* 1st edition, SIAM, 2010.
DOI: 10.1137/1.9780898719383

[52] Deshmukh, A P and J T Allison. "Simultaneous Structural and Control System Design for Horizontal Axis Wind Turbines." *Proceedings of the AIAA/ASME/ASCE/AHS/ASC 2013 Structures, Structural Dynamics, and Materials Conference*, Boston, MA, USA, Apr. 2013.
DOI: 10.2514/6.2013-1533

[53] Bertsekas, D P. *Nonlinear Programming,* 2nd edition, Athena Scientific, 1999.
ISBN: 9781886529007

[54] Ruszczyński, A. *Nonlinear Optimization,* 1st edition, Vol. 13, Princeton University Press, 2006.
ISBN: 9780691119151

[55] Papalambros, P Y and D J Wilde. *Principles of Optimal Design,* 2nd edition, Cambridge University Press, 2000.
ISBN: 9780521627276

[56] Betts, J T. *Practical Methods for Optimal Control and Estimation Using Nonlinear Programming,* 2nd edition, SIAM, 2009.
ISBN: 9780898716887

[57] Sussmann, H J and J C Willems. "300 Years of Optimal Control: From the Brachystochrone to the Maximum Principle." *Control Systems*, IEEE. ***17*** (3), June 1997, pp. 32–44.
DOI: 10.1109/37.588098

[58] Liberzon, D. *Calculus of Variations and Optimal Control Theory: A Concise Introduction,* 1st edition, Princeton University Press, 2012.
ISBN: 9780691151878

[59] Hespanha, J P. *Linear Systems Theory,* 1st edition, Princeton University Press, 2009.
ISBN: 9780691140216

[60] Feehery, W F and P I Barton. "Dynamic Optimization with State Variable Path Constraints." *Computers & Chemical Engineering*, Elsevier. ***22*** (9), Aug. 1998, pp. 1241–1256.
DOI: 10.1016/S0098-1354(98)00012-X

[61] Spong, M W, S Hutchinson, and M Vidyasagar. *Robot Modeling and Control,* 1st edition, John Wiley & Sons, 2005.
ISBN: 9780471649908

[62] Walsh, A N. "Space Station Minimum Energy Optimal Control Problem." Honors Thesis. University of Florida: Gainesville, FL, USA, Apr. 2013.
URL: http://www.honors.ufl.edu/apps/Thesis.aspx/Details/2082

[63] Rao, A V et al. "Algorithm 902: GPOPS, A MATLAB Software for Solving Multiple-Phase Optimal Control Problems Using the Gauss Pseudospectral Method." *Transactions on Mathematical Software*, ACM. ***37*** (2), Apr. 2010, pp. 22:1–39.
DOI: 10.1145/1731022.1731032

[64] Benson, D. "A Gauss Pseudospectral Transcription for Optimal Control." Ph.D. Dissertation. Massachusetts Institute of Technology: Cambridge, MA, USA, Feb. 2005.
URL: http://hdl.handle.net/1721.1/28919

[65] Karbowski, D, S Pagerit, J Kwon, A Rousseau, and K-F F v Pechmann. "'Fair' Comparison of Powertrain Configurations for Plug-In Hybrid Operation using Global Optimization." *Proceedings of the SAE 2009 World Congress & Exhibition*, No. 2009-01-1334, Detroit, MI, USA, Apr. 2009.
DOI: 10.4271/2009-01-1334

[66] Hadj, N B, S Tounsi, R Neji, and F Sellami. "Real Coded Genetic Algorithm for Permanent Magnet Motor Mass Minimization for Electric Vehicle Application." *Proceedings of the IEEE 2007 International Symposium on Computational Intelligence and Intelligent Informatics*, Agadir, Morocco, Mar. 2007, pp. 153–158.
DOI: 10.1109/ISCIII.2007.367380

[67] Ravichandran, T, D Wang, and G Heppler. "Simultaneous Plant-Controller Design Optimization of a Two-Link Planar Manipulator." *Mechatronics*, Elsevier. ***16*** (3–4), Apr. 2006, pp. 233–242.
DOI: 10.1016/j.mechatronics.2005.09.008

[68] Wang, Q and J S Arora. "Several Simultaneous Formulations for Transient Dynamic Response Optimization: An Evaluation." *International Journal for Numerical Methods in Engineering*, John Wiley & Sons. ***80*** (5), Oct. 2009, pp. 631–650.
DOI: 10.1002/nme.2655

[69] Guo, T and J T Allison. "On the Use of MPCCs in Combined Topological and Parametric Design of Genetic Regulatory Circuits." *Proceedings of the ISSMO 2013 World Congress on Structural and Multidisciplinary Optimization*, Orlando, FL, USA, May 2013.

[70] Kang, B S, G J Park, and J S Arora. "A Review of Optimization of Structures Subjected to Transient Loads." *Structural and Multidisciplinary Optimization*, Springer. ***31*** (2), Feb. 2006, pp. 81–95.
DOI: 10.1007/s00158-005-0575-4

[71] Barthelemy, J-F M and R T Haftka. "Approximation Concepts for Optimum Structural Design: A Review." *Structural Optimization*, Springer. ***5*** (3), Sept. 1993, pp. 129–144.
DOI: 10.1007/BF01743349

[72] Haug, E J and J S Arora. *Applied Optimal Design: Mechanical and Structural Systems,* 1st edition, Wiley-Interscience, 1979.
ISBN: 9780471041702

[73] Kim, M-S and D-H Choi. "Min-Max Dynamic Response Optimization of Mechanical Systems Using Approximate Augmented Lagrangian." *International Journal for Numerical Methods in Engineering*, John Wiley & Sons. ***43*** (3), Oct. 1998, pp. 549–564.
DOI: 10.1002/(SICI)1097-0207(19981015)43:3<549::AID-NME446>3.0.CO;2-V

[74] Bowling, A P, J E Renaud, J T Newkirk, N M Patel, and H Agarwal. "Reliability-Based Design Optimization of Robotic System Dynamic Performance." *Journal of Mechanical Design*, ASME. ***129*** (4), Apr. 2006, pp. 449–454.
doi: 10.1115/1.2437804

[75] Sunar, M and S S Rao. "Simultaneous Passive and Active Control Design of Structures Using Multiobjective Optimization Strategies." *Computers and Structures*, Elsevier. ***48*** (5), Sept. 1993, pp. 913–924.
doi: 10.1016/0045-7949(93)90513-D

[76] Frischknecht, B D, D L Peters, and P Y Papalambros. "Pareto Set Analysis: Local Measures of Objective Coupling in Multiobjective Design Optimization." *Structural and Multidisciplinary Optimization*, Springer. ***43*** (5), May 2011, pp. 617–630.
doi: 10.1007/s00158-010-0599-2

[77] Peters, D L, P Y Papalambros, and A G Ulsoy. "Control Proxy Functions for Sequential Design and Control Optimization." *Journal of Mechanical Design*, ASME. ***133*** (9), Sept. 2011, pp. 091007.
doi: 10.1115/1.4004792

[78] Rao, A V. *Pseudospectral Methods for Optimal Control: Theory and Practice*. Online. Lecture Notes. 2012.
url: http://vdol.mae.ufl.edu/Presentations/pseudospectralMethods.pdf.

[79] Bryson, A E and Y C Ho. *Applied Optimal Control: Optimization, Estimation and Control,* Taylor & Francis, 1975.
isbn: 0891162283

[80] Herber, D R. *Solving Optimal Control Problems using Simscape Models for State Derivatives*. Tech. rep. UIUC-ESDL-2014-01. Engineering System Design Lab, May 2014.
url: http://systemdesign.illinois.edu/publications/Her14b.pdf.

[81] Haftka, R T. "Simultaneous Analysis and Design." *AIAA Journal*. ***23*** (7), July 1985, pp. 1099–1103.
doi: 10.2514/3.9043

[82] Darby, C L and A V Rao. "A Mesh Refinement Algorithm for Solving Optimal Control Problems Using Pseudospectral Methods." *Proceedings of the AIAA 2009 Guidance, Navigation, and Control Conference*, No. AIAA 2009-5791, Chicago, IL, USA, Aug. 2009.
doi: 10.2514/6.2009-5791

[83] Garg, D. "Advances in Global Pseudospectral Methods for Optimal Control." Ph.D. Dissertation. University of Florida: Gainesville, FL, USA, Aug. 2011.
url: http://etd.fcla.edu/UF/UFE0043196/garg_d.pdf

[84] Darby, C L. "*hp*-Pseudospectral Method for Solving Continuous-Time Nonlinear Optimal Control Problems." Ph.D. Dissertation. University of Florida: Gainesville, FL, USA, May 2011.
url: http://ufdc.ufl.edu/UFE0042778/00001

[85] Rao, S S. "Combined Structural and Control Optimization of Flexible Structures." *Engineering Optimization*, Taylor & Francis. ***13*** (1), 1988, pp. 1–16.
DOI: 10.1080/03052158808940943

[86] Butsuen, T. "The Design of Semi-Active Suspensions for Automotive Vehicles." Ph.D. Dissertation. Massachusetts Institute of Technology: Cambridge, MA, USA, June 1989.
URL: http://hdl.handle.net/1721.1/14220

[87] Friedland, B. *Advanced Control System Design,* 1st edition, Prentice-Hall, 1996.
ISBN: 0130140104

[88] Roos, F. "Towards a Methodology for Integrated Design of Mechatronic Servo Systems." Ph.D. Dissertation. Royal Institute of Technology: Stockholm, Sweden, Sept. 2007.
URL: http://urn.kb.se/resolve?urn=urn:nbn:se:kth:diva-4473

[89] Trivedi, D, D Dienno, and C D Rahn. "Optimal, Model-Based Design of Soft Robotic Manipulators." *Journal of Mechanical Design*, ASME. ***130*** (9), Aug. 2008, pp. 091402.
DOI: 10.1115/1.2943300

[90] Deshmukh, A P. "Multidisciplinary Design Optimization of Dynamic Systems Using Surrogate Modeling Approach." M.S. Thesis. University of Illinois at Urbana-Champaign: Urbana-Champaign, IL, USA, May 2013.
URL: http://hdl.handle.net/2142/44209

[91] Fonseca, I M. "Integrated Structural and Control Optimization." *Journal of Vibration and Control*, SAGE. ***10*** (10), Oct. 2004, pp. 1377–1391.
DOI: 10.1177/1077546304042043

[92] Kang, W and N Bedrossian. "Pseudospectral Optimal Control Theory Makes Debut Flight, Saves NASA $1M in Under Three Hours." *SIAM News*. ***40*** (7), Sept. 2007.

[93] Vlases, W G, S W Paris, R M Lajoie, M J Martens, and C R Hargraves. *Optimal Trajectories by Implicit Simulation*. Tech. rep. WRDC-TR-90-3056. Wright-Patterson AFB, 1990.

[94] Betts, J T and W P Huffman. *Sparse Optimal Control Software SOCS. Mathematics and Engineering Analysis Technical Document*. Tech. rep. MEA-LR-085. Boeing Information and Support Services, July 1997.

[95] *GESOP & ASTOS: The New Generation of Optimization Software*. Institute of Flight Mechanics and Control. 2003.
URL: https://www.astos.de/products.

[96] Ross, I M and F Fahroo. *User's Manual for DIDO 2001 α: A MATLAB Application for Solving Optimal Control Problems*. Tech. rep. TR-AAS-01-03. Dept. of Aeronautics and Astronautics, Naval Postgraduate School, 2001.

[97] Williams, P. *User's Guide for DIRECT 2.0.* User's Manual. Royal Melbourne Institute of Technology, 2008.

[98] Rutquist, P E and M M Edvall. *PROPT—MATLAB Optimal Control Software*, User's Manual, Tomlab Optimization, 2010.
URL: http://tomopt.com/docs/TOMLAB_PROPT.pdf

[99] Milam, M B. "Real-Time Optimal Trajectory Generation for Constrained Dynamical Systems." Ph.D. Dissertation. California Institute of Technology: Pasadena, CA, USA, May 2003.
URL: http://resolver.caltech.edu/CaltechETD:etd-06022003-114340

[100] Becerra, V M. "Solving Complex Optimal Control Problems at No Cost with $\mathcal{PSOPT}$." *Proceedings of the IEEE 2010 International Symposium on Computer-Aided Control System Design*, Yokohama, Japan, Sept. 2010, pp. 1391–1396.
DOI: 10.1109/CACSD.2010.5612676

[101] Heath, M T. *Scientific Computing An Introductory Survey,* 2nd edition, McGraw-Hill, 1997.
ISBN: 0072399104

[102] Huntington, G T and A V Rao. "Comparison of Global and Local Collocation Methods for Optimal Control." *Journal of Guidance, Control, and Dynamics*, AIAA. ***31*** (2), Mar.–Apr. 2008, pp. 432–436.
DOI: 10.2514/1.30915

[103] Patterson, M A and A V Rao. "Exploiting Sparsity in Direct Collocation Pseudospectral Methods for Solving Optimal Control Problems." *Journal of Spacecraft and Rockets*, AIAA. ***49*** (2), Mar.–Apr. 2014, pp. 354–377.
DOI: 10.2514/1.A32071

[104] Kasturi, P and P Dupont. "Constrained Optimal Control of Vibration Dampers." *Journal of Sound and Vibration*, Elsevier. ***215*** (3), Aug. 1998, pp. 499–509.
DOI: 10.1006/jsvi.1998.1661

[105] Herber, D R, J W McDonald, O S Alvarez-Salazar, G Krishnan, and J T Allison. "Reducing Spacecraft Jitter During Satellite Reorientation Maneuvers via Solar Array Dynamics." *Proceedings of the AIAA/ISSMO 2014 Multidisciplinary Analysis and Optimization Conference*, No. AIAA 2014-3278, Altanta, GA, USA, June 2014.
DOI: 10.2514/6.2014-3278

[106] Son, H and K-M Lee. "Open-Loop Controller Design and Dynamic Characteristics of a Spherical Wheel Motor." *Transactions on Industrial Electronics*, IEEE. ***57***, Oct. 2010, pp. 3475–3482.
DOI: 10.1109/TIE.2009.2039454

[107] Schaal, S and C G Atkeson. "Open Loop Stable Control Strategies for Robot Juggling." *Proceedings of the IEEE 1993 International Conference on Robotics and Automation*, Vol. 3, Atlanta, GA. USA, May 1993, pp. 913–918.
DOI: 10.1109/ROBOT.1993.292260

[108] Mourik, S v, H Zwart, and K J Keesman. "Integrated Open Loop Control and Design of a Food Storage Room." *Biosystems Engineering*, Elsevier. ***104*** (4), Dec. 2009, pp. 493–502.
DOI: 10.1016/j.biosystemseng.2009.09.010

[109] Karkee, M and B L Steward. "Study of the Open and Closed Loop Characteristics of a Tractor and a Single Axle Towed Implement System." *Journal of Terramechanics*, Elsevier. ***47*** (6), Dec. 2010, pp. 379–393.
DOI: 10.1016/j.jterra.2010.05.005

[110] Journée, J M J and W W Massie. *Offshore Hydromechanics,* 1st edition, Delft University of Technology, 2001.
URL: http://www.shipmotions.nl/DUT/LectureNotes/OffshoreHydromechanics.pdf

[111] McTaggart, K. *Modelling and Simulation of Seaways in Deep Water for Simulation of Ship Motions.* Tech. rep. DRDC-ATLANTIC-TM-2003-190. Defence R&D Canada, Sept. 2003.

[112] ITTC. "The Specialist Committee on Waves-Final Report and Recommendations to the 23rd ITTC." *Proceedings of the ITTC 2002 International Towing Tank Conference*, Vol. 2, Venice, Italy, Sept. 2002, pp. 505–551.
URL: http://ittc.sname.org/proc23/Waves.pdf

[113] Valério, D, P Beirão, and J S d Costa. "Optimisation of Wave Energy Extraction with the Archimedes Wave Swing." *Ocean Engineering*, Elsevier. ***34*** (17–18), Dec. 2007, pp. 2330–2344.
DOI: 10.1016/j.oceaneng.2007.05.009

[114] Bachynski, E E, Y L Young, and R W Yeung. "Analysis and Optimization of a Tethered Wave Energy Converter in Irregular Waves." *Renewable Energy*, Elsevier. ***48***, Dec. 2012, pp. 133–145.
DOI: 10.1016/j.renene.2012.04.044

[115] Li, Y and Y-H Yu. "A Synthesis of Numerical Methods for Modeling Wave Energy Converter-Point Absorbers." *Renewable and Sustainable Energy Reviews*, Elsevier. ***16*** (6), Aug. 2012, pp. 4352–4364.
DOI: http://dx.doi.org/10.1016/j.rser.2011.11.008

[116] Lattanzio, S M and J T Scruggs. "Maximum Power Generation of a Wave Energy Converter in a Stochastic Environment." *Proceedings of the IEEE 2011 International Conference on Control Applications*, Denver, CO, USA, Sept. 2011, pp. 1125–1130.
DOI: 10.1109/CCA.2011.6044428

[117] McIver, P and D V Evans. "The Occurrence of Negative Added Mass in Free-Surface Problems Involving Submerged Oscillating Bodies." *Journal of Engineering Mathematics*, Springer. ***18*** (1), Mar. 1984, pp. 7–22.
DOI: 10.1007/BF00042895

[118] Cummins, W E. "The Impulse Response Function and Ship Motions." *Schiffstechnik.* ***9***, Oct. 1962, pp. 101–109.
URL: http://hdl.handle.net/1721.3/49049

[119] Yu, F and J Falnes. "State-Space Modelling of a Vertical Cylinder in Heave." *Applied Ocean Research*, Elsevier. ***17*** (5), Oct. 1995, pp. 265–275.
DOI: 10.1016/0141-1187(96)00002-8

[120] Yeung, R W. "Added Mass And Damping of a Vertical Cylinder in Finite-Depth Waters." *Applied Ocean Research*, Elsevier. ***3*** (3), July 1981, pp. 119–133.
DOI: 10.1016/0141-1187(81)90101-2

[121] Bhatta, D D. "Computations of Hydrodynamic Coefficients, Displacement-Amplitude Ratios and Forces for a Floating Cylinder due to Wave Diffraction and Radiation." *International Journal of Non-Linear Mechanics*, Elsevier. ***46*** (8), Oct. 2011, pp. 1027–1041.
DOI: 10.1016/j.ijnonlinmec.2011.04.022

[122] Clément, A H. "Using Differential Properties of the Green Function in Seakeeping Computational Codes." *Proceedings of the 1999 International Conference on Numerical Ship Hydrodynamics*, Nantes, France, July 1999, pp. 6.5.

[123] Korsmeyer, F T, H B Bingham, and J N Newman. *TiMIT: A Panel-Method Program for Transient Wave-Body Interactions*, May 1999.
URL: http://www.wamit.com/Publications/TiMITmanual.pdf

[124] *WAMIT User Manual Version 7.0*, May 2013.
URL: http://www.wamit.com/manual.htm

[125] *AquaDyn Description*. Scientific Software Group. Apr. 4, 2014.
URL: http://www.scisoftware.com/products/aquadyn_details/aquadyn_details.html.

[126] Forrester, A, A Sobester, and A Keane. *Engineering Design via Surrogate Modelling: A Practical Guide,* 1st edition, John Wiley & Sons, 2008.
ISBN: 0470060689

[127] Hoen, M K T. "Modeling and Control of Wave Energy Converters." M.S. Thesis. Norwegian University of ScienceTechnology: Trondheim, Norway, May 2009.
URL: http://urn.kb.se/resolve?urn=urn:nbn:no:ntnu:diva-8960

[128] Garcia-Rosa, P B et al. "Wave-to-Wire Model and Energy Storage Analysis of an Ocean Wave Energy Hyperbaric Converter." *Journal of Oceanic Engineering*, IEEE. ***39*** (2), Apr. 2014, pp. 386–397.
DOI: 10.1109/JOE.2013.2260916

[129] Hoerner, S F. *Fluid Dynamic Drag,* Hoerner Fluid Dynamics, 1965.
ISBN: 9993623938

[130] Korde, U A. "Control System Applications in Wave Energy Conversion." *Proceedings of the OCEANS 2000 MTS/IEEE Conference and Exhibition*, Providence, RI, USA, Sept. 2000, pp. 1817–1824.
DOI: 10.1109/OCEANS.2000.882202

[131] Pitti, A, M Lungarella, and Y Kuniyoshi. "Exploration of Natural Dynamics through Resonance and Chaos." *Proceedings of the 2006 International Conference on Intelligent Autonomous Systems*, Tokyo, Japan, Mar. 2006, pp. 558–565.

[132] Falnes, J and J Hals. "Heaving Buoys, Point Absorbers and Arrays." *Philosophical Transactions of the Royal Society A*, Royal Society Publishing. ***370*** (1959), Jan. 2012, pp. 246–277.
doi: 10.1098/rsta.2011.0249

[133] Valerio, D, P Beirao, M J G Mendes, and J Sa da Costa. "Comparison of Control Strategies Performance for a Wave Energy Converter." *Proceedings of the IEEE 2008 Mediterranean Conference on Control and Automation*, Ajaccio, France, June 2008, pp. 773–778.
doi: 10.1109/MED.2008.4602139

[134] Salter, S H, J R M Taylor, and N J Caldwell. "Power Conversion Mechanisms for Wave Energy." *Proceedings of the Institution of Mechanical Engineers, Part M: Journal of Engineering for the Maritime Environment*, SAGE. ***216*** (1), June 2002, pp. 1–27.
doi: 10.1243/147509002320382103

[135] Ringwood, J. "Practical Challenges in Harvesting Wave Energy." *Journal of Ocean Technology.* ***5*** (2), 2010, pp. 73–91.
url: http://www.eeng.nuim.ie/coer/doc/PUB0008_J161JOTC.pdf

[136] Speyer, J L. "Periodic Optimal Flight." *Journal of Guidance, Control, and Dynamics*, AIAA. ***19*** (4), July–Aug. 1996, pp. 745–755.
doi: 10.2514/3.21695

[137] Boyd, S and L Vandenberghe. *Convex Optimization,* 7th edition, Cambridge University Press, 2009.
isbn: 0521833787

ERRATA

#	Location	Reads	Correction
1	p. 15, Eqn. (2.6)	$e^{\mathbf{A}t}\boldsymbol{\xi}_0 + \int_{t_0}^{t_f}$	$e^{\mathbf{A}(t-t_0)}\boldsymbol{\xi}_0 + \int_{t_0}^{t}$
2	p. 18, Eqn. (2.7)	$\xi_{n+1}(t_0) = 0$	$\xi_{n+1}(t_0) = t_0$
3	p. 21, Eqn. (2.14)	$e^{\mathbf{A}(\mathbf{x_p})t}\boldsymbol{\xi}_0 + \int_{t_0}^{t_f}$	$e^{\mathbf{A}(\mathbf{x_p})(t-t_0)}\boldsymbol{\xi}_0 + \int_{t_0}^{t}$
4	p. 30, Figure 2.4	**d)** DT global collocation	[1]
5	p. 40, Eqn. (3.18)	$\boldsymbol{\xi}[t_{k-1}] + \mathbf{k}_3$	[2] $\boldsymbol{\xi}[t_{k-1}] + h_k\mathbf{k}_3$
6	p. 41, Eqn. (3.20)	$\approx \frac{1}{2}\sum_{k=0}^{n_t-1}$	$\approx \sum_{k=0}^{n_t-1}$
7	p. 69, Eqn. (4.43)	$\boldsymbol{\xi}(t_f) - \boldsymbol{\xi}(0) \leq \mathbf{0}$	$\boldsymbol{\xi}(t_f) - \boldsymbol{\xi}(0) = \mathbf{0}$
8	p. 110, Eqn. (A.10)	(A.10a) twice	(A.10a)–(A.10g)

[1] This illustration should have defect constraints for the derivative of the polynomial approximation rather than the polynomial itself. This is one of the main differences between time-marching (integration) direct transcription methods and pseudospectral (differentiation) direct transcription methods.

[2] Each stage of the formula has derivative functions with increments on $\boldsymbol{\xi}[t_{k-1}]$. All of these increments should have $h_k\mathbf{k}$ instead of $\mathbf{k}$ (if present). The fourth-order Runge-Kutta equations have different but equivalent definitions in different texts. The previous set of equations was a misprint of two common representations.

A number of minor typographical errors have also been corrected.